# CONTROLLERS FOR AIR TO FUEL RATIO REGULATION OF SI ENGINES


ANURAK JANSRI





A DISSERTATION SUBMITTED IN PARTIAL FULFILLMENT
OF THE REQUIREMENT FOR THE DEGREE OF
DOCTOR OF ENGINEERING IN ELECTRICAL ENGINEERING
FACULTY OF ENGINEERING
KING MONGKUT'S INSTITUTE OF TECHNOLOGY LADKRABANG
2013

KMITL-2013-EN-D-018-184

| | |
|---|---|
| **หัวข้อวิทยานิพนธ์** | ตัวควบคุมสำหรับอัตราส่วนอากาศต่อเชื้อเพลิงของเครื่องยนต์จุดระเบิดด้วยประกายไฟ |
| **นักศึกษา** | นายอนุรักษ์ จันทร์ศรี |
| **รหัสประจำตัว** | 51060009 |
| **ปริญญา** | วิศวกรรมศาสตรดุษฎีบัณฑิต |
| **สาขาวิชา** | วิศวกรรมไฟฟ้า |
| **พ.ศ.** | 2556 |
| **อาจารย์ที่ปรึกษาวิทยานิพนธ์** | รศ.ดร.ปิติเขต สู้รักษา |

## บทคัดย่อ

วิทยานิพนธ์นี้ศึกษาการควบคุมอัตราส่วนปริมาณอากาศต่อปริมาณเชื้อเพลิงสำหรับเครื่องยนต์จุดระเบิดด้วยประกายไฟ โดยนำแบบจำลองเครื่องยนต์ค่ากลางมาประยุกต์และปรับปรุงค่าสัมประสิทธิ์การคายอากาศ จึงได้เสนอแบบจำลองเชิงคณิตศาสตร์การคายอากาศของลิ้นปีกผีเสื้อ รวมทั้งเพิ่มเติมสัญญาณรบกวนที่สร้างจากสัญญาณอลวนแบบโลจิสติก สำหรับกลวิธีการควบคุมอัตราส่วนปริมาณอากาศต่อปริมาณเชื้อเพลิงได้ออกแบบจากแนวคิดทฤษฎีตรรกศาสตร์วิภัชนัยโดยใช้สัดส่วนและผลรวมของค่าผิดพลาดระบบมาประมวลผล ตัวควบคุมแบบตรรกศาสตร์วิภัชนัยดังกล่าวสามารถควบคุมอัตราส่วนปริมาณอากาศต่อประมาณเชื้อเพลิงได้อย่างมีประสิทธิภาพ และมีคุณสมบัติที่ง่ายต่อการปรับแต่งสัมประสิทธิ์ มีความคงทนต่อสัญญาณรบกวน และ มีสถาปัตยกรรมในรูปแบบง่าย ผลการทดลองพบว่าแบบจำลองมีความตรง ผลการทดสอบสมรรถนะพบว่าตัวควบคุมตรรกศาสตร์วิภัชนัยแบบพีไอให้ผลดีที่สุด

| | |
|---|---|
| **Thesis Title** | Controllers for Air to Fuel Ratio Regulation of SI Engines |
| **Student** | Mr. Anurak Jansri |
| **Student ID.** | 51060009 |
| **Degree** | Doctor of Engineering |
| **Program** | Electrical Engineering |
| **Year** | 2013 |
| **Thesis Advisor** | Assoc.Prof.Dr.Pitikhate Sooraksa |


## ABSTRACT

This thesis is study of air to fuel ratio (AFR) regulation for spark ignition engines. With the engine model, a mean value engine model (MVEM) is utilized. For realistic operations of throttle valve, the MVEM is improved on static discharge coefficient to dynamic discharge coefficient. Moreover, the throttle operations are added a disturbance signal by chaotic generator. The AFR control strategy is designed by using a discrete fuzzy PI algorithm, which provides easy tuning, robustness and rapid development with a simple architecture. Results and Performance index (J) of fuel regulation are presented by computer simulation and standard evolution criteria respectively. Experimental results reveal validity of the model. Performance tests also reveal that the fuzzy PI controller outperforms the others in comparison.

# ACKNOWLEDGEMENTS

The author would like to sincerely express his gratitude to his advisor, Dr. Pitikhate Sooraksa, for supporting his research and continuing encouragement along the entire period of his study. Guidance from his advisor either in his academic life and social life are countless and unforgettable. The author would also like to thank to his Co-advisor, Prof. Hisayuki Aoyama, who gave many experiences in academic research at University of Electro-Communications, Tokyo, Japan.

The author would like to thank to all committee members: Dr. Surapan Airpiboon, Dr. Attasit Lasakul, Dr. Vanvisa Chutchawong and Dr. Veerapol Monyakul for the time spent reviewing this dissertation's document. Thanks to Dr. Withawat Withayachumnankul of the University of Adelaide Australia for comments and proofreading to the journal paper. Thanks also addressed to all laboratory members and his lovely family.

The author would be grateful to Thailand Research Fond for fully supporting to him under Royal Golden Jubilee Ph.D. program and big thanks to Bangkok NGV Company, National Electronic & Computer Technology Center (NECTEC), National Innovation Agency (NIA) and National Research Council of Thailand (NRCT) for research material supporting.

Anurak Jansri

# TABLE OF CONTENTS

# TABLE OF CONTENTS (cont.)

# TABLE OF CONTENTS (cont.)

# LIST OF FIGURES

# LIST OF FIGURES (cont.)

# LIST OF FIGURES (cont.)

# LIST OF TABLES

# NOMENCLATURE

| | |
|---|---|
| $A_{th}(\alpha)$ | Area of throttle $(m^2)$ |
| $D$ | Diameter of throttle $(m)$ |
| $\alpha$ | Angle of throttle plate $(Radius)$ |
| $d$ | Diameter of throttle lot $(m)$ |
| $k$ | $d/D$ |
| $\dot{m}_{ath}$ | Air mass flow rate pass throttle plate $(kg/s)$ |
| $p_0$ | Front of throttle pressure $(Pa)$ |
| $T_0$ | Front of throttle temperature $(Kalvin)$ |
| $C_d$ | Discharge coefficient $(0 \leftrightarrow 1)$ |
| $R$ | Gas constant $\left(287J/(k_g * K)\right)$ |
| $p_i$ | Intake manifold pressure $(Pa)$ |
| $p_e$ | Exhaust pressure $(Pa)$ |
| $\gamma$ | Specific heat ratio |
| $M_a$ | Mass of air $(Kg)$ |
| $T_i$ | Intake manifold temperature $(Kalvin)$ |
| $r_c$ | Cylinder ratio |
| $\eta_v$ | Volumetric efficiency |
| $\rho_{ai}$ | Intake manifold density |
| $V_m$ | Manifold volume $(m^3)$ |
| $N$ | Crankshaft speed $(rpm)$ |
| $\dot{m}_{ac}$ | Air mass flow rate in cylinder $(kg/s)$ |
| $\dot{m}_{fi}$ | Injected fuel mass flow rate $(kg/s)$ |
| $\dot{m}_{ff}$ | Fuel film mass flow rate $(kg/s)$ |
| $\dot{m}_{fv}$ | Fuel vapor mass flow rate $(kg/s)$ |
| $\dot{m}_{fc}$ | Fuel mass flow rate in cylinder $(kg/s)$ |
| $t_{inj}$ | Time of fuel injection $(s)$ |
| $t_0$ | Time delay of fuel injector $(s)$ |
| $\tau_s$ | Time delay of oxygen sensor $(s)$ |
| $\tau_d$ | Time delay of cylinder cycle $(s)$ |

# Chapter 1
# Introduction

## 1.1 Background

In basic public transportations and private transportations, many vehicles can be moved by thermal power using closed systems. Such the systems are motor cycles, boats, cars, trains, and aircrafts. The closed system is called internal combustion engine became it can generate driving torques by combustion of air and fuel. After the air and fuel are fired, they are transformed to exhaust out to environment. Consequently, bad pollutions are clouded. Note that this is a problem. Typically, the driving powers are generated by amount of air and amount of fuel inside combustion chamber as a regular variation form. This implies that if there are more amount of air and amount of fuel then more driving power is required. Conversely, less amount of air and less amount of fuel yields less driving power. Since fuel economy topic is highly impact thus designs of engine and engine controller are challenging. Note that this is a challenging problem as well. As the problems, amount of air and amount of fuel are especially focused; hence, air to fuel ratio (AFR) regulation is remarked. For various fuels namely gasoline, natural gas vehicle (NGV), liquid petroleum gas (LPG) and others are shown the AFR ratio in Appendix E.

## 1.2 Objectives

The objectives of this research are:

(1) to establish combustion engine model for computer simulation;

(2) to simulate the air to fuel ratio control by using various controllers;

(3) to simulate an air regulator control by using various controllers;

(4) to verify validity of (1), (2), and (3) by experiment.

## 1.3 Literature review

As the reasons in Subsection 1.1, several AFR feedback algorithms have been proposed for controlling AFR. The basic observer-based controller using state variable technique is presented in [1,2], To improve amount of air mass in transient state, a nonlinear steady state fuelling controller is described in [3,4]. Gaeta et al [5] has recently proposed a control strategy incorporating a feedforward controller, inner feedback PI model-based controller, and Smith predictor. Comparison on PI controller, PID controller and sliding mode controller is simulated in [6]. Choi and

Hedrick [7] developed an observer-based fuel injection control algorithm using sliding mode strategy. Wang and Yu [8] improved Choi and Hedrick's algorithm by introducing the second-order sliding mode control with an RBF neural network for gain adjustment. However, these strategies might cause a chattering problem. For improvement, Wang et al. [9] proposed an adaptive neural network strategy, which employed a radial basis function (RBF) network type, together with the recursive k-means and recursive least-squares algorithms for training the network. Wang and Yu [10] also proposed a parameter estimation for dynamic sliding mode control (DSMC) by using an adaptive radial basis function network strategy. However, these neural network algorithms are too complicated to embed into a microcontroller and the physical meaning of each parameter might not be clear enough.

In addition, for air regulation, it is also called electronic throttle valve. The electronic throttle control strategies to control the ETV have three approaches stand out: a conventional proportional-integral-derivative (PID) controller with compensators, a sliding mode control, and a neural network control. Of the first scenario, Deur et al proposed a PID controller with the nonlinear friction and limp-home compensators [11]. Pavkovic et al improved Deur's work with adaptive strategy for auto-tuning the PID controller gains [12]. Mercorelli implemented a real-time self-tuning of an approximated proportional-derivative (PD) regulator for the tracking error caused by inexact feedback linearization [13]. Grepl and Lee studied the four models of controllers each with a spring compensator, a model-based friction compensator, a smooth-sliding mode friction compensator, and PID controller [14]. Recently, Corno et al presented an adaptive control using gain-scheduled approach for PID controller to control a pair of ETV of the racing motorcycles [15].

Of the second scenario, Baric et al employed a sliding mode controller to achieve a tracking of smooth reference signal and estimated the parameters of ETV using the neural network approach [16]. Reichhartinger and Horn proposed a control scheme, which consists of a twisting algorithm and a super-twisting algorithm, both of which are based on second-order sliding mode concept [17]. Moreover, the sliding mode strategy has been chosen to estimate an angle velocity and a motor current for variable-structure controller [18].

For the last scenario, in more recent years to identify the ETV model, the neuro-computing has been used. Yuan et al proposed an adaptive inverse model control system that employs two radial basis functions for both a model regulation and a model identifier [19]. In another work of Yuan et al, a fuzzy neural network controller

and a neural network identifier based on back propagation algorithm are proposed in [20].

## 1.4 Research scope

(1) The combustion engine model is established based on thermodynamic principle and mechanical design.

(2) MATLAB/SIMULINK is utilized to simulate the performance of model.

Referring to the several AFR feedback algorithms in Section 1.3, however, existing literature have not been investigated on controlling AFR with a simple fuzzy PI structure well-designed in [21, 22]. A fuzzy PI controller proposed in Ref [21, 22] has been thoroughly proved and well-understood many years ago due to its simple structure, easy tuning, excellent tracking performance, and high robustness.

(3) The discrete fuzzy PI control is used for air to fuel ratio regulation in computer simulation.

(4) The air regulator or called electronic throttle valve is employed for computer simulation and real experiment by using various controllers: discrete PI controller, discrete PD controller, discrete PID controller, discrete PD+I controller, discrete PID with anti-windup controller, discrete fuzzy PI with anti-windup controller as well as sliding mode controller.

## 1.5 Dissertation outline

Chapter 2 details the mathematical modeling of both an internal combustion engine and an electronic throttle body. The internal combustion engine is described by the mean value engine model (MVEM); then, the MVEM remarks systems upon: air, fuel, temperature, pressure, torque, speed and sensor. The electronic throttle valve (ETV) is also presented as mathematical model.

Chapter 3 discusses the simple controls namely proportional integral derivative (PID) control, fuzzy control and sliding mode control (SMC). The PID is a classical control that widely used in various industries. The fuzzy logic and fuzzy system are well known in the area of Artificial intelligence, expert system as well as granular computing for computer science, computer engineering and control engineering. The SMC is one approach in a set of robust control strategies that need exact process model as well.

Chapter 4 presents air to fuel ratio regulation of spark ignition engine by computer simulation. The MVEM is used for a mathematical engine model that consists of various components a throttle plate, intake pipe, injector, combustion

chamber, crankshaft and exhaust oxygen sensor. The discrete fuzzy PI controller is used for regulator. For robustness tests, the chaotic signals are injected to disturb both throttle degree and engine speed of the systems.

Chapter 5 presents electronic throttle control by computer simulation. The ETV mathematical model that consists of dynamic parts is remarked. The discrete PID, discrete fuzzy PI and SMC-ERL schemes are employed to control the throttle degree. For robustness tests, the disturbance signal is added to disturb feedback position of the ETV.

In Chapter 6, from mathematical model, computer simulation, controller design and parameter tuning knowledge of electronic throttle valve as described in Chapter 5 , this chapter presents ETV control in experiment.

Chapter 7 gives conclusion of Chapters 2-6.

# Chapter 2
# Process Model

## 2.1 Introduction

Currently, for more convenience on pre-design process in automotive engineering, many vehicle parts are computerized machine. This chapter details the mathematical modeling of both an internal combustion engine and an electronic throttle body. The internal combustion engine is described by the mean value engine model (MVEM); then, the MVEM remarks systems upon: air, fuel, temperature, pressure, torque, speed and sensor. The model is following Section 2.2.

Section 2.3 moves to other vehicle part namely an electronic throttle valve (ETV). The ETV is one important that is placed on the air system to regulate air mass flow. It consists of three dynamic elements: a direct-current (dc) motor, a gear train box, and a return spring. From the elements, a numerous load torque is occurred such as static friction, column friction and spring load torque. Therefore, performing of ETV is based on nonlinear behavior.

## 2.2 Engine Model

The MVEM is a mathematical engine model of single cylinder system and consists of various components such as throttle valve, intake pipe, injector, combustion chamber, crankshaft, exhaust pipe and exhaust oxygen sensor. They are shown in Fig. 2.1. The details for each subsystem are described in Section 2.2.1-2.2.7.

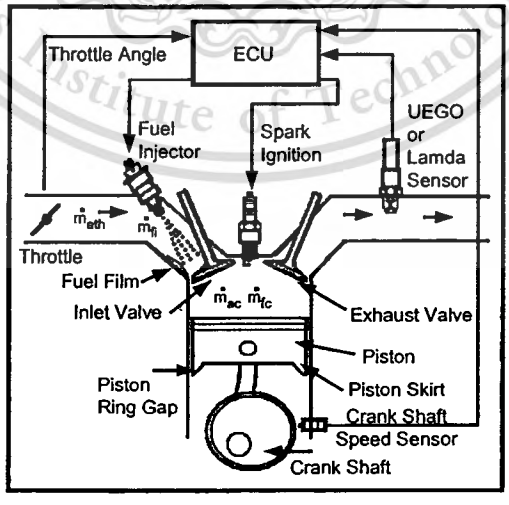


**Fig. 2.1** The internal combustion system

### 2.2.1 Air Flow

In spark ignition engines, air is an essential compound for the internal combustion process. The air flow system directly influences the engine performance, i.e., the power, torque, speed and low emission, as detailed below. For the sake of convenience, the mathematical notation appeared in the equations used throughout this research is listed in the nomenclature page.

### 2.2.2 Area of throttle

A throttle plate is an air-flowing valve separating a filter side and an intake side. The throttle provides a flow area for an amount of air into the intake manifold. The flow area can be adjusted by a throttle angle and can be expressed by [23]

$$A_{th}(\alpha) = \frac{\pi D^2}{4}\left(1-\frac{\cos\alpha}{\cos\alpha_0}\right)+\frac{D^2}{2}\left\{\frac{k}{\cos\alpha}\left(\cos^2\alpha-k^2\cos^2\alpha_0\right)^{1/2}\right.$$
$$\left.-\frac{\cos\alpha}{\cos\alpha_0}\sin^{-1}\left(\frac{k\cos\alpha_0}{\cos\alpha}\right)-k\left(1-k^2\right)^{1/2}+\sin^{-1}k\right\} \quad (2.1)$$

### 2.2.3 Mass of air after the throttle

After the throttle plate opens, the air in front of the throttle can pass into an intake manifold. To calculate the volume of the passing air, a differential equation has been used [3, 23]. The air mass flow rate can be described by the relationship among the area of the throttle, discharge coefficient, pressure in the front of the throttle, intake manifold pressure, temperature in front of the throttle, gas constant, and specific heat ratio, as

$$\dot{m}_{ath} = \frac{C_d A_{th} p_0}{\sqrt{RT_0}}\left(\frac{2\gamma}{\gamma-1}\right)^{1/2}\left[\left(\frac{p_i}{p_0}\right)^{2/\gamma}-\left(\frac{p_i}{p_0}\right)^{(\gamma+1)/\gamma}\right]^{1/2} \quad (2.2)$$

According to the experiment in [24], we use a linear regression method to establish a formula for the dynamic discharge coefficient. The formula is described by the third-order polynomial as

$$C_d(P_0,P_i) = -1.47\left(\frac{P_i}{P_0}\right)^3+1.06\left(\frac{P_i}{P_0}\right)^2-0.21\left(\frac{P_i}{P_0}\right)+1.01 \quad (2.3)$$

Note that extant literatures do not clearly describe the dynamic behaviors of the air passing through the throttle. This discharge coefficient is now explicitly described in our work as shown in Eq. (2.3).

### 2.2.4 Volumetric efficiency

The volumetric efficiency is a necessary parameter used in a four-stroke engine [23, 25]. It is a ratio between the actual mass of the air flowing into the cylinder and the mass of the air given on theoretical volume. Ideally, the volumetric efficiency is defined as a function of the following variables: the mass of air, pressure in front of the throttle, intake manifold pressure, exhaust pressure, temperature at front of the throttle, intake manifold temperature, specific heat ratio, cylinder ratio, and fuel to air ratio [26]

$$\eta_v = \left(\frac{M}{M_a}\right)\left(\frac{p_i}{p_0}\right)\left(\frac{T_0}{T_i}\right)\left(\frac{1}{1+(F/A)}\right)\left\{\frac{r_c}{r_{c-1}} - \frac{1}{\gamma(r_c-1)}\left[\left(\frac{p_e}{p_i}\right)+(\gamma-1)\right]\right\} \tag{2.4}$$

### 2.2.5 Intake manifold density

The intake manifold density, $\rho_{ai}$, is one important parameter greatly influencing the mass of air passing into the cylinder. The density can be expressed by

$$\rho_{ai} = \frac{p_i}{RT_i} \tag{2.5}$$

, where

$$\dot{p}_i = \frac{RT_i}{V_m}\dot{m}_{ath} - \frac{\eta_v N V_d p_i}{120 V_m} \tag{2.6}$$

From Eqs. (2), (4) and (6), for the air flow system, an actual amount of air passing into the cylinder can be calculated by

$$\dot{m}_{ac} = \frac{\eta_v N V_d \rho_{ai}}{2(60)} \tag{2.7}$$

### 2.2.6 Fuel Flow

A fuel injector is an electromechanical device electrically controlled to activate a solenoid valve. An amount of fuel injected into the intake manifold can be expressed by

$$m_{fi} = K\left(t_{inj} - t_0\right) \tag{2.8}$$

In Eq. (2.8), the injected time $\left(t_{inj}\right)$ is dynamic behavior because it is calculated from various speeds of engine by the electronic control unit (ECU). The response time of the solenoid $\left(t_0\right)$ represents a mechanical delay and is a small constant about microseconds [1]. After the fuel is injected, the fuelling dynamic process begins [1, 3,28].The simplest fuel-film-flow model of the MVEM depicted in Fig. 2.2 can be described by

$$\dot{m}_{ff} = \frac{1}{\tau_f}\left(-\dot{m}_{ff} + X\dot{m}_{fi}\right) \tag{2.9}$$

$$\dot{m}_{fv} = \left(1 - X\right)\dot{m}_{fi} \tag{2.9.1}$$

$$\dot{m}_f = \dot{m}_{fv} + \dot{m}_{ff} \tag{2.9.2}$$

where $\tau_f$ is the time constant of fuel evaporation. The term $X$ is a fraction of the injected fuel, which is deposited on both the intake manifold wall and the inlet valve.

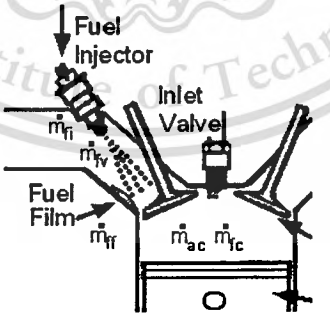


**Fig. 2.2** Fuel film description

After the inlet valve is closed, the actual air to fuel ratio inside the cylinder can be calculated by using

$$A/F = \frac{\dot{m}_{ac}}{\dot{m}_{fc}} \tag{2.10}$$

, and the lambda input can be calculated simultaneously by using

$$\lambda_i = \frac{A/F}{(A/F)_s} \tag{2.11}.$$

The relationship between the actual and measured lambdas is provided by the following transfer function [26]

$$\lambda_m = \frac{\lambda_i e^{-\tau_d s}}{\tau_s s + 1} \tag{2.12}$$

Note that $s$ is the complex variable written in frequency domain fashion, $\tau_s$ is the time constant of the oxygen sensor, and $\tau_d$ is the transport delay between the injector and the exhaust gas oxygen sensor. Hence, the transfer function is specific to the first-order pulse dynamic dead time (FOPDDT) system [1,28,29].

### 2.2.7 Crankshaft

Since the output of the system is the engine speed, we first need to calculate the crankshaft velocity. To start with, the work of the crankshaft system depends on the relationship between the pressure and torque [23-25, 30-32]. The crankshaft velocity can be calculated by an integral of the resulting torque divided by the engine inertia [33], and can be expressed by

$$\dot{\omega} = \frac{1}{J_{eng}}\left(T_c - T_f - T_p - T_l\right) \tag{2.13}$$

where $\dot{\omega}$ is the engine speed, $T_c$ is the combustion torque after sparks, $T_f$ is the friction torque while the piston moves up and down, $T_p$ is the pumping torque , $T_l$ is the load torque and $J_{eng}$ is the engine inertia. In other words, the crankshaft velocity can be explained by using the pressure term or the mean effective pressure term as

$$\dot{\omega} = \frac{1}{J_{eng}}\left[\frac{V_d\left(imep - tfmep\right)}{4\pi} - T_l\right] \tag{2.14}$$

where *imep* is the net indicated mean effective pressure for a four-stroke engine without a supercharger, and it is a result of subtraction between the gross indicate mean effective pressure (*gmep*) and pumping indicate mean effective pressure (*pmep*). We now have

$$imep = gmep - pmep \tag{2.15}$$

and the *imep* can then be computed by

$$imep = \frac{120\eta_f \dot{m}_f Q_{HV} \min(\lambda,1)}{V_d N} \tag{2.16}$$

where $\eta_f$ is the fuel conversion efficiency, $Q_{HV}$ is the fuel low heat value and $\dot{m}_f$ is the fuel mass flow rate. The first and second parameters are strongly related to a fuel type. *tfmap* is the friction mean effective pressure and it is also a result of summation between the mechanical friction mean effective pressure (*mfmep*) and accessory mean effective pressure (*afmep*). Here *tfmap* is defined as

$$tfmep = mfmep + amep \tag{2.17}$$

The variables and effects used for calculation of *tfmep* are as follows. The mechanical friction mean effective pressure is related to the journal-bearing friction, piston and rings friction, and valve train friction. The journal-bearing friction is highly dependent on the viscosity and cleanness of engine oil. The piston and rings friction is caused by scratch between the piston skirt and the ring pack with the cylinder bore. The valve train friction arises from three parts: the overhead camshaft, the pivot rockers and the valve components. The accessory mean effective pressure involves oil pump, water pump and non-charging alternator friction. Combining all these effects, the friction-mean effective pressure can be written as a function of the engine speed as

$$tfmep = 0.97 + 0.15\left(\frac{N}{1000}\right) + 0.05\left(\frac{N}{1000}\right)^2 \tag{2.18}$$

Finally, the formula for the engine speed can be written as

$$N = \left[ 60\left( \int_0^t \dot{\omega} dt \right) \right] \Big/ 2\pi \tag{2.19}$$

## 2.3 Electronic Throttle Valve

With reference to [8, 34], an electronic throttle valve (ETV) consists of three dynamic elements: a direct-current (dc) motor, a gear train box, and a return spring, all of which are of greatest influence upon design of a precise control algorithm. The ETV structure is shown in Fig. 2.3. The dc motor is a torque transducer that converts electric energy into mechanical energy. Its mathematical model can be described as:

$$0 = Vi_a - VL_a - VR_a - V_b \tag{2.20}$$

$$Vi_a - V_b = L_a \frac{di_a}{dt} + i_a R_a \tag{2.21}$$

$$V_b = K_{emf} \omega_m \tag{2.22}$$

$$T_m = K_m i_a \tag{2.23}$$

$$0 = T_m - T_b - T_{app} - T_L \tag{2.24}$$

$$J_m \frac{d\omega_m}{dt} = T_m - T_b - T_L \tag{2.25}$$

where $V$ is a input control voltage, $i_a$ a dc motor armature current, $L_a$ a dc motor armature inductance, $R_a$ a dc motor armature resistance, $V_b$ a back-emf voltage, $\omega_m$ a rotor angular velocity, $K_{emf}$ a back-emf constant, $K_m$ a motor torque constant, $T_m$ a motor torque determined by its current, $T_b$ a viscous-friction torque, $T_{app}$ a applied torque, $T_L$ a load torque due to the air mass flow force, and $J_m$ a rotor inertia.

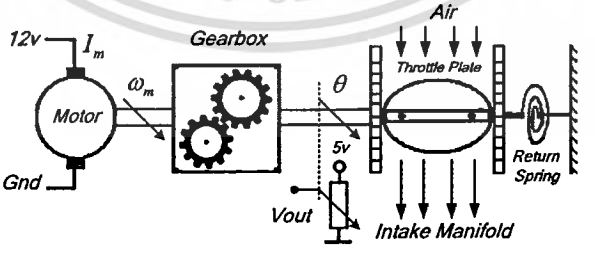


**Fig. 2.3** Structure of electronic throttle valve

Of the second part, after the motor has been spun, the gear train box is employed to transmit the motor torque to open a throttle plate. Simultaneously, the

gear train box has generated the backlash nonlinear behavior, transmission friction as well as throttle plate friction. Several frictions can be explained in terms of physics based on a friction model of the LuGre model [8, 11, 12 and 34]. The model is based on dynamic behavior as expressed below:

$$T_f = \sigma_0 z + \sigma_1 \dot{z} + \sigma_2 \omega_m \tag{2.26}$$

$$\dot{z} = \omega_m - \frac{\sigma_0 |\omega_m|}{g(\omega_m)} z \tag{2.27}$$

$$g(\omega_m) = F_c + (F_s - F_c) e^{-|\omega_m/\omega_s|^2} \tag{2.28}$$

where $T_f$ is friction torque, and $\sigma_0$ and $\sigma_1$ represent dynamic friction parameters as asperity stiffness and damping coefficients, $\sigma_2$ is a viscous friction, $z$ is an internal state of friction that is a function of angular velocity $(\omega_m)$, a Coulomb friction $(F_c)$, a static friction $(F_s)$, and the Stribeck velocity $(\omega_s)$. Note that the static friction is higher than Coulomb friction. While the ETV is performed, the most load torque is a spring torque. Therefore, the damping coefficient $\sigma_1 \dot{z}$ and the viscous friction $\sigma_2 \omega_m$ are neglected. In addition, the Stribeck friction model can be defined the Coulomb friction curve as $F_c = F_s$ and the LuGre friction model is reduced to the Dahl friction model as

$$T_f = \sigma_0 z \tag{2.29}$$

$$g(\omega_m) = F_c \tag{2.30}$$

$$\dot{z} = \omega_m - \frac{\sigma_0 |\omega_m|}{F_c} z \tag{2.31}$$

, take derivative on (2.29)

$$\dot{T}_f = \sigma_0 \dot{z} \tag{2.32}$$

, give $\dot{z}$ in (2.32) by (2.31)

$$\dot{T}_f = \sigma_0 \left( \omega_m - \frac{\sigma_0 |\omega_m|}{F_c} z \right) \tag{2.33}$$

, give $\sigma_0 z$ in (2.33) by (2.29)

$$\dot{T}_f = \sigma_0 \left( \omega_m - \frac{|\omega_m|}{F_c} T_f \right) \tag{2.34}$$

, and also its characteristic is shown in fig. 2.4.

Of the last part, the return spring, to avoid damage in a car accident or lack of control, the throttle plate is extremely forced into closed position; hence, the return

spring torque $(T_{sp})$ is enormous. The return spring torque is computed from both static stiffness torque $(K_s)$ and throttle opened torque; also, its characteristic is shown in Fig. 2.5. The torque can be described as:

$$T_{sp} = K_t(\theta - \theta_0) + K_s \operatorname{sgn}(\theta - \theta_0) \qquad (2.35)$$

where $K_t$ is torsion stiffness torque.

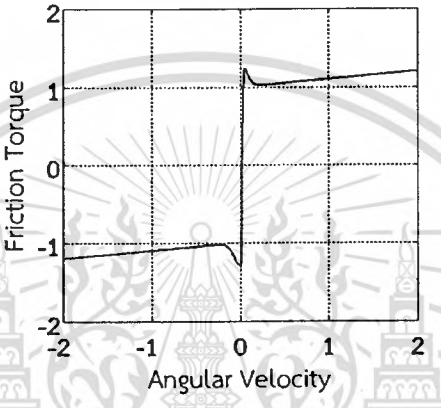


Fig. 2.4 A nonlinear characteristic of Dahl friction

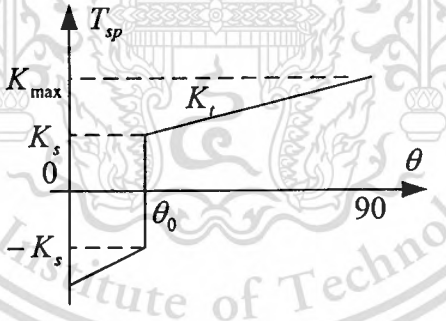


Fig. 2.5 A nonlinear characteristic of return spring

## 2.4 Summary

For the first step in analyzing, designing and controller tuning, mathematical modeling is an important significantly. Equations mentioned in Section 2.2 will be used as the plant model for computer simulation in Chapter 4. The equations mentioned in Section 2.3 will be used in Chapter 5.

# Chapter 3
# Control Strategies

## 3.1 Introduction

This chapter now presents the simple controls namely proportional integral derivative (PID) control, fuzzy control and sliding mode control (SMC). The PID is a classical control that widely used in various industries. The fuzzy logic and fuzzy system are well known in the area of Artificial intelligence, expert system as well as granular computing for computer science, computer engineering and control engineering. In this chapter, the control engineering is selected. Also, the SMC is one approach in a set of robust control strategies that need exact process model.

For this chapter organization, in Section 3.2, the first topic, a classical PID on frequency model is mentioned and discrete model is transformed by using a backward approximation method. In Section 3.3, Design of discrete fuzzy PI controller is described such as two inputs and an output membership function for fuzzification, four rules for fuzzy interference, a center of area calculation for defuzzification and ten increment control outputs. Section 3.4, the SMC based on exponential reaching law is described. Section 3.5, two fitness functions, an integral absolute error (IAE) and an integral square error (ISE) are employed to compute a performance index of controller.

## 3.2 Discrete PID Controller

To begin with, considering of a control action of a typical PID controller described in the frequency domain by

$$U_{PID}(s) = K\left(1 + \frac{1}{st_i} + st_d\right)E(s) \tag{3.1}$$

where $K$ is the controller gain, $t_i$ the integral time, $t_d$ the derivative time, and $E(s)$ error signal. To transform the analog PID controller to a discrete version, a backward approximation method [29] is employed:

$$s = \frac{\left(1 - z^{-1}\right)}{T} \tag{3.2}$$

, to obtain

$$U_{PID}(z)=K\left(1+\frac{1}{t_i}\left(\frac{T}{1-z^{-1}}\right)+\left(\frac{1-z^{-1}}{T}\right)t_d\right)e(z) \tag{3.3}$$

$$U_{PID}(z)=\left(K_p+K_i\left(\frac{1}{1-z^{-1}}\right)+K_d\left(1-z^{-1}\right)\right)e(z) \tag{3.4}$$

$$U_{PID}(z)=\left(\frac{K_p\left(1-z^{-1}\right)+K_i+K_d\left(1-z^{-1}\right)\left(1-z^{-1}\right)}{\left(1-z^{-1}\right)}\right)e(z) \tag{3.5}$$

$$U_{PID}(z)\left(1-z^{-1}\right)=\left\{K_p\left(1-z^{-1}\right)+K_i+K_d\left(1-z^{-1}\right)\left(1-z^{-1}\right)\right\}e(z) \tag{3.6}$$

$$U_{PID}(z)\left(1-z^{-1}\right)=\left\{K_p\left(1-z^{-1}\right)+K_i+K_d\left(1-2z^{-1}+z^{-2}\right)\right\}e(z) \tag{3.7}$$

$$\begin{aligned}U_{PID}(KT)-U_{PID}(KT-1)&=K_p\{e(KT)-e(KT-1)\}\\&\quad+K_i\{e(KT)\}+K_d\{e(KT)-2e(KT-1)+e(KT-2)\}\end{aligned} \tag{3.8}$$

$$\begin{aligned}\Delta U_{PID}(KT)&=K_p\{e(KT)-e(KT-1)\}+K_i\{e(KT)\}\\&\quad+K_d\{e(KT)-2e(KT-1)+e(KT-2)\}\end{aligned} \tag{3.9}$$

where $K_p$ is a proportional gain, $K_i=KT/2t_i$ is an integral gain and $K_d=Kt_d/T$ is a derivative gain.

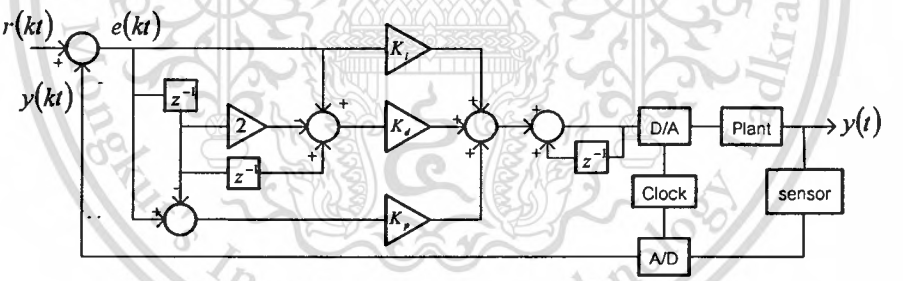


Fig. 3.1 The discrete PID control scheme.

## 3.3 Discrete Fuzzy PI Controller

This section introduces a brief review of the discrete fuzzy PI control in [21, 22] that has been proved to have superior performance over the classical PID one. Similarly, to start with, a typical PID controller described in Eq. (3.1) as

$$U_{PID}(s)=K\left(1+\frac{1}{st_i}+st_d\right)E(s) \tag{3.10}$$

For PI control, let $t_d$ = 0. To transform the analog PI controller to a discrete version, a bilinear approximation method [29] is employed:

$$s = \frac{2}{T}\left(\frac{1-z^{-1}}{1+z^{-1}}\right) \tag{3.11}$$

to obtain

$$U_{PI}(z) = K\left(1+\frac{1}{t_i}\left(\frac{T}{2}\left(\frac{1+z^{-1}}{1-z^{-1}}\right)\right)\right)E(z) \tag{3.12}$$

with simple algebra and taking inverse z-transform, we arrive at the incremental control

$$U_{PI}(z) = \left(K_p + K_i\left(\frac{1+z^{-1}}{1-z^{-1}}\right)\right)E(z) \tag{3.13}$$

$$U_{PI}(z) = \left(\frac{K_p(1-z^{-1}) + K_i(1+z^{-1})}{(1-z^{-1})}\right)E(z) \tag{3.14}$$

$$U_{PI}(z)(1-z^{-1}) = \{K_p(1-z^{-1}) + K_i(1+z^{-1})\}E(z) \tag{3.15}$$

$$U_{PI}(KT) - U_{PI}(KT-1) = K_p\{e(KT) - e(KT-1)\} + K_i\{e(KT) + e(KT-1)\} \tag{3.16}$$

$$\Delta U_{PI}(kT) = K_p\{e(kT) - e(kT-T)\} + K_i\{e(kT) + e(kT-T)\} \tag{3.17}$$

where $K_p$ is a proportional gain and $K_i = KT/2t_i$ is an integral gain. The system represented by Eq. (3.17) can be illustrated by Fig. 3.2.

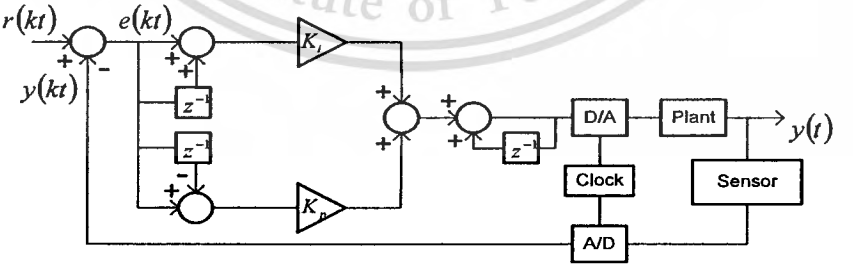


**Fig. 3.2** The discrete PI control scheme

In designing a simple discrete fuzzy PI controller, a fuzzy decision block with fuzzy gains $K_u$ is simply added into the conventional one in Fig. 3.2 to obtain the fuzzy version in Fig. 3.3. The discrete fuzzy PI controller is derived by using an error

and a rate of error for fuzzification, four rule bases and min-max Mamdani's method for fuzzy inference, and a center of area calculation for defuzzification. Inputs and output membership function are shown in Figs. 3.4 and 3.5, respectively. Combination of the two input membership function forms the 2-D error phase plane that is illustrated in Fig. 3.4 (Top view).

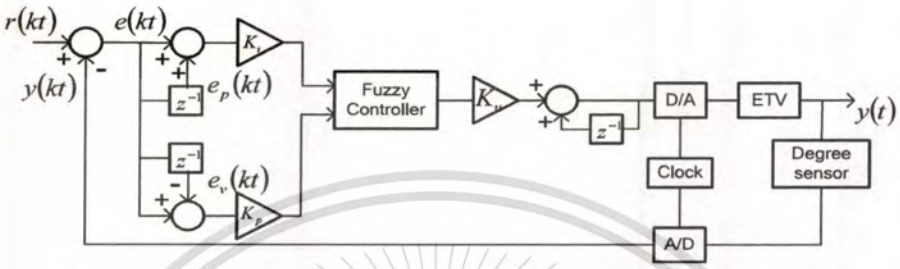


**Fig. 3.3** The discrete fuzzy PI control scheme

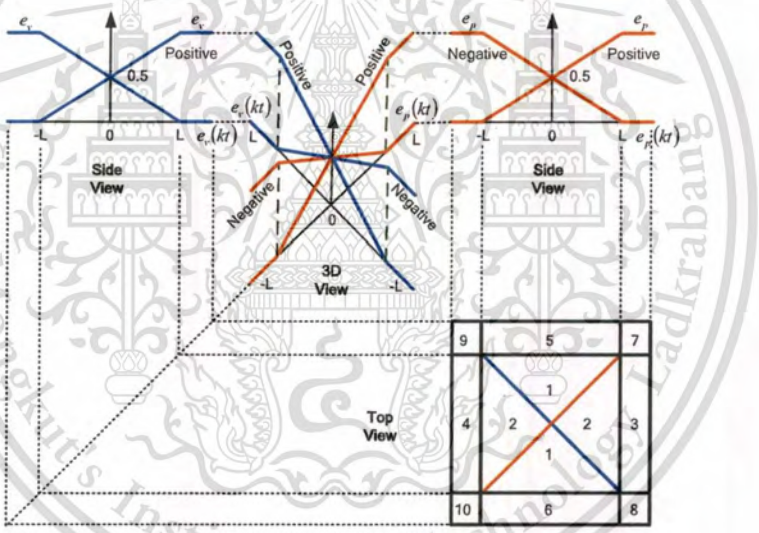


**Fig. 3.4** The input membership function and input combination of possible cases on the error phase plane.

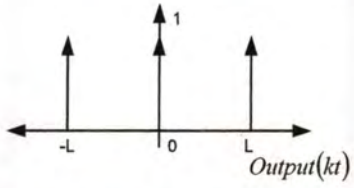


**Fig. 3.5** The output membership function

Mathematically, Fig. 3.4 can be directly read out as

$$e_p \cdot Positive = \frac{K_i e_p(kt) + L}{2L}, e_p \cdot Negative = \frac{-K_i e_p(kt) + L}{2L} \quad (3.18)$$

$$e_v \cdot Positive = \frac{K_p e_v(kt) + L}{2L}, e_v \cdot Negative = \frac{-K_p e_v(kt) + L}{2L} \quad (3.19)$$

Similarly, Fig. 3.5 states that $\mu_o(z_i)$, which is the value of the output membership function, has three types of solutions: $Positive = L, Zero = 0$, $Negative = -L$. For interference, the inner fuzzy outputs are produced by both fuzzy rule base and fuzzy logic operator

$$\max\{\min\{\mu(e_v), \mu(e_p)\}\} \quad (3.20)$$

where $\mu(e_v)$ and $\mu(e_p)$ are the output of the input membership functions. Four rule bases for natural tracking are shown in fig. 3.6 and employed as:

- R1: If $e_p$ is Positive and $e_v$ is Positive Then Output is Positive
- R2: If $e_p$ is Positive and $e_v$ is Negative Then Output is Zero
- R3: If $e_p$ is Negative and $e_v$ is Positive Then Output is Zero
- R4: If $e_p$ is Negative and $e_v$ is Negative Then Output is Negative.

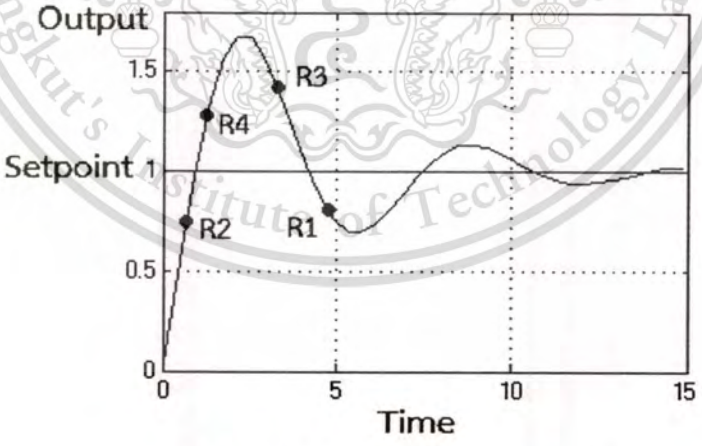


**Fig. 3.6** The natural tracking

For defuzzification, the center of the area is expressed by

$$\text{Center of Area} = \frac{\sum_{i=1}^{n} u_i \mu_i}{\sum_{i=1}^{n} \mu_i} \tag{3.21}$$

Then, the final formulas of each input region as shown in Fig. 3.4 (top view) can be found as following:

$$\Delta u_{pi}(kt) = \frac{L\{K_i e_p(kt) + K_p e_v(kt)\}}{2\{2L - K_p|e_v(kt)|\}} \quad \text{Area 1} \tag{3.22}$$

$$\Delta u_{pi}(kt) = \frac{L\{K_i e_p(kt) + K_p e_v(kt)\}}{2\{2L - K_i|e_p(kt)|\}} \quad \text{Area 2} \tag{3.23}$$

$$\Delta u_{pi}(kt) = 0.5\{K_p e_v(kt) + L\} \quad \text{Area 3} \tag{3.24}$$

$$\Delta u_{pi}(kt) = 0.5\{K_p e_v(kt) - L\} \quad \text{Area 4} \tag{3.25}$$

$$\Delta u_{pi}(kt) = 0.5\{K_i e_p(kt) + L\} \quad \text{Area 5} \tag{3.26}$$

$$\Delta u_{pi}(kt) = 0.5\{K_i e_p(kt) - L\} \quad \text{Area 6} \tag{3.27}$$

$$\Delta u_{pi}(kt) = -L \quad \text{Area 7} \tag{3.28}$$

$$\Delta u_{pi}(kt) = 0 \quad \text{Areas 8, 9} \tag{3.29}$$

$$\Delta u_{pi}(kt) = L \quad \text{Area 10} \tag{3.30}$$

For obvious understanding how to find whole formulas of each input region, an appendix A is described.

## 3.3 Sliding Mode Control based on Exponential Reaching Law

This section reveals both sliding mode and reaching law for a SMC regulator. A sliding mode is based on a sliding line that is negative slop (-m). The sliding line is also called sliding phase that drive system close to equilibrium point. A reaching law is algorithm of reaching phase that drive system is to treat a stable manifold. Typically, the sliding surface is described as

$$s(t) = \dot{e}(t) + ce(t). \tag{3.31}$$

Let

$$e(t) = SP(t) - PO(t) \tag{3.32}$$

, take derivative on Eq. (3.32)

$$\dot{e}(t) = \frac{d(SP(t))}{dt} - \frac{d(PO(t))}{dt} \tag{3.33}$$

, denote that $SP(t)$ = set point and $PO(t)$ = process output. The reaching law uses an exponential algorithm that is expressed by

$$\dot{s}(t) = -h\text{sgn}(s) - ks \tag{3.34}$$

Then, for sliding mode control based on exponential reaching law (SMC-ERL), the final system can be written as

$$-h\text{sgn}(s) - ks = \ddot{e}(t) + c\dot{e}(t) \tag{3.35}$$

## 3.4 Measure of Controlled Performance

For controlled system, rise time, peak time, settling time, overshoot value, under shoot value and cost of control signal are significant. They are indicator value of controlling performance because they are treated by adjusting a controlled parameter. Several indicator values can be realized on quantitative form as shown in Fig. 3.7. Hence, an integral absolute error (IAE) and an integral square error (ISE) are considered. The performance index (J) can be calculated by both.

$$IAE = \int_0^\infty |e(t)|dt \tag{3.36}$$

$$ISE = \int_0^\infty e^2 dt \tag{3.37}$$

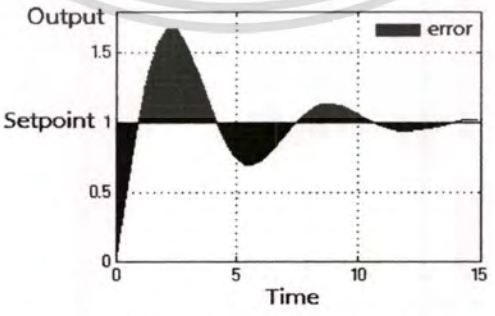


Fig. 3.7 An amount of error

## 3.5 Summary

The discrete PID controller, the discrete fuzzy PI controller and the sliding mode controller have been briefly reviewed. To design the control system using these approaches, three following parameters can be adjusted: error gain $K_i$, rate of error gain $K_p$ and $K_d$ for PID. Four following parameters can be adjusted: error average gain $K_i$, rate of error gain $K_p$, output gain $K_u$ and input membership length $L$ for fuzzy PI. Also, three following parameters can be adjusted: error gain $c$, switching manifold gain $h$ and exponential gain $c$ for SMC-ERL. Controllers presented in this section are applied to the process models obtained in Chapter 2 with the results presented in the Chapter 4 and Chapter 5.

# Chapter 4
# Computer Simulation of SI Engine

## 4.1 Introduction

This chapter presents air to fuel ratio regulation of spark ignition engine by computer simulation. The MVEM is used for a mathematical engine model that consists of various components a throttle plate, intake pipe, injector, combustion chamber, crankshaft and exhaust oxygen sensor. The discrete fuzzy PI controller as described in Chapter 3 is employed for regulator. For robustness tests, the chaotic signals are injected to disturb both throttle degree and engine speed of the systems.

Section 4.2 presents schematic diagram of spark ignition engine with air to fuel control, MATLAB/SIMULINK diagram of MVEM and chaotic model. Section 4.3 details about simulation results such as the AFR response, corresponding control signals and associated dynamic responses. Performance evaluations are presented in Section 4.4.

## 4.2 Air to Fuel Ratio Control

The workflow of the SI engine with an AFR (A/F ratio) control is clearly shown in Fig. 4.1. We consider the workflow based on the feedback control strategy. The figure summarizes the plant described mathematically in Chapter 2. For simulation, we have run the SI engine model by using MATLAB/SIMULINK shown in Fig. 4.2 and more details are described in Appendix B.

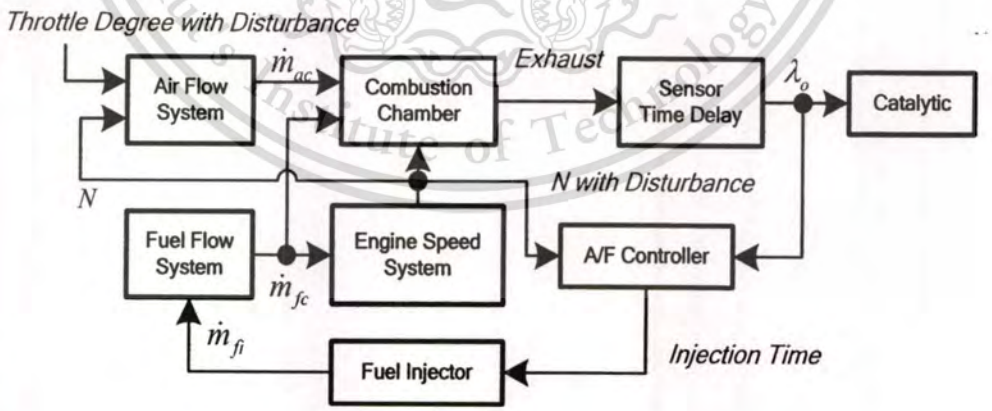


**Fig. 4.1** Block diagram of the SI engine with AFR control

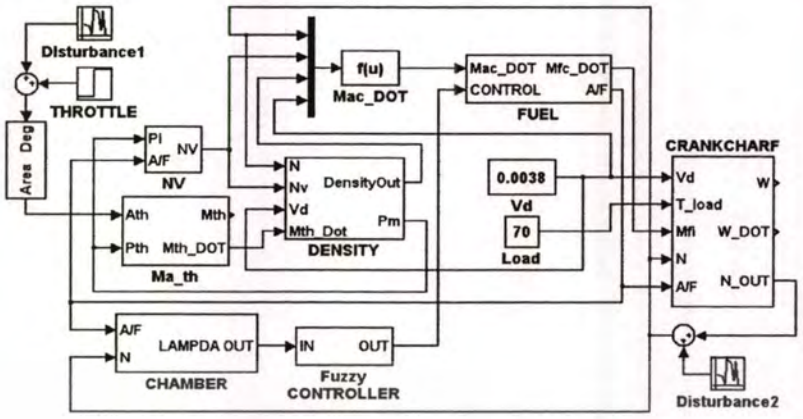


**Fig. 4.2** The system in MATLAB/SIMULINK representation

The simulation parameters based on a real-world specification are as follows: the cylinder displacement volume of 0.0038 $m^3$ [7] and compression ratio of 10. For an NA engine car [24], the pressure in front of the throttle is 101330 $Pa$ (1 bar), and the temperature in front of the throttle is 300 $K$. In the case of gasoline fuel [23-25, 30-32], the ideal gas constant is 287 $J/(k_g * K)$; the specific heat ratio is 1.4; the specific heat value is 44300 $J$; the fuel conversion efficiency is 0.7. The load torque is 70 N-m [7]. Each engine revolution has both a static time delay and dynamic time delay. For the static delay, the fuel injector time delay is 0.00041 s and the oxygen sensor time delay is 0.45 s [1]. The dynamic time delay is the cylinder cycle time delay that can be expressed as [28]

$$\tau_d = \frac{120}{N} \tag{4.1}$$

In Fig. 4.2, the throttle disturbance and the speed disturbance are involved. The disturbance is generated by a logistic map with a law frequency. The logistic map function is expressed as

$$x(k+1) = ax(k)(1-x(k)) \tag{4.2}$$

where $a = 3.8$ and $x(0) = 0.1$. The disturbance patterns are presented with realistic magnitudes shown in Figs. 4.3-4.4 to test the robustness of the designed control system.

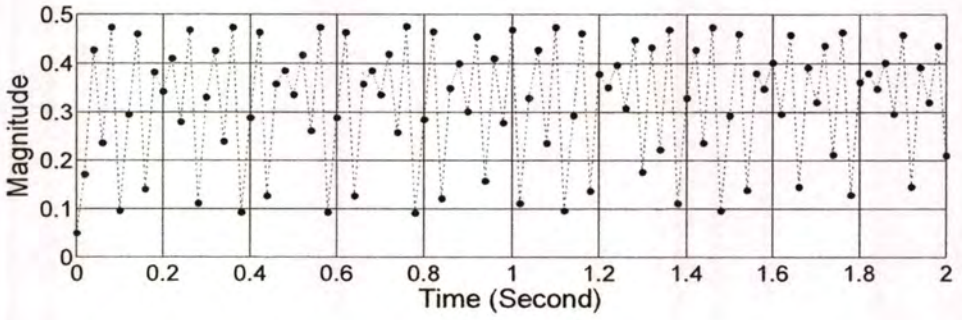


Fig. 4.3 Throttle disturbance

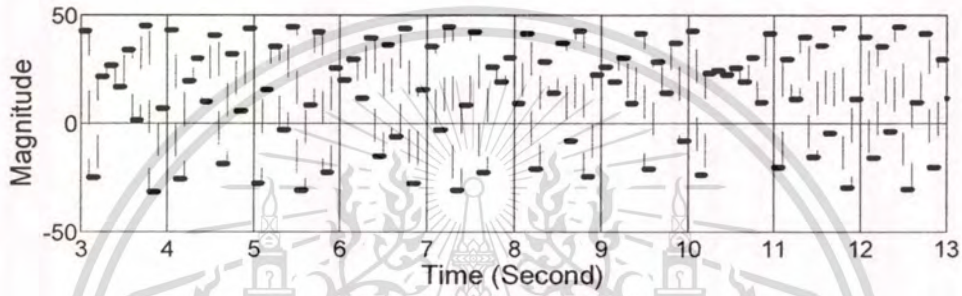


Fig. 4.4 Engine speed disturbance

For throttle inputs, three accelerations with disturbance are assigned: single step, double step and sine step, as shown in Figs. 4.5, 4.6 and 4.7 respectively. In control, the fuzzy PI controller is employed in accordance with several details as follow: the sampling time of the controller is 20 ms; the controller gains are: $K_p$ =7.0, $K_i$ =1.4, $K_u$ =0.012 and $L$ =5.0; with an integral time $t_i$ =50 ms. To evaluate the performance of fuzzy PI controller, an integral of absolute error (ITAE), an integral of square error (ISE), an integral of absolute control output (IACO) and an integral absolute error (IAE) are employed. They are numerically shown in Table 4.1.

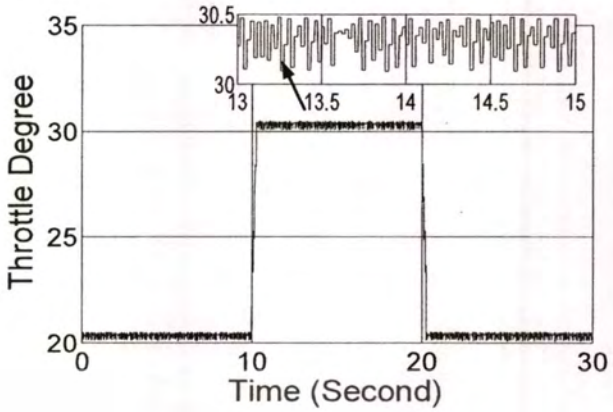


Fig. 4.5 The single-step acceleration

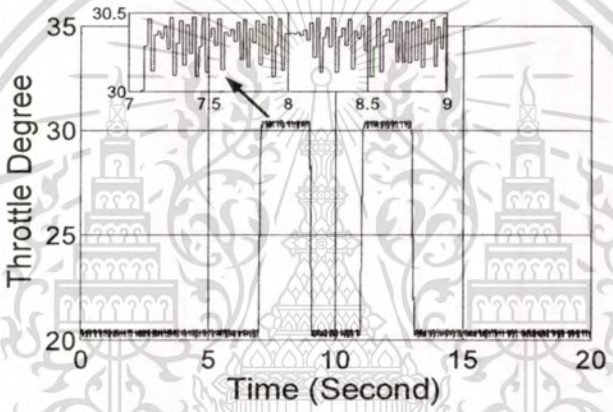


Fig. 4.6 The double-step acceleration

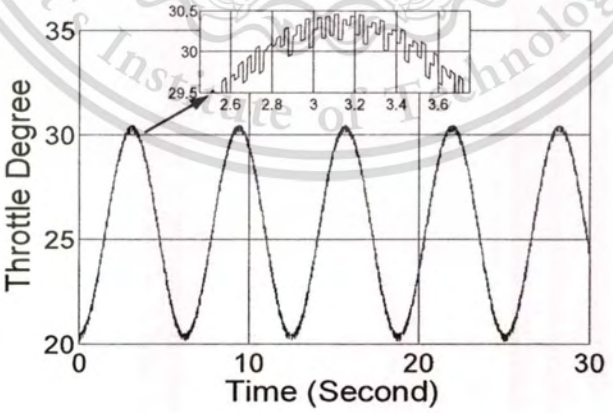


Fig. 4.7 The sine-step acceleration

## 4.3 Simulation Results

In Fig. 4.8 the throttle is executed on the single step corresponds to the situation that the driver pushes on the acceleration pedal only one time. Figure 4.8 shows the measured signal of AFR (a), control signal of controller (b), amount of air mass (c), amount of fuel mass (d), number of volumetric efficiency (e), number of intake pressure (f), value of indicated torque (g), value of friction torque (h) and engine speed (g). During 0 s to 3 s is start time of simulated engine; consequently, the results divert out from actuality of engine operation. Therefore, the results can be considered suitably after 3 s. The magnitude of the AFR corresponding to the step up of the throttling from 20 to 30 degrees is 10% higher than the stoichiometric ratio (14.7/1) and the settling time is only 2.5 s. Conversely, at the step down of the throttling from 30 degrees to 20 degrees, the ratio is 15% lower than the stoichiometric ratio and the settling time is 4 s. The settling time of the step down is higher than the step up because the engine running at a low speed generates a higher exhausted delay as evident in engine speed. The air mass minimum and maximum are around 0.015 and 0.05 kg/s respectively. The fuel mass minimum and maximum are around 0.001 and 0.0035 kg/s respectively. With the air mass flow and fuel mass flow into cylinder are used to demonstrate the effectiveness of the system model, according to the AFR, have a correct order of magnitude. In addition, the average of volume metric efficiency is about 0.6 and the average of intake pressure is about 60 kPa. The values confirm that not only the volume metric efficiency does not exceed 1 but also the intake manifold pressure does not exceed 1 *bar*. With engine power, the indicate torque is much larger than friction torque; then, engine speed is occurred. The results are reasonably acceptable.

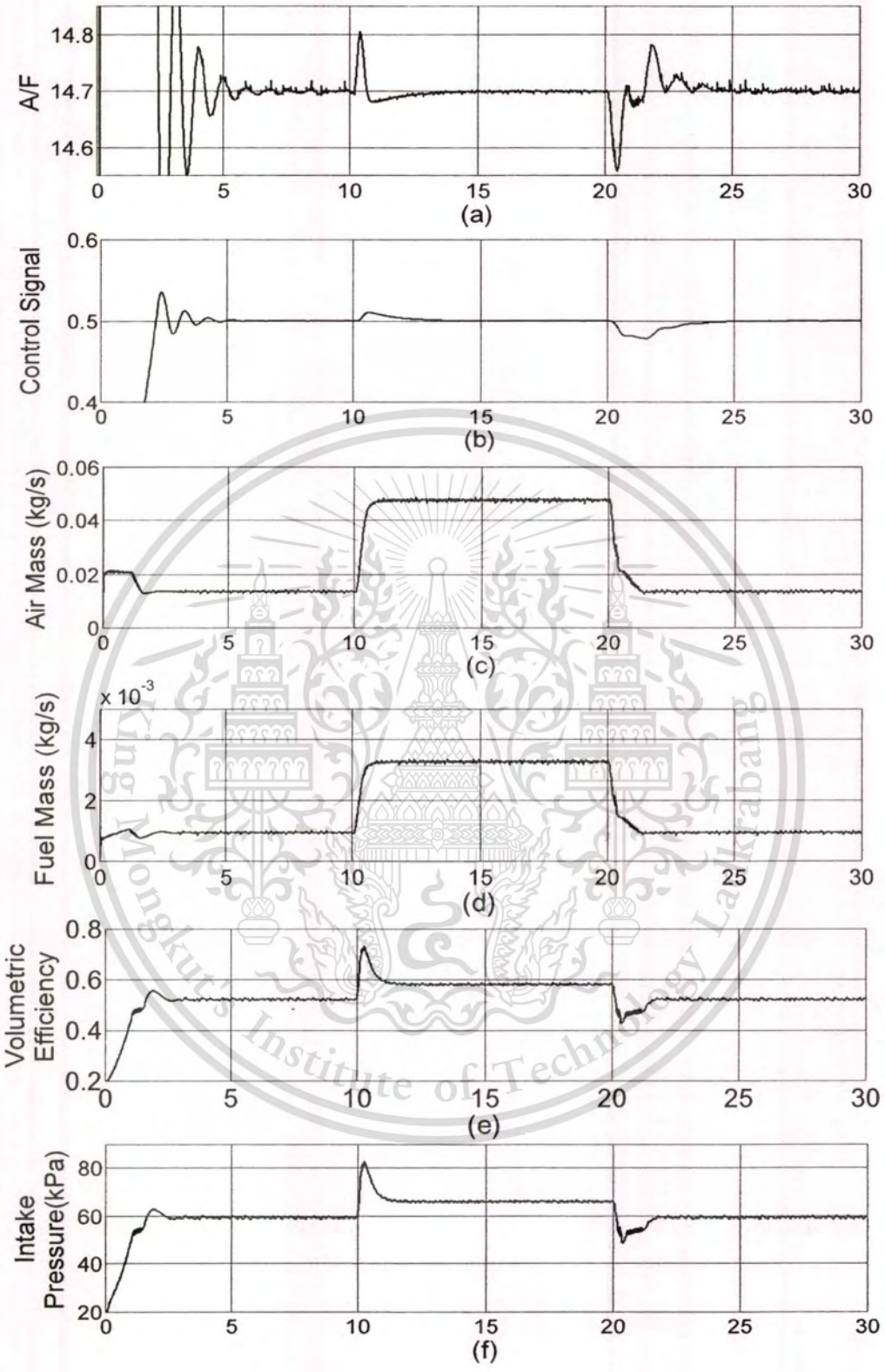


**Fig. 4.8** Engine operations with single-step acceleration (Cont.)

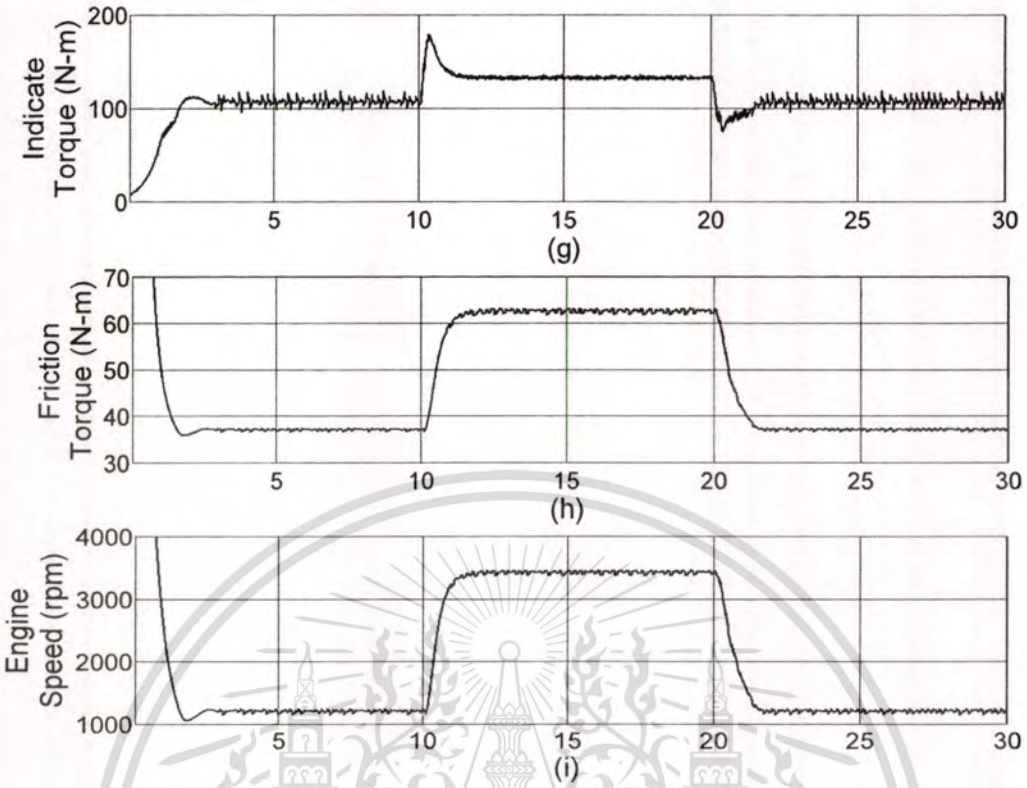


**Fig. 4.8** Engine operations with single-step acceleration

In Fig. 4.9 the throttle is executed on the double step that the driver pushes on the acceleration pedal two times. The Figure 4.9 shows the measured signal aspects same as Fig. 4.8. Similarly, the results are considered after 3 s. The maximum magnitude of the AFR corresponding to the step up of the throttling from 20 to 30 degrees is 15% higher than the stoichiometric ratio and the settling time is only 2 s. Conversely, at the step down of the throttling from 30 degrees to 20 degrees, the ratio is 18% lower than the stoichiometric ratio and the settling time is 4 s. The air mass minimum and maximum are around 0.015 and 0.048 kg/s respectively. The fuel mass minimum and maximum are around 0.001 and 0.0031 kg/s respectively. The average of volume metric efficiency is about 0.58 and the average of intake pressure is about 65 kPa. They do not exceed basic value of NA engine. The average of indicate torque is about 130 Nm and average of friction torque is about 50 Nm. The engine speed can be occurred around 1100 to 3400 rpm.

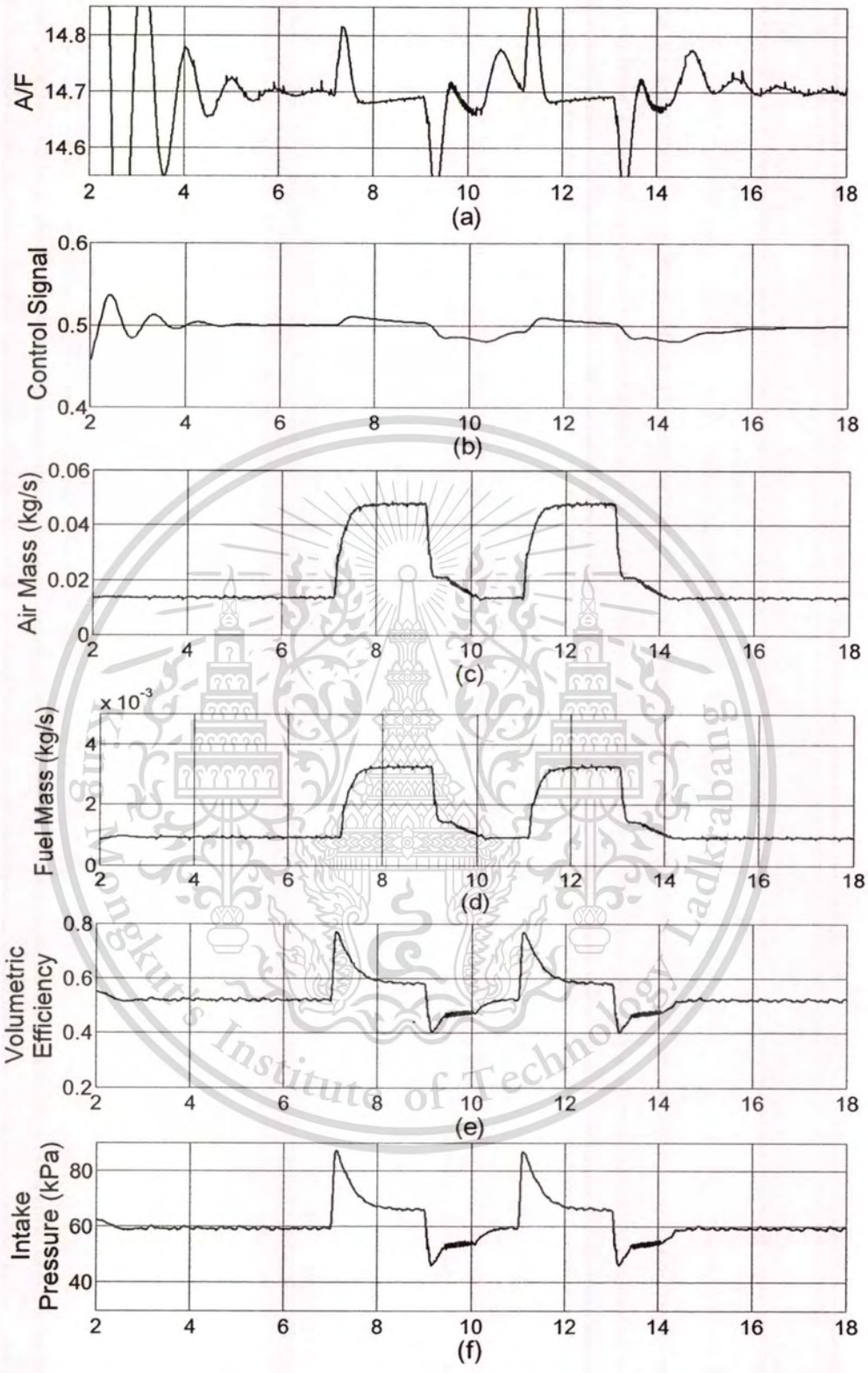


**Fig. 4.9** Engine operations with double-step acceleration (Cont.)

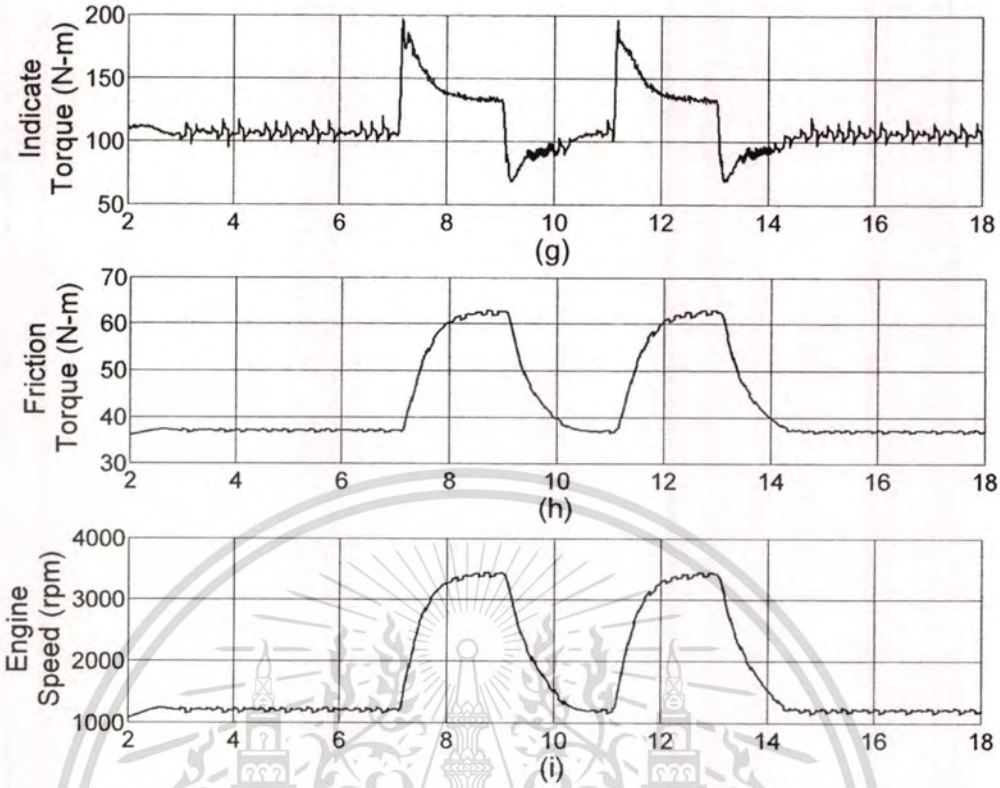


Fig. 4.9 Engine operations with double-step acceleration

In Fig. 4.10 the throttle is executed on the sine step that change position of the acceleration pedal every time; then, all measured signals have behavior seem like unstable. The maximum magnitude of the AFR is 5% higher than the stoichiometric ratio and the minimum magnitude is 3% lower than the stoichiometric ratio. The settling time is off set. The air mass and the fuel mass are nearly the value of double step acceleration. The average of volume metric efficiency is about 0.55 and the average of intake pressure is about 61 kPa. The average of indicate torque is about 120 Nm and average of friction torque is about 50 Nm. The engine speed is generated around 1100 to 3400 rpm.

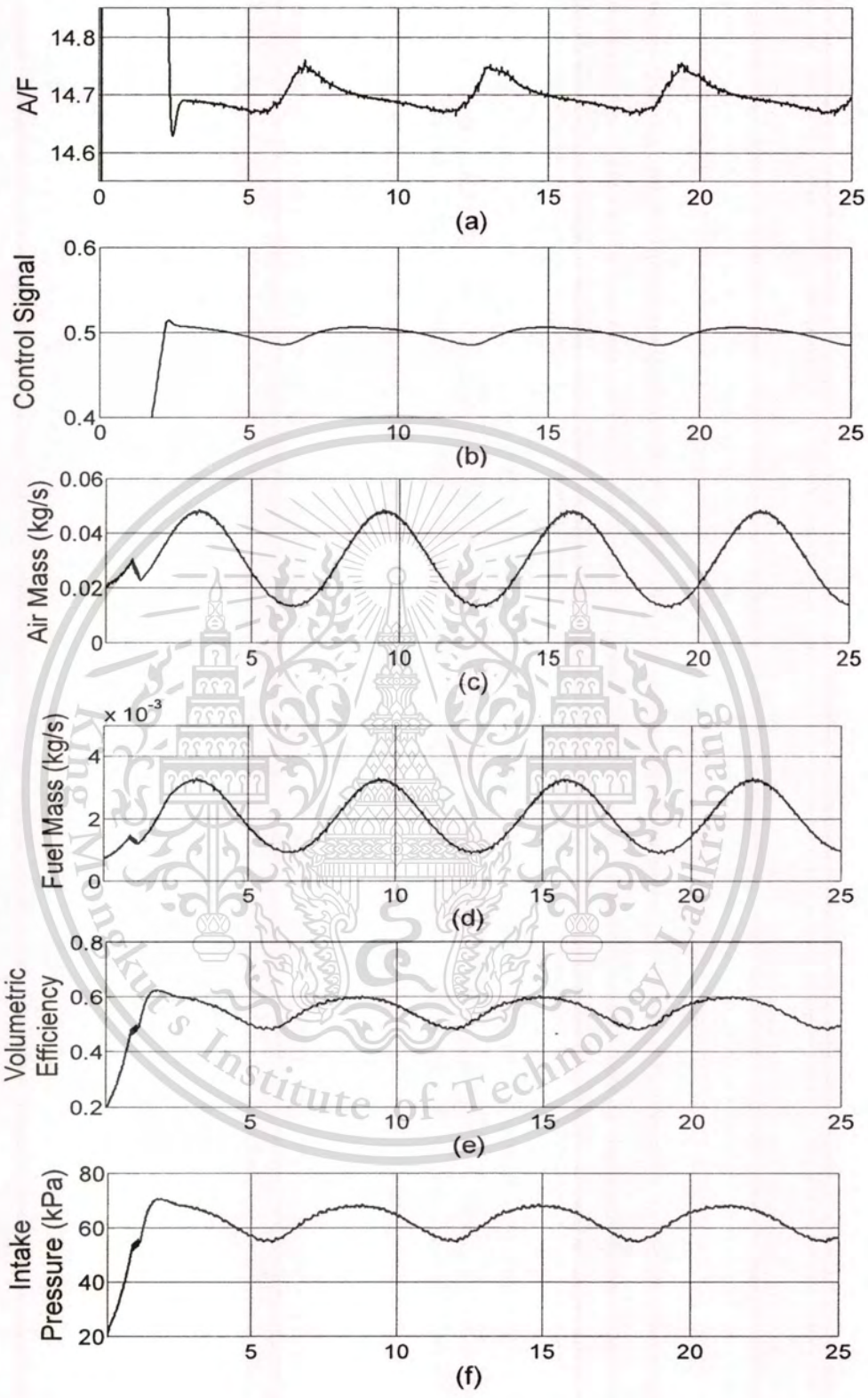


**Fig. 4.10** Engine operations with sine-step acceleration (Cont.)

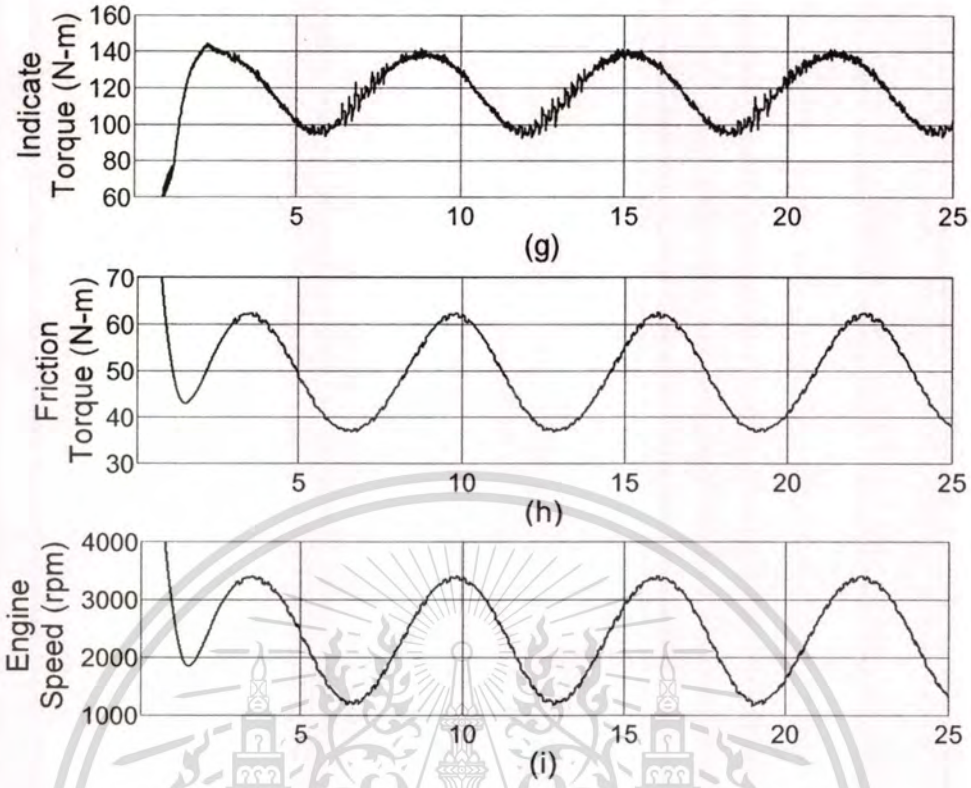


Fig. 4.10 Engine operations with sine-step acceleration

## 4.4 Summary

As the simulation, the results from control of spark ignition engine by using discrete fuzzy PI controller such as AFR, control signal of controller, air mass, fuel mass, volumetric efficiency, intake manifold pressure, indicated torque, friction torque and engine speed are graphically described. With, the results can reasonably guarantee the MVEM. In addition, the performance evaluation for AFR control is shown in Table 4.1. Obviously, the ITAE, ISE and IAE of the single-step are less than other because two short pulses have an overall shorter time duration and are acquired less control inputs; sine pulse change throttle position every time.

**Table 4.1** Various performance indices for evaluation of AFR control

| Accelaration | ITAE | ISE | IACO | IAE |
|---|---|---|---|---|
| Single step (30s) | 3.2598 | 0.008758 | 12.9753 | 0.2061 |
| Double step (17s) | 3.314 | 0.0207 | 6.4611 | 0.3113 |
| Sine step (25s) | 4.7219 | 0.00745 | 10.4449 | 0.3329 |

Next chapter is computer simulation of the electronic throttle control. The mathematical model of electronic throttle body as described in Chapter 2 is used and three controllers in Chapter 3 are applied to control the degree of throttle.

# Chapter 5
# Computer Simulation of Electronic Throttle Valve

## 5.1 Introduction

This chapter presents electronic throttle control by computer simulation. The ETV mathematical model that consists of dynamic parts is remarked. The discrete PID, discrete fuzzy PI and SMC-ERL schemes as described in Chapter 3 are employed to control the throttle degree. For robustness tests, the disturbance signal is added to disturb feedback position of the ETV.

In Section 5.2, Laplace transform of ETV is presented. With the SMC-ERL controller is designed explicitly as in Section 5.3. In Section 5.4, various parameters of ETV and the controllers are assigned. Two accelerations with disturbance are assigned as sine step and multi step. The simulation results, such as throttle degree response, error signal and current consumption, are presented. Section 5.5, average of performance indices using an integral of absolute current input ($IAC_i$) and other as in previous chapter are discussed.

## 5.2 Electronic Throttle Valve

Figure 5.1 is a Laplace form of ETV that includes a direct-current motor model, Dahl friction and spring load. The dc motor part is operated by sufficient voltage and current; in consequence, dynamic action of rotor is occurred based on direct variation with value of electric power. The dynamic action of a rotor is rotating action that generates speed and degree. Speed is an input for Dahl Friction model and degree is an input for the spring load model.

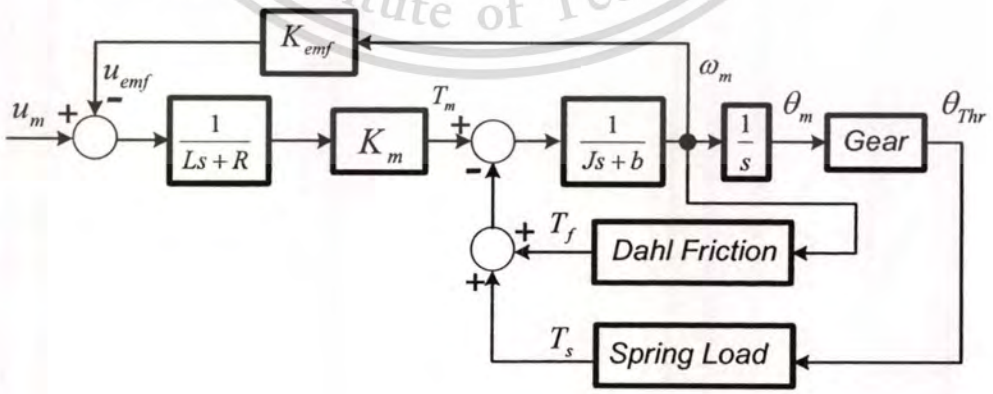


**Fig. 5.1** ETV diagram based on Laplace form

## 5.3 Electronic Throttle Control

The single input single output (SISO) feedback control strategy is utilized for simulation on MATLAB/SIMULINK. In Fig. 5.2, the controller block is the control algorithms mentioned in Chapter 3. There are PID algorithm, fuzzy PI algorithm and SMC-ERL algorithm to control the degree of ETV. For PID and fuzzy PI, the control schemes in Sections 3.2 and 3.3 are employed respectively, but the SMC-ERL is expanded of the design in Section 5.3.1.

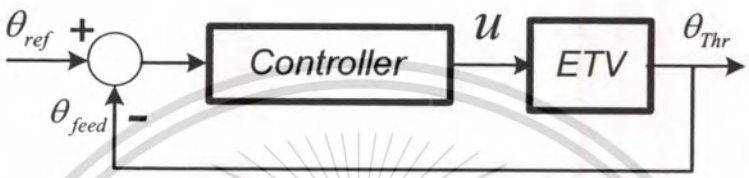


**Fig. 5.2** SISO feedback control strategy for ETV control

**5.3.1** Design of SMC-ERL controller with ETV

Let consider

$$J_m\ddot{\theta} = T_m - T_{sp} - T_f \tag{5.1}$$

$$T_m = K_m \cdot i_a \tag{5.2}$$

$$T_m = K_m \cdot (E_a - K_{emf} \cdot \omega_m) / R_a \tag{5.3}$$

, where the parameters are mentioned in Chapter 2. Let $K_{emf}$ be $K_m$,

$$T_m = (K_m \cdot E_a - K_m^2 \cdot \omega_m) / R_a \tag{5.4}$$

$$T_{sp} = K_t(\theta - \theta_0) + K_s \operatorname{sgn}(\theta - \theta_0) \tag{5.5}$$

, and let $T_f$ be Dahl friction model, then

$$J_m\ddot{\theta} = \{(K_m \cdot E_a - K_m^2 \cdot \omega_m) / R_a\} - \{K_t(\theta - \theta_0) + K_s \operatorname{sgn}(\theta - \theta_0)\} - T_f \tag{5.6}$$

$$s = \dot{e} + ce \tag{5.7}$$

$$e = \theta_{ref} - \theta_{feed} \tag{5.8}$$

$$\dot{e} = \dot{\theta}_{ref} - \dot{\theta}_{feed} \tag{5.9}$$

$$\dot{s} = (\ddot{\theta}_{ref} - \ddot{\theta}_{feed}) + c(\dot{\theta}_{ref} - \dot{\theta}_{feed}) \tag{5.10}$$

, and let $\ddot{\theta}_{feed}$ be $\ddot{\theta}$ from equation (5.6), then

$$\dot{s} = \ddot{\theta}_{ref} + c(\dot{\theta}_{ref} - \dot{\theta}_{feed}) - [\{(K_m \cdot E_a - K_m^2 \cdot \omega_m)/R_a\} - \{K_t(\theta - \theta_0) + K_s \operatorname{sgn}(\theta - \theta_0)\} - T_f]/J_m \quad (5.11)$$

For exponential reaching law, we have

$$\dot{s} = -h \cdot \operatorname{sgn}(s) - ks \quad (5.12)$$

, and then, we have the following equation:

$$-h \cdot \operatorname{sgn}(s) - ks = \ddot{\theta}_{ref} + c(\dot{\theta}_{ref} - \dot{\theta}_{feed}) - [\{(K_m \cdot E_a - K_m^2 \cdot \omega_m)/R_a\} - \{K_t(\theta - \theta_0) + K_s \operatorname{sgn}(\theta - \theta_0)\} - T_f]/J_m \quad (5.13)$$

$$-h \cdot \operatorname{sgn}(\dot{e} + ce) - k \cdot (\dot{e} + ce) = \ddot{\theta}_{ref} + c(\dot{\theta}_{ref} - \dot{\theta}_{feed}) - (K_m \cdot E_a - K_m^2 \cdot \omega_m)/R_a J_m [\{K_t(\theta - \theta_0) + K_s \operatorname{sgn}(\theta - \theta_0)\} + T_f]/J_m \quad (5.14)$$

$$-h \cdot \operatorname{sgn}(\dot{e} + ce) - k \cdot (\dot{e} + ce) = \ddot{\theta}_{ref} + c(\dot{\theta}_{ref} - \dot{\theta}_{feed}) - \frac{K_m E_a}{R_a J_m} + \frac{K_m^2 \cdot \omega_m}{R_a J_m} + \frac{K_t(\theta - \theta_0)}{J_m} + \frac{K_s \operatorname{sgn}(\theta - \theta_0)}{J_m} + \frac{T_f}{J_m} \quad (5.15)$$

$$\frac{K_m E_a}{R_a J_m} = h \cdot \operatorname{sgn}(\dot{e} + ce) + k \cdot (\dot{e} + ce) + \ddot{\theta}_{ref} + c(\dot{\theta}_{ref} - \dot{\theta}_{feed}) + \frac{K_m^2 \cdot \omega_m}{R_a J_m} + \frac{K_t(\theta - \theta_0)}{J_m} + \frac{K_s \operatorname{sgn}(\theta - \theta_0)}{J_m} + \frac{T_f}{J_m} \quad (5.16)$$

$$E_a = \frac{R_a J_m}{K_m} \cdot \left\{ h \cdot \operatorname{sgn}(\dot{e} + ce) + k \cdot (\dot{e} + ce) + \ddot{\theta}_{ref} + c(\dot{\theta}_{ref} - \dot{\theta}_{feed}) + \frac{K_m^2 \cdot \omega_m}{R_a J_m} + \frac{K_t(\theta - \theta_0)}{J_m} + \frac{K_s \operatorname{sgn}(\theta - \theta_0)}{J_m} + \frac{T_f}{J_m} \right\} \quad (5.17)$$

Finally we obtain

$$u_m = E_a \tag{5.18}$$

## 5.4 Computer Simulation

In this simulation, the ETV simulation model is detailed in Appendix B (B.6); the ETV parameters in electrical part and mechanical part are identified form Appendix C. Whole parameters are in Table 5.1. In control, the sampling time of the controller is 1 ms; the PID controller is set in accordance with several details as follow: the controller gains are: $K_p$ =12.0, $K_i$ =0.12, $K_d$ =120, $t_i$ =100 ms, $t_d$ =10 ms; the fuzzy PI controller with several details as follow: the controller gains are: $K_p$ =12, $K_i$ =0.06, $K_u$ =12 and $L$ =2000; the SMC-ERL controller with several details as follow: the controller gains are: $h$ =1, $k$ =300 and $c$ =100.

To evaluate the performance of controllers, an integral of absolute current output ($IAC_i$), an integral of absolute error (IAE) and an integral of square error (ISE) are defined. The throttle inputs, two accelerations with disturbance are assigned: sine step and multi step, as shown in Figs. 5.3 and 5.4.

**Table 5.1** ETV parameters

| Part | Value | Part | Value |
|---|---|---|---|
| L | 0.006 | $K_m$, $K_{emf}$ | 7.0 |
| R | 6 | Gear | 14/40 |
| J | 0.00245 | $K_t$ | 0.046 |
| B | 0.002 | $K_s$ | 5.2125 |

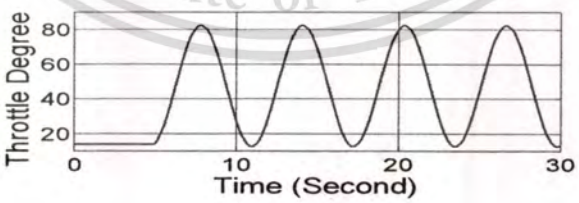


**Fig. 5.3** Sine-step acceleration

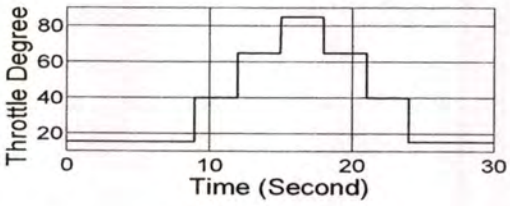


**Fig. 5.4** Multi-step acceleration

**5.4.1** The results corresponding to sine acceleration without disturbance

This subsection figures results of ETV control in details as degree response, error sinal and current consumtion. The details which are result from PID controller, fuzzy PI controller and SMC-ERL controller as illustrated in Figs. (a), (b) and (c) respectivly. Figure 5.5 shows the response of throttle degree between reference input and feedbak output. Hence, seen that time at 5 s, the responses have overshoot: 4 degrees for PID control as shown in Fig. 5.5(a) and 2 degrees for fuzzy PI control as shown in Fig. 5.5(b). Figure 5.6 more emphasizes on the responses by using error signal. With the Figure 5.6(b) reveals that fuzzy PI controller is greater control than other. In addition, fuzzy PI controller have smallest IAE value and ISE value that are signified in Table 5.2. Figure 5.7 shows that current consumptions are around 0 to 2 Amperes for driving the throttle valve.

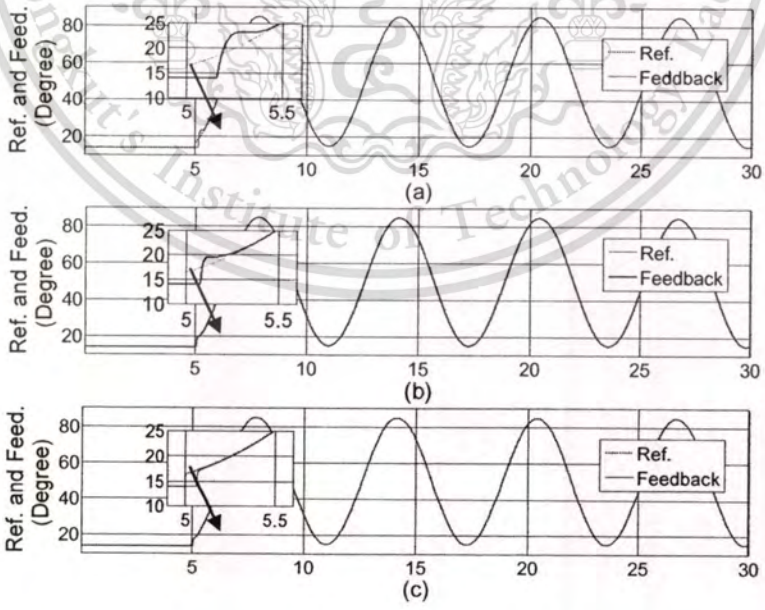


**Fig. 5.5** Responses of sine-step acceleration

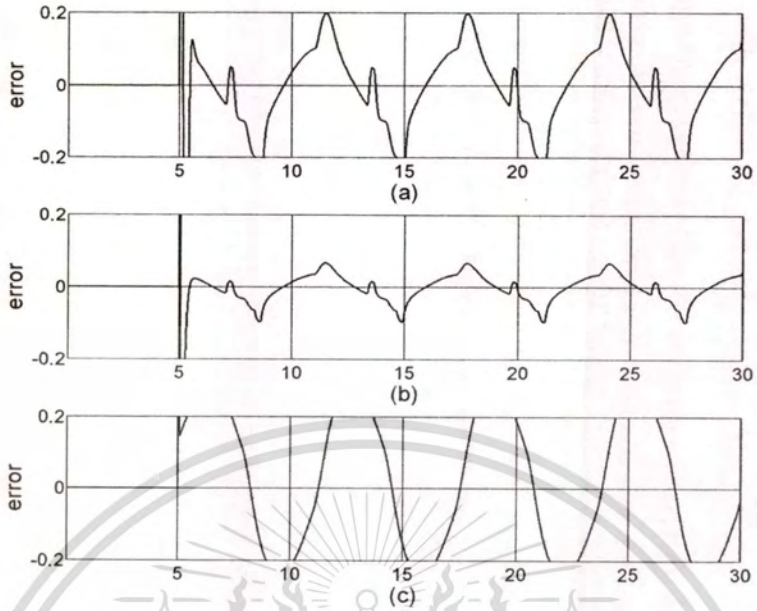


Fig. 5.6 Error signals of sine-step acceleration

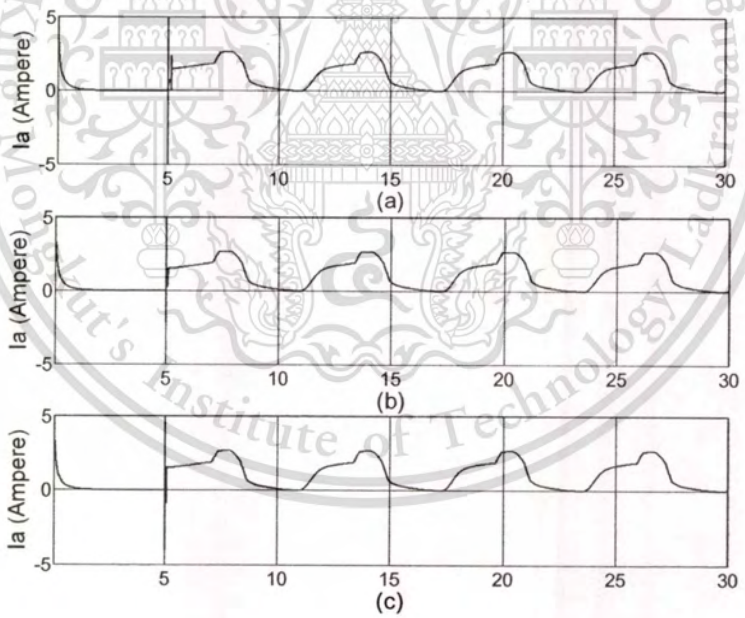


Fig. 5.7 Used currents of sine-step acceleration

**Table 5.2** Performance indices of controls corresponding to sine step

| Controller | $IAC_i$ (Ampere) | IAE (Degree) | ISE (Degree) |
|---|---|---|---|
| PID | 28.6962 | 3.1927 | 3.2388 |
| Fuzzy-PI | 28.6935 | 1.1412 | 0.9 |
| SMC-ERL | 28.5327 | 4.7611 | 1.4885 |

**5.4.2** The results corresponding to multi acceleration without disturbance

In this subsection, the acceleration input of ETV control is changed from sine step to multi step for control in transient situation. Figure 5.8 shows that every push on acceleration padle; the responses have 4 degrees overshoot and 0.35 s settling time for PID control as shown in Fig. 5.8(a), 3.3 degrees overshoot and 0.25 s settling time for fuzzy PI control as shown in Fig. 5.8(b), 0.03 s settling time for SMC-ERL control as shown in Fig. 5.8(c). Similarly, every withdraw acceleration padle, the responses have 2.5 degrees undershoot and 0.35 s settling time for PID control, 1.5 degrees undershoot and 0.2 s settling time for fuzzy PI control. Figure 5.9 reveals that error signals are generated belong transient inputs. For the PID control and fuuzzy PI control, error signals are keeped to zero after transient action. But, error signals of SMC-ERL control are not closed to zero. Current consumptions are around 0.2 to 2.5 Amperes as shown in Fig. 5.10.

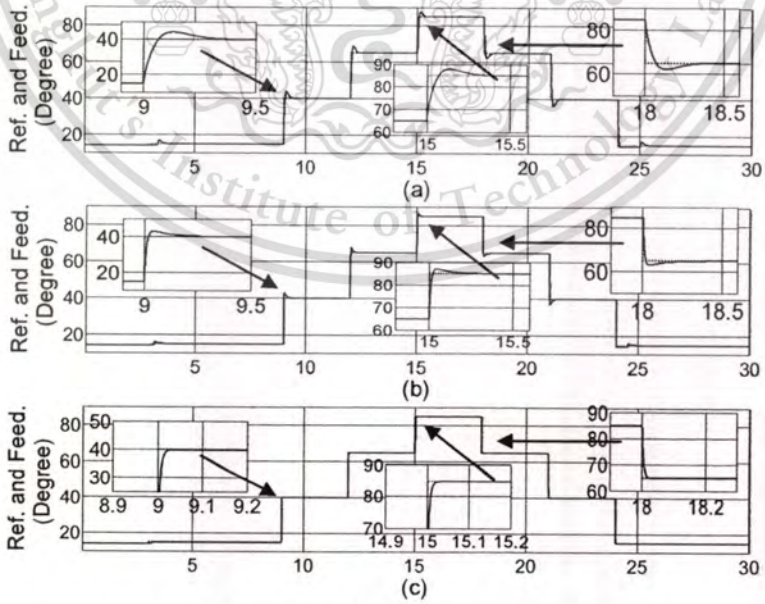


**Fig. 5.8** Responses of multi-step acceleration

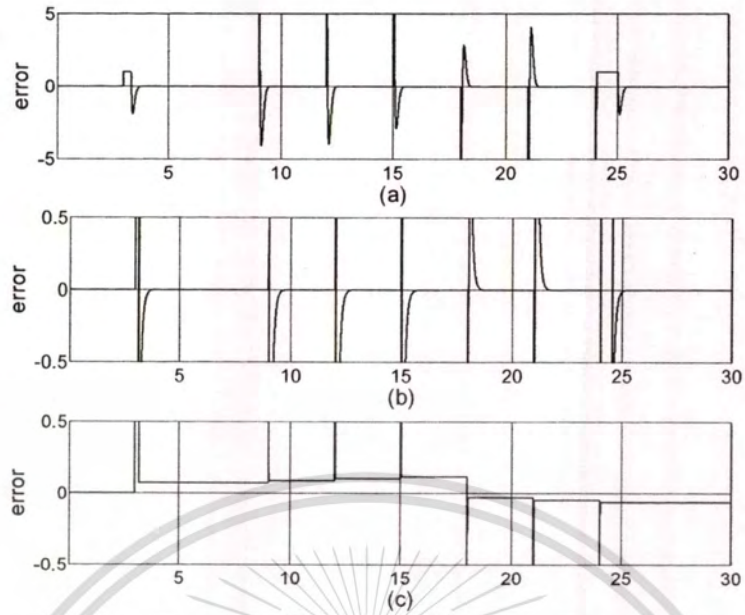


Fig. 5.9 Error signals of multi-step acceleration

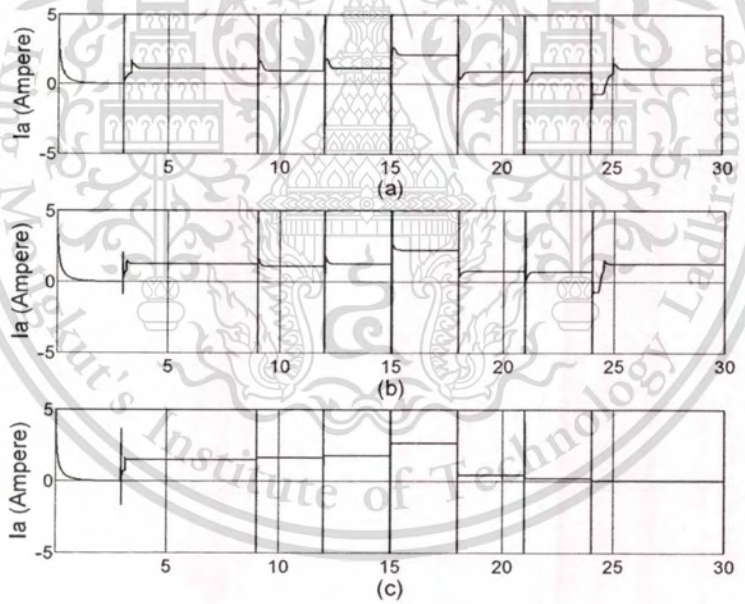


**Fig. 5.10** Used currents of multi-step acceleration

**Table 5.3** Performance indices of controls corresponding to multi step

| Controller | $IAC_i$ (Ampere) | IAE (Degree) | ISE (Degree) |
|---|---|---|---|
| PID | 30.5044 | 7.6367 | 56.5113 |
| Fuzzy-PI | 31.1482 | 3.303 | 18.4007 |
| SMC-ERL | 27.2649 | 2.6482 | 10.7836 |

**5.4.3** The results corresponding to sine acceleration with disturbance

When the distubance is added to feedback signal, fluctuation behavior of responces is appeared as illustrated in Figs 5.11-5.13. Figure 5.12 shows that the average of error signals are about 1.5 degrees. From Fig.5.13, average of current consumption can be calculated as follow: 8 Amperes for PID control, 2 Amperes for fuzzy PI control and 2.5 Amperes for SMC-ERL control. Therefore, a smallest current consumption $IAC_i$, the performance comparison is shown in Table 5.4.

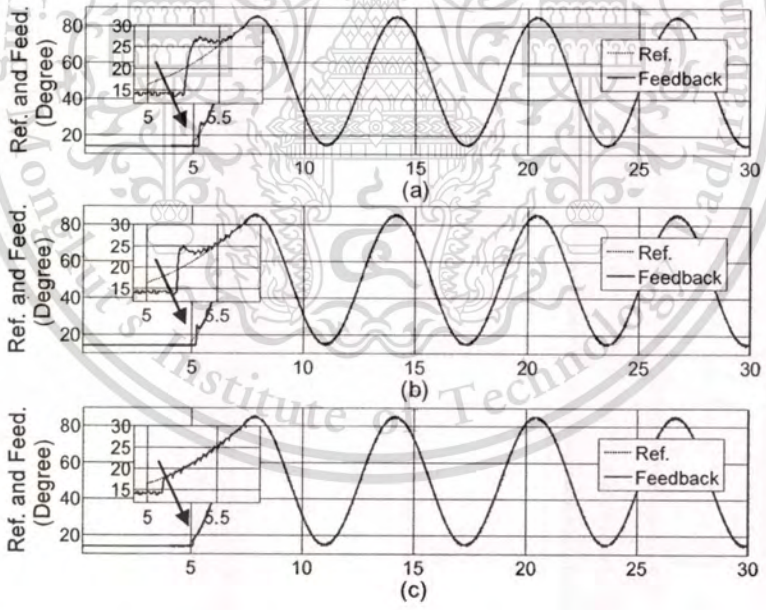


**Fig. 5.11** Responses of sine-step acceleration with disturbance

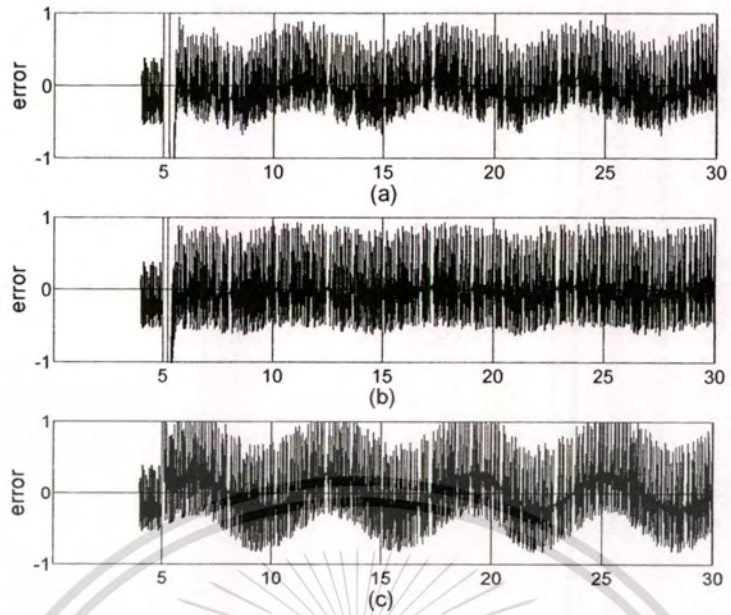


Fig. 5.12 Error signals of sine-step acceleration with disturbance

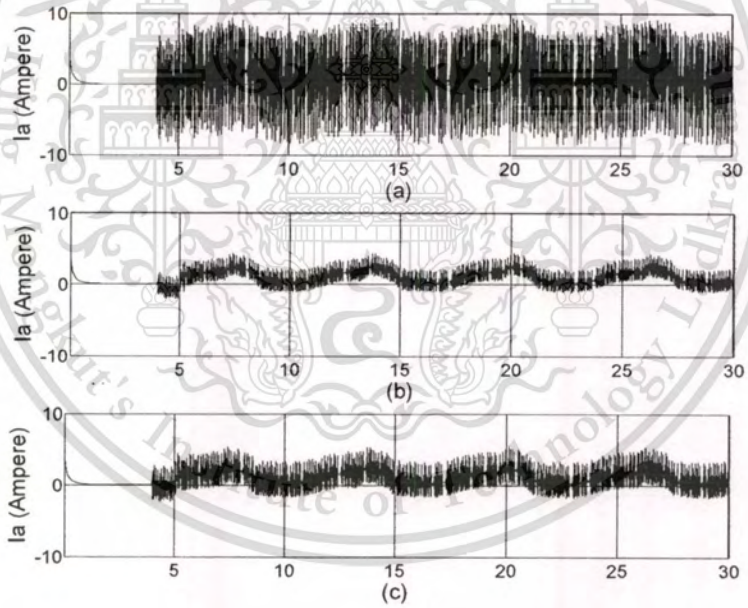


**Fig. 5.13** Used currents of sine-step acceleration with disturbance

**Table 5.4** Performance indices of controls corresponding to sine step with disturbance

| Controller | $IAC_i$ (Ampere) | IAE (Degree) | ISE (Degree) |
|---|---|---|---|
| PID | 42.5278 | 6.7639 | 8.7461 |
| Fuzzy-PI | 29.0532 | 6.083 | 6.3253 |
| SMC-ERL | 29.5156 | 5.8297 | 2.8839 |

**5.4.4** The results corresponding to multi acceleration with disturbance

This subsection is the last simulation of ETV control that tests about transient situations with feed back distubance. Figure 5.14 shows that every push on acceleration padle; the responses have 5 degrees overshoot and 0.4 s settling time for PID control as shown in Fig. 5.14(a), 3.5 degrees overshoot and 0.25 s settling time for fuzzy PI control as shown in Fig. 5.14(b), 0.03 s settling time for SMC-ERL control as shown in Fig. 5.14(c). Similarly, every withdraw acceleration padle, the responses have 2.5 degrees undershoot and 0.4 s settling time for PID control, 2.0 degrees undershoot and 0.1 s settling time for fuzzy PI control. From Fig.5.16, it can be claculated average of current consumption as follow: 8 Amperes for PID control, 3 Amperes for fuzzy PI control and 4 Amperes for SMC-ERL control.

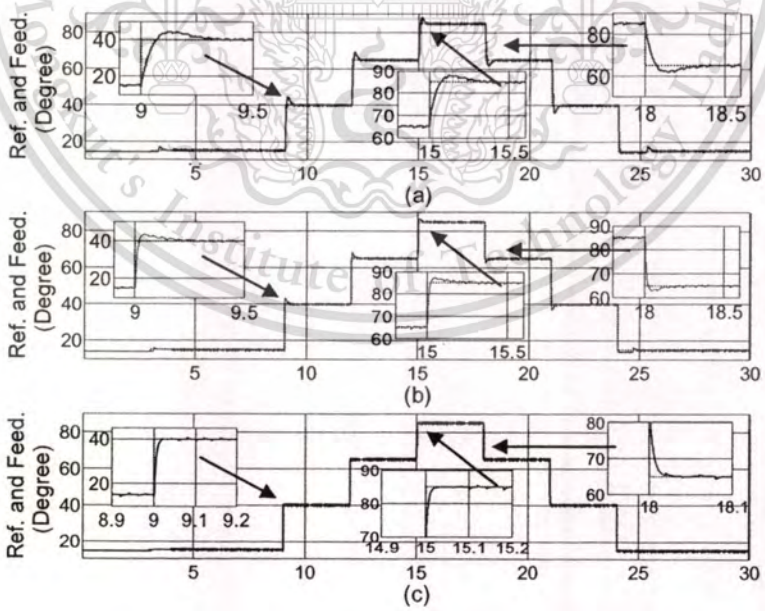


**Fig. 5.14** Responses of multi-step acceleration with disturbance

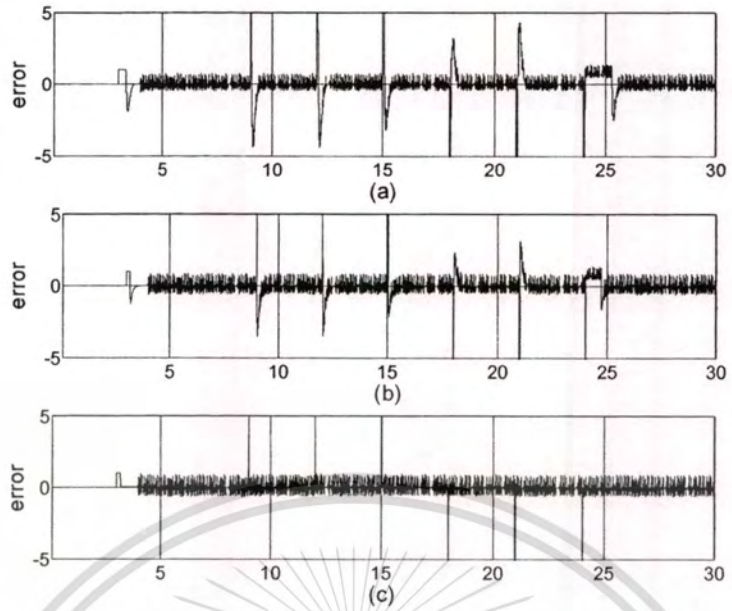


Fig. 5.15 Error signals of multi-step acceleration with disturbance

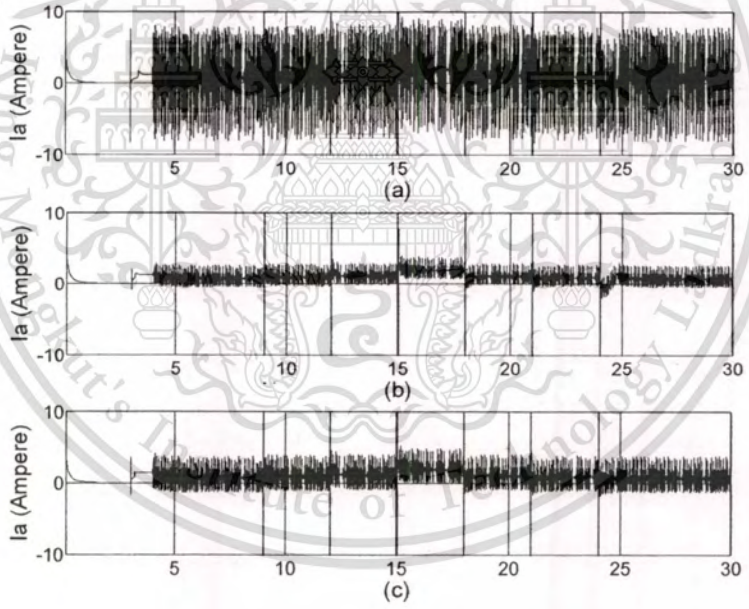


Fig. 5.16 Used currents of multi-step acceleration with disturbance

**Table 5.5** Performance indices of controls corresponding to multi step with disturbance

| Controller | $IAC_i$ (Ampere) | IAE (Degree) | ISE (Degree) |
|---|---|---|---|
| PID | 41.4854 | 11.8789 | 58.6436 |
| Fuzzy-PI | 26.2208 | 7.6766 | 20.3925 |
| SMC-ERL | 27.3334 | 4.0173 | 11.9202 |

## 5.5 Summary

The mathematical model of electronic throttle valve is described in Laplace transform. The model consists of DC motor, small friction (Dahl friction model) as well as biggest load torque (return spring torque). The MATLAB/SIMULINK is utilized for simulation. There are PID strategy, fuzzy PI strategy and SMC-ERL strategy to control the degrees of throttle plate. The throttle inputs with disturbance are assigned as single sine step and multi step. With the simulation, the several results from control such as throttle degree response, error signal and current consumption are graphically described. In addition, the performance indices are $IAC_i$, IAE and ISE for estimation of control parameters. As the Table 5.6 is average of performance indices for three controllers. The table shows that the SMC-ERL controller is the most effective.

**Table 5.6** Average performance indices of control in simulation

| Controller | $IAC_i$ (Ampere) | IAE (Degree) | ISE (Degree) |
|---|---|---|---|
| PID | 35.8034 | 7.368 | 31.7849 |
| Fuzzy-PI | 28.7789 | 4.551 | 11.5048 |
| SMC-ERL | **28.1617** | **4.3141** | **6.7691** |

Next chapter is experiment of the electronic throttle control by using PID, PID with anti-windup, fuzzy PI, fuzzy PI with anti-windup, SMC-ERL strategies. The knowledge in this chapter about control parameter tuning will be used in next chapter.

# Chapter 6
# Experiment of Electronic Throttle Valve

## 6.1 Introduction

From mathematical model, computer simulation, controller design and parameter tuning knowledge of electronic throttle valve as described in previous chapter, this chapter presents ETV control on experiment.

In Section 6.2, details about an electronic control scheme, a single-phase driver circuit and controller parameters are remarked. Section 6.3 shows experiment results from PID control, PID with anti-windup control, fuzzy PI with anti-windup control and SMC-ERL control; moreover, experiment results from PI control, PD control and PD+I control are also explained in appendix D. Section 6.4, performance indices by using a maximum of overshoot degree, a maximum of settling time and other as in previous chapter are also discussed.

## 6.2 Hardware Setup

The electronic throttle control system is organized and designed based on SISO feedback control strategy as shown in Fig. 6.1. For the apparatus of this experiment, it is clearly shown in Fig. 6.3. As the controller part, we have used a dsPic30f2010 microcontroller to generate a Pulse-Width-Modulation (PWM) control signal in 200 Hz for TLP250 isolator, and the controller has been embedded four control algorithm: PID, PID-AW, fuzzy PI-AW and SMC-ERL. The TLP250 isolator amplifies the PWM control signal from 5 to 12 V to activate a chopper driver that is an IRF840 MOSFET for high-current motor driving. The chopper driver is based on a single phase which can source high current of 8 Amperes as presented in Fig. 6.2. The ETV is of HITACHI SERA576-01 model as referred to Appendix C. For an actual position feedback of throttle plate, a potentiometer placed inside the ETV is used and NI analog to digital module is also used for data acquisition based on 0.0391 sample time. There are two electrical supplies: a main supply of 12 V for all parts and a controller supply of 5 V.

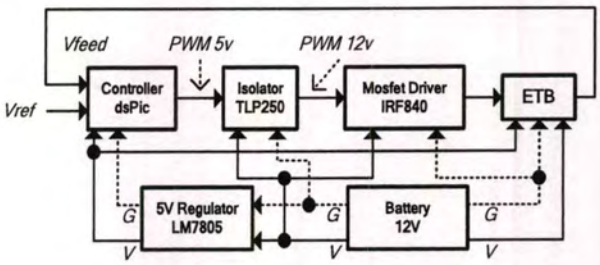


**Fig. 6.1** An electronic throttle control scheme

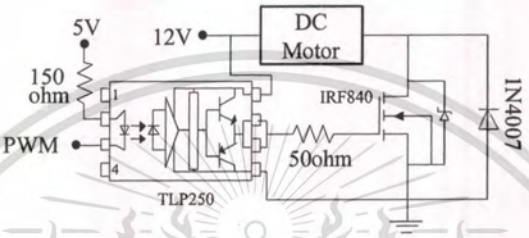


**Fig. 6.2** A single phase chopper driver

**Fig. 6.3** Apparatus of electronic throttle control

According to, the sampling time of all controllers are 1 ms; the PID controller is set in accordance with several details as follow: the controller gains are: $K_p$ =9.0, $K_i$ =0.045, $K_d$ =9.0; the PID-AW controller with the controller gains are: $K_p$ =9.0, $K_i$ =0.045, $K_d$ =9.0 and $K_w$ =0.8; the fuzzy PI-AW controller with the controller gains are: $K_p$ =20, $K_i$ =0.043, $K_u$ =3.0 and $L$ =250, $K_w$ =1.05; the SMC-ERL controller with the controller gains are: $h$ =1, $k$ =150 and $c$ =20. For throttle inputs, three types are employed: single-ramp step, sine step and multi-step accelerations. They are illustrated in Fig. 6.4.

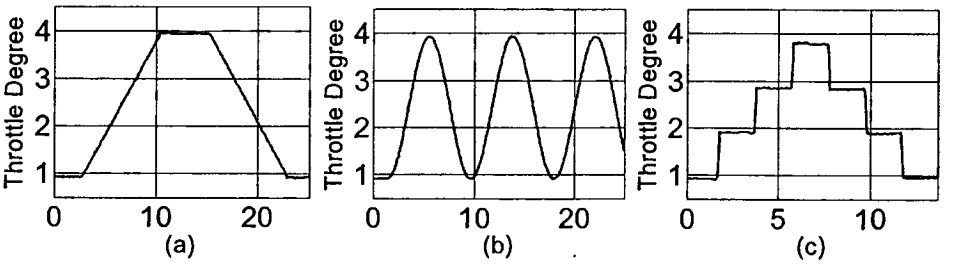


**Fig. 6.4** The throttle inputs for experimentation

## 6.3 Control Results

This section presents results of ETV control in detail as degree response. With the result, y-axis is a throttle degree in voltage level. The relationship between throttle degree and voltage level is 0 to 90 degrees equal 0 to 4.3 V. X-axis is operation time.

### 6.3.1 Proportional-Integral-Derivative (PID) strategy

In this subsection, the discrete PID controller is implemented. Figures 6.5 and 6.6 are tracking responses but Figure 6.7 is transient response. Figure 6.5 reveals that the response of step up is greater than step down, and the reponse is closed to referent input during 10 s to 15 s. Figure 6.6 reveals that the response can be tracked with referrence intput but it has offset state at both maximum and minimun of reference input. For transient response, Figure 6.6 presents that every step up of referenc input; the responses have 6.4 degrees overshoot and 0.5 s settling time. Similarly, every step down, the responses have 8.3 degrees undershoot and 0.5 s settling time.

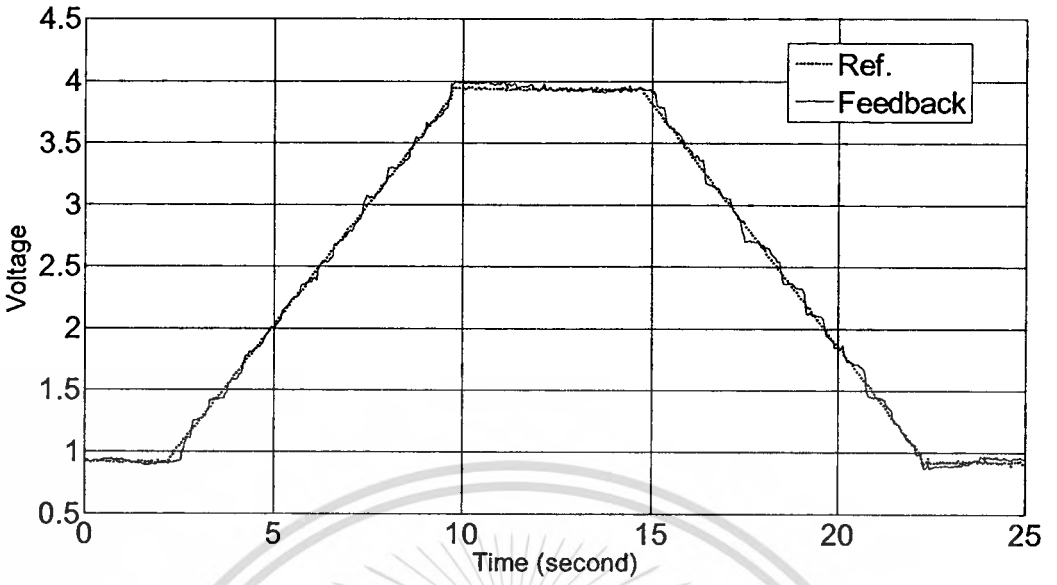


Fig. 6.5 Ramp-step response of PID controller

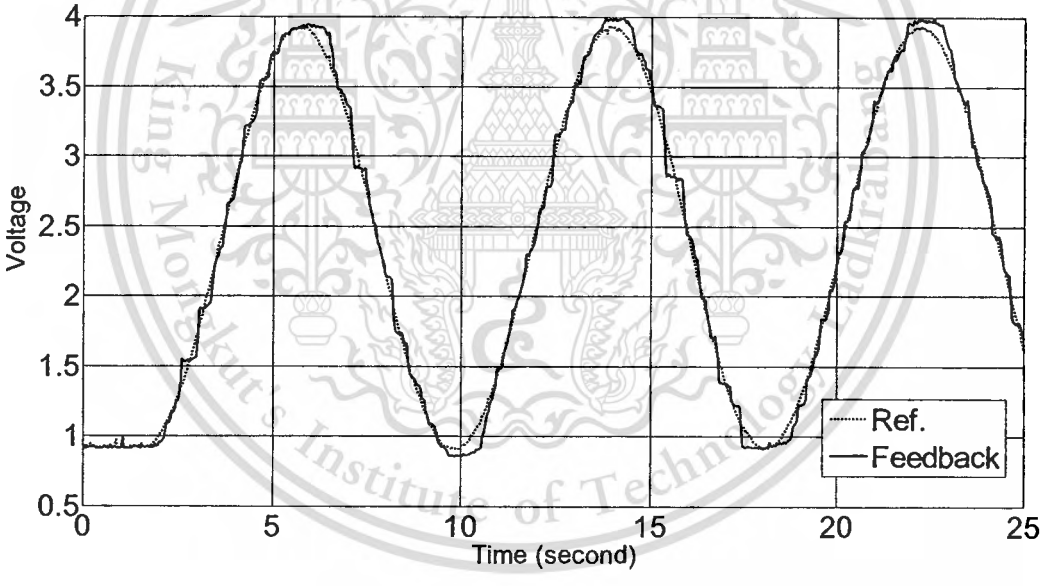


Fig. 6.6 Sine-step response of PID controller

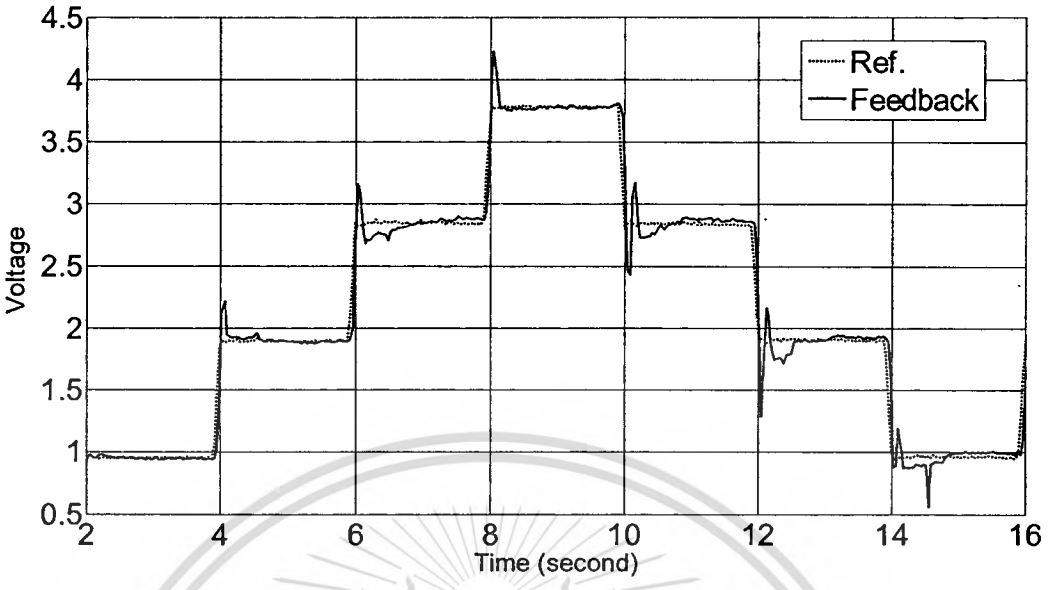


**Fig. 6.7** Multi-step response of PID controller

6.3.2 Proportional-Integral-Derivative with anti-windup strategy

This subsection presents the discrete PID controller in previous operate with an anti-windup module, its shcematic is depicted in below.

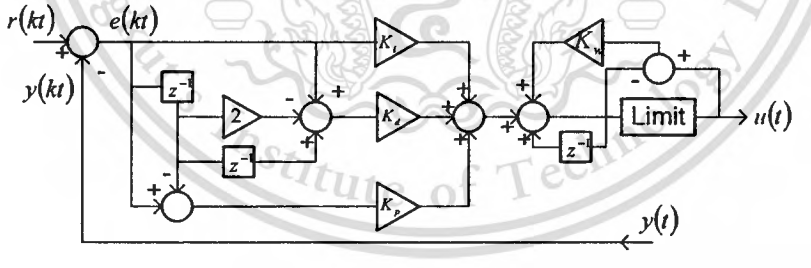


**Fig. 6.8** The discrete PID control with anti-windup scheme

Figures 6.9 and 6.10 are tracking response that can be tracked with referrence intput but offset states are occurred at both maximum and minimun of reference input as Fig. 6.10. For transient response, Figure 6.11 presents that every step up of referenc input and the responses have no overshoot and 0.5 s settling time. Similarly, every step down, the responses have no degrees undershoot and 0.5 s settling time. Therefore, the added anti-windup can decrease overshoots and undershoots effectively.

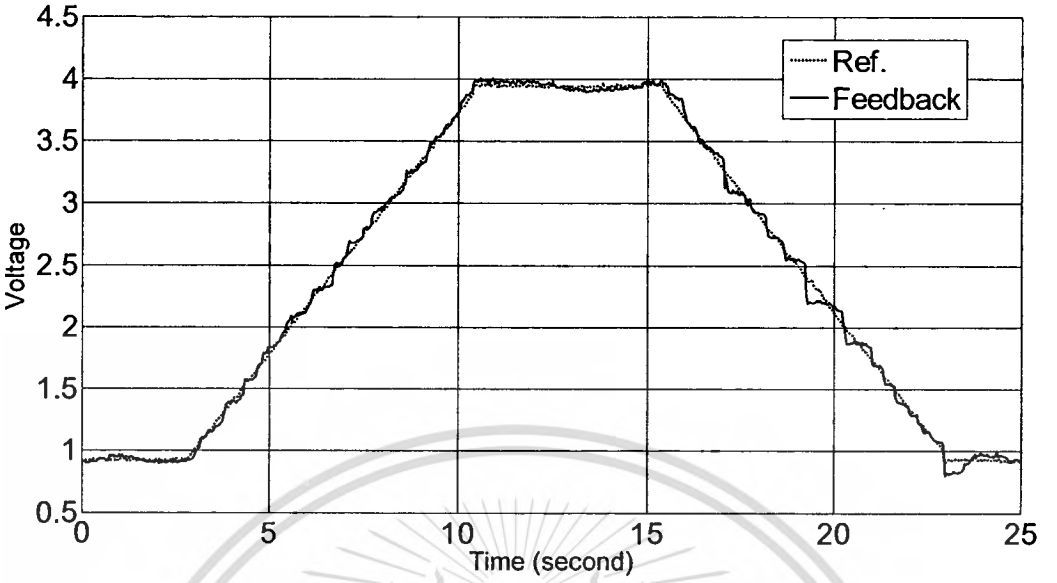


Fig. 6.9 Ramp-step response of PID-AW controller

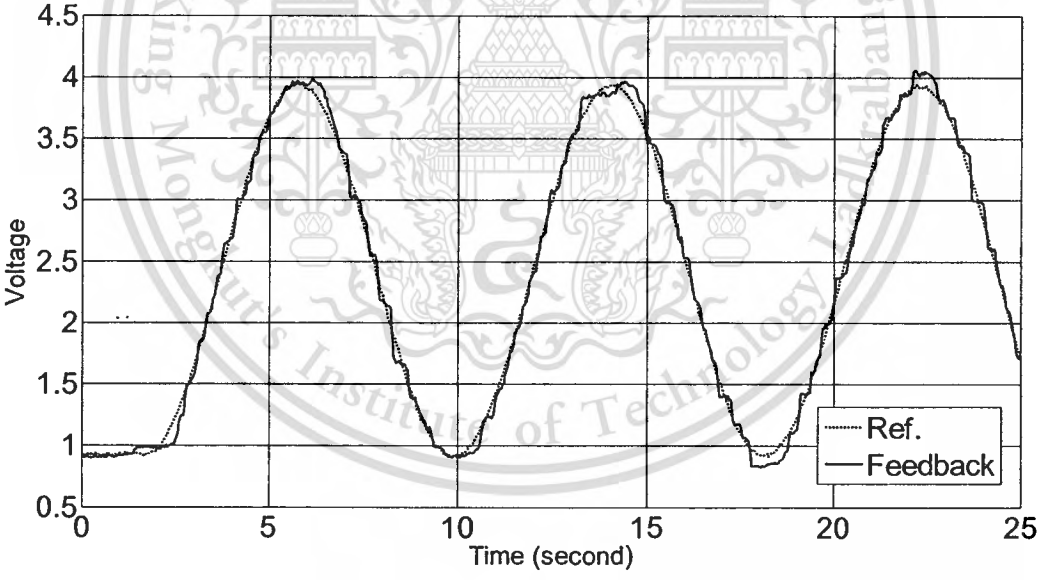


**Fig. 6.10** Sine-step response of PID-AW controller

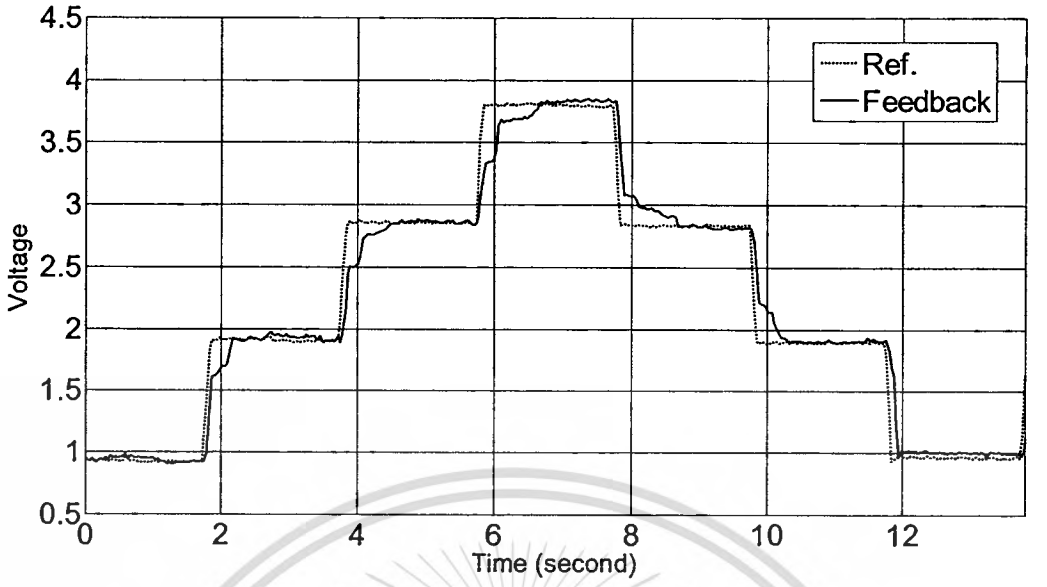


**Fig. 6.11** Multi-step response of PID-AW controller

6.3.3 Fuzzy-PI with anti-windup strategy

In this subsection, the discrete fuzzy PI controller as in Chapter 3 with the anti-windup as in Subsection 6.3.2 is implemented. For the resultes of tracking responce is illustrated in Figs 6.12-6.13, there are effective alike with both previous controllers. But, transient responses about setteling time, the discrete fuzzy PI controller outperforms effectively than those counterparts as shown in Fig. 6.14.

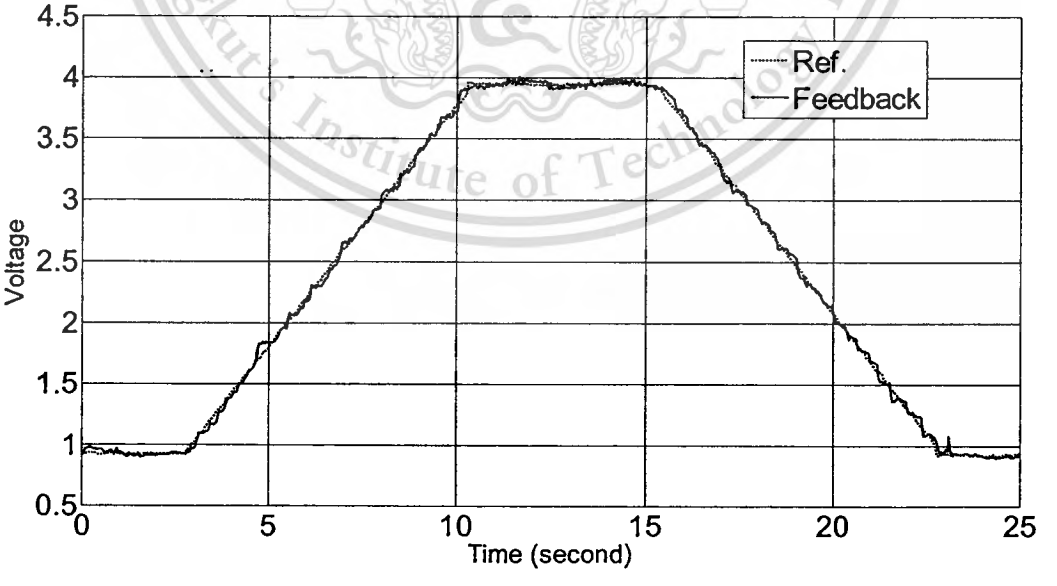


**Fig. 6.12** Ramp-step response of fuzzy PI-AW controller

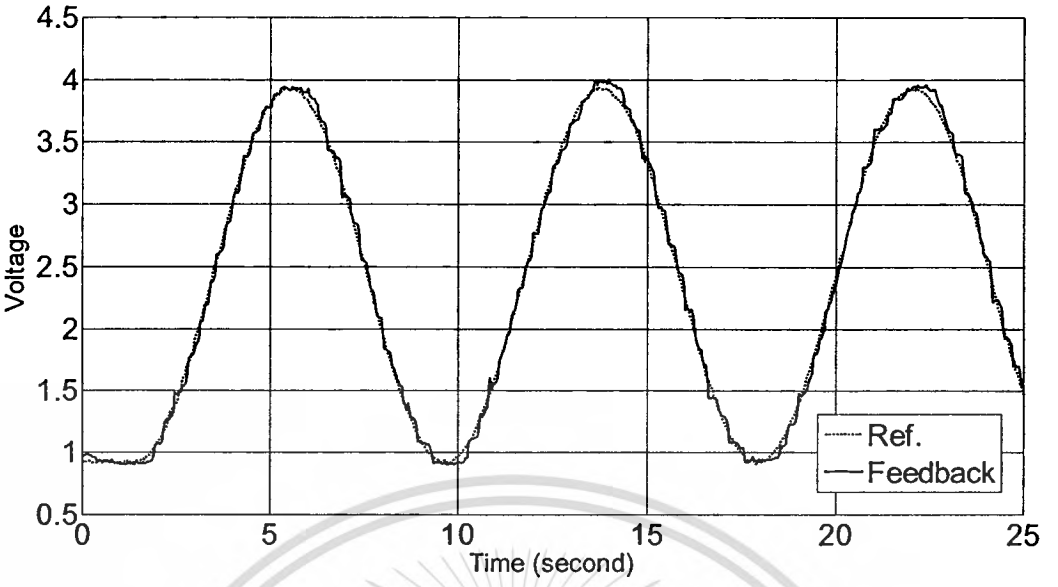


Fig. 6.13 Sine-step response of fuzzy PI-AW controller

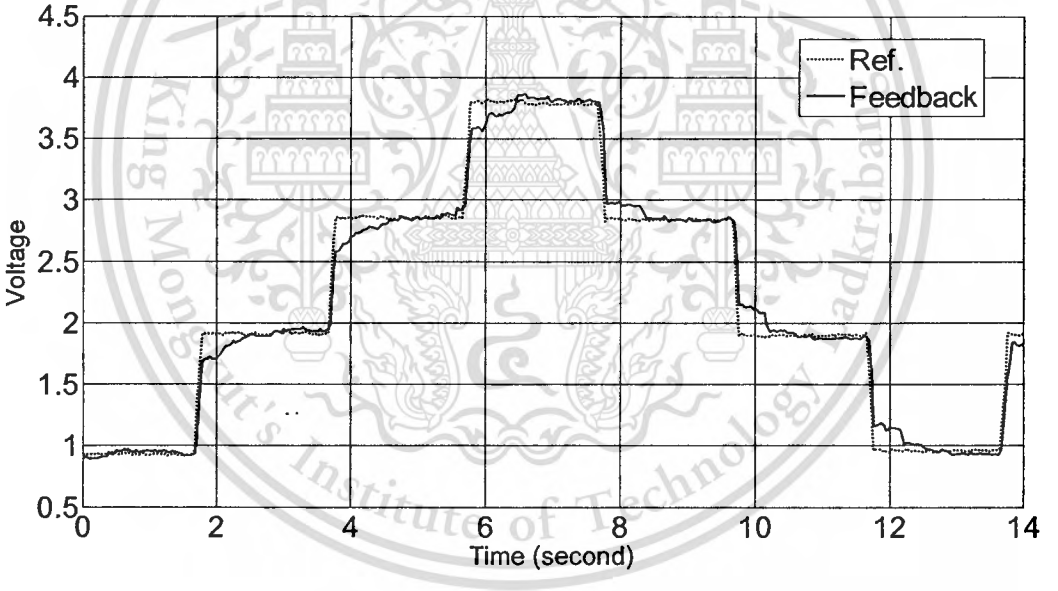


Fig. 6.14 Multi-step response of fuzzy PI-AW controller

**6.3.4** Sliding Mode Control using Exponential Reaching Law

This is a final subsection, the SMC-ELR controller is implemented. With the whole results of responses, offet states are occurred. There are 5.2 degrees for ramp step up, 5.0 degrees for ramp step down, 5.3 degrees for sine step up, 4.3 degrees for sine step down, 2.0 degrees for multi step up and 2.5 degrees for multi step down. Figure 6.17 presents that overshoot is 4.18 degrees and undershoot is 10.4 degrees.

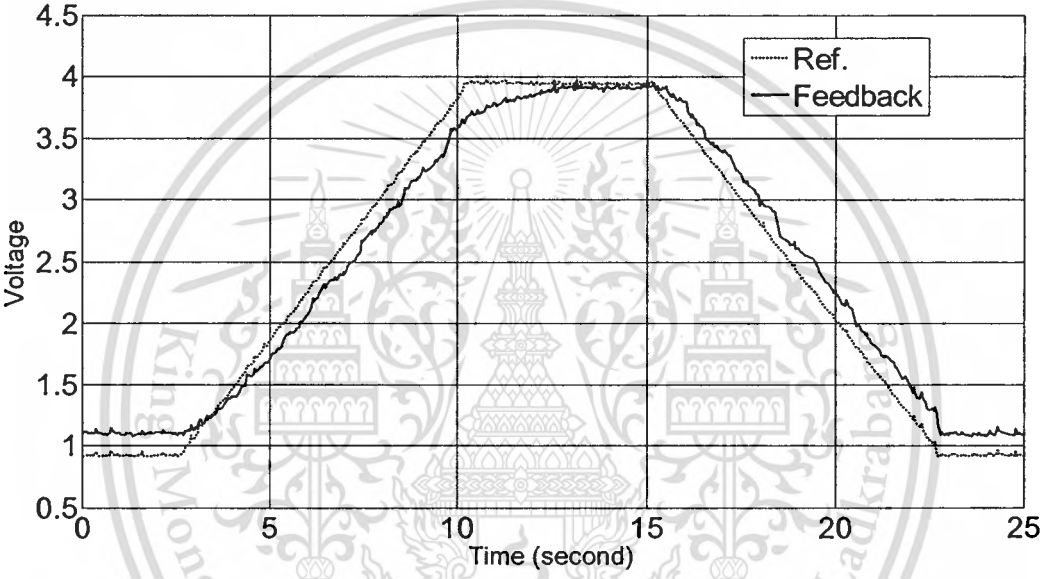


**Fig. 6.15** Ramp-step response of SMC-ERL controller

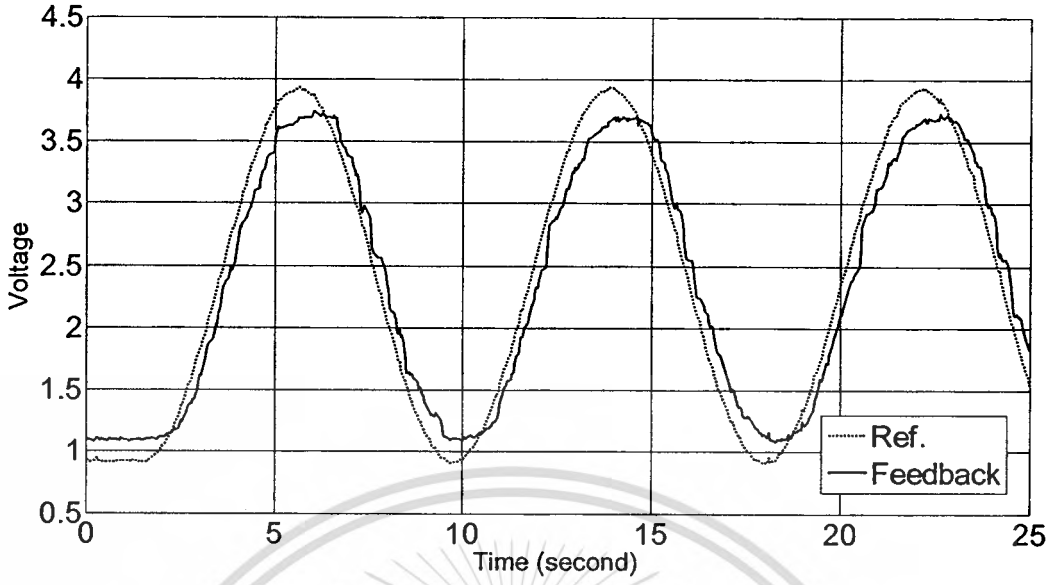


**Fig. 6.16** Sine-step response of SMC-ERL controller

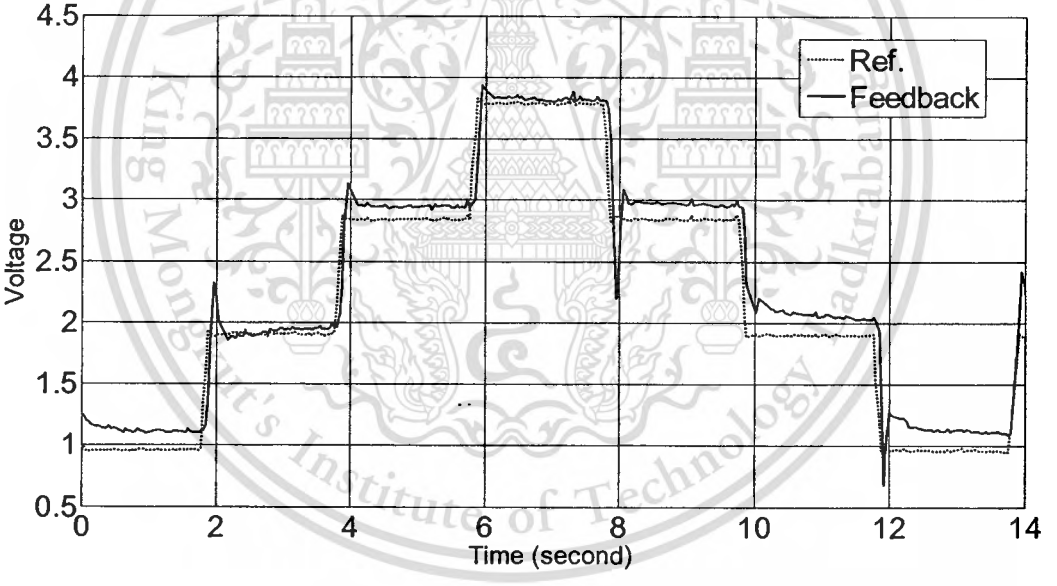


**Fig. 6.17** Multi-step response of SMC-ERL controller

## 6.4 Summary

This chapter presents the electronic throttle control in experiment that utilizes four control algorithms namely PID, PID-AW, fuzzy PI-AW and SMC-ERL. They are implemented into a 16-bits microcontroller. The performances of each controller are indicated in Table 6.1. In comparison FPI-AW controller is the best one. For average performance indices of controls in experiment, the readers are referred to Appendix G.

**Table 6.1** Performance indices of controls in experiment

| Acceleration | Controller | IAE (Degree) | ISE (Degree) | OV Max (Degree) | Settling Time Max (Second) |
|---|---|---|---|---|---|
| Ramp step | PID | 0.7741 | 0.0369 | 0 | - |
| | PID-AW | 0.895 | 0.0524 | 0 | - |
| | FPI-AW | **0.6989** | **0.0299** | 0 | - |
| | SMC-ERL | 3.7808 | 0.7261 | 0 | Off set |
| Sine step | PID | 1.3518 | 0.1199 | 0 | - |
| | PID-AW | 1.4311 | 0.1261 | 0 | - |
| | FPI-AW | **1.1468** | **0.0757** | 0 | - |
| | SMC-ERL | 4.7607 | 1.1461 | 0 | Off set |
| Multi step | PID | 0.8931 | 0.2215 | 0.6318 | 0.93 |
| | PID-AW | 1.1291 | 0.3221 | 0 | **0.81** |
| | FPI-AW | **0.9533** | **0.1529** | 0 | 0.72 |
| | SMC-ERL | 1.809 | 0.441 | 0.6671 | Off set |

# Chapter 7
# Conclusions

This research deals with computer simulation and experiment of car engine and air to fuel ratio regulator. The car engine is such a spark ignition engine that describes as a mean value engine model. The air to fuel ratio regulator is based on control algorithm for example a discrete fuzzy PI controller. With the car engine model, a dynamic discharge coefficient and chaotic disturbance signal are proposed. The includes control of spark ignition engine such as air to fuel ratio, control signal of controller, air mass, fuel mass, volumetric efficiency, intake manifold pressure, indicated torque, friction torque and engine speed. The proposed discrete fuzzy PI controller can guarantee the spark ignition model and stoichiometric ratio. According to the experiment as shown by average performance indices, the FPI-AW outperforms the others control schemes.

# References


[1] C. F. Chang, N. P. Fekete, A. Amstutz and J. D. Powell, "Air-Fuel Ratio Control Spark-Ignition Engines Using Estimation Theory," IEEE Transactions on Control Systems Technology, Vol. 3, No.1, MAR 1995, pp. 22-30.

[2] J. D. Powell, N. P. Fekete and C. F. Chang, "Observer-Based Air-Fuel Ratio Control," IEEE Control System Magazine, 1998, pp. 83.

[3] M. A. Franchek, J. Mohrfeld and A. Osburn, "Transient Fueling Controller Identification for Spark Ignition Engines," ASME Journal of Dynamic System Measurement and Control, Vol.128, No. 3, SEP 2006, pp. 499-509.

[4] A. W. Osburn and M. A. Franchek, "Transient Air/Fuel Ratio Controller Identification Using Repetitive Control," ASME Journal of Dynamic System Measurement and Control, Vol.126, No. 4, DEC 2004, pp. 781-789.

[5] A. D. Gaeta, U. Montanaro and V. Giglio, "Model-Based Control of the Air Fuel Ratio for Gasoline Direct Injection Engines via Advanced Co-Simulation: An Approach to Reduce the Development Cycle of Engine Control Systems," ASME Journal of Dynamic System Measurement and Control, Vol. 133, No. 6, NOV 2011, pp. 1-17.

[6] J. R. Wagner, D. M. Dawson, and L. Zeyu, "Nonlinear Air-to-Fuel Ratio and Engine Speed Control for Hybird Vehicles," IEEE Transactions on Vehicular Technology, Vol. 52, No.1, JAN 2003, pp. 184-195.

[7] S. B. Choi and J. K. Hendrick, "An Observer-Based Controller Design Method for Improving Air/Fuel Characteristics of Spark Ignition Engines," IEEE Transactions on Control Systems Technology, Vol. 6, No. 3, MAY 1998, pp. 325-334.

[8] S. W. Wang and D. L. Yu, "A New Development of Internal Combustion Engine Air-Fuel Ratio Control with Second-Order Sliding Mode," ASME Journal of Dynamic System Measurement and Control, Vol. 129, No. 6, NOV 2007, pp. 757-766.

[9] S. W. Wang, D. L. Yu, J. B. Gomm, G. F. Page and S. S. Douglas, "Adaptive Neural Network Model Based Predictive Control for Air-Fuel Ratio of SI Engines," Engineering Applications of Artificial Intelligence, Vol. 19, No. 2, 2006, pp. 189-200.

[10] S. W. Wang and D. L Yu, "Adaptive RBF Network for Parameter Estimation and Stable Air-Fuel Ratio Control," Neural Network, Vol. 21, No. 1, 2008, pp. 102-112.

[11] J. Deur, D. Pavkovic, N. Peric, M. Jansz and D. Hrovat, "An Electronic Throttle Control Strategy Including Compensation of Friction and Limp-Home Effects," IEEE Transactions on Industry Applications, Vol. 40, No. 3, May/Jun 2004, pp. 821-834.

[12] D. Pavkovic, J. Deur, M. Jansz and N. Peric, "Adaptive Control of Automotive Electronic Throttle," Control Engineering Practice, Vol. 14, 2006, pp. 121-136.

[13] P. Mercorlli, "Robust Feedback Linearization using An Adaptive PD Regulator for A Sensorless Control of A Throttle Valve," Mechatronics, Vol. 19, 2009, pp. 1334-1345.

[14] R. Grepl, and B. Lee, "Modeling Parameter Estimation and Nonlinear Control of Automotive Electronic Throttle using A Rapid-Control Prototyping Techique," International Journal of Automotive Technology, Vol. 11, No. 4, 2010, pp. 601-610.

[15] M. Corno, M. Tanelli, S. M. Savaresi, and L. Fabbri, "Design and Validation of A Gain-Scheduled Controller for the Electronic Throttle Body in Ride-by-Wire Racing Motorcycles," IEEE Transactions on Control Systems Technology , Vol. 19, No. 1, JAN. 2011, pp. 18-30.

[16] M. Baric, I. Petrovic, and N. Peric, "Neural Network-Based Sliding Mode Control of Electronic Throttle," Engineering Applications of Artificial Intelligence, Vol. 18, 2005, pp. 951-961.

[17] M. Reichhartinger, and M. Horn, "Application of Higher Order Sliding-Mode Concepts to A Throttle Actuator for Gasoline Engines," IEEE Transactions on Industrial Electronics, Vol. 56, No. 9, SEP. 2009, pp. 3322-3329.

[18] Y. Pan, U. Ozguner and O. H. Dagci, "Variable-Structure Control of Electronic Throttle Valve," IEEE Transactions on Industrial Electronics, Vol. 55, No. 11, NOV. 2008, pp. 3899-3907.

[19] Y. Xiaofang, W. Yaonan, S. Wei and W. Lianghong, "RBF Networks-Based Adaptive Inverse Model Control System for Electronic Throttle," IEEE Transactions on Control Systems Technology , Vol. 18, No. 3, MAY. 2010, pp. 750-756.

[20] X. Yuan, Y. Wang, L. Wu, X. Zhang, and W. Sun, "Neural Network Based Self-Learning Control Strategy for Electronic Throttle Valve," IEEE Transactions on Vehicular Technology, Vol. 59, No. 8, OCT. 2010, pp. 3757-3765.

[21] G. Chen, and H. Ying, "Stability Analysis of Nonlinear Fuzzy PI Control Systems", International Conference on Industrial Fuzzy Control and Intelligent Systems, DEC. 1993, pp. 128-133.

[22] H. A. Malki, H. Li and G. Chen, "New Design and Stability Analysis of Fuzzy Proportional-Derivative Control Systems," IEEE Transactions on Fuzzy Systems, Vol. 2, No. 4, NOV. 1994, pp. 245-254.

[23] J. B. Heywood, International Combustion Engine Fundamentals, McGraw-Hill, New York, 1998.

[24] P. Anderson, Air Charge Estimation in Turbocharged Spark Ignition Engines, PhD thesis, Linkoping University, 2005.

[25] C. R. Ferguson and A. T. Kirkpatrick, International Combustion Engines Applied Thermosciences, second ed., John Wiley & Sons, New York, 2001.

[26] G. Gnanam, S. R. Habibi, R. T. Burton and M. T. Sulatisky, "Neural Network Control of Air-to-Fuel Ratio in a Bi-Fuel Engine," IEEE Transactions on Systems Man and Cybernatics Part C: Applications and Reviews, Vol. 36, No.5, 2006, pp. 656-667.

[27] R. Weeks, J.J. Moskwa, Automotive Engine Modeling for Real-Time Control Using Matlab/Simulink, SAE Paper No.950417, 1995.

[28] F. Zhang, K. M. Grigoriadis, M. A. Franchek and H. L. Makki, "Linear Parameter-Varying Lean Burn Air-Fuel Ratio Control for a Spark Ignition Engine," ASME Journal of Dynamic System Measurement and Control, Vol. 129, No. 4, 2007, pp. 404-414.

[29] G. F. Franklin, J. D. Powell and A. E. Naeini, Feedback Control of Dynamic Systems, fifth ed., Pearson International Edition, Singapore, 2006.

[30] V. Ganesan, International Combustion Engines, second ed., Tata McGraw-Hill, Singapore, 2004.

[31] U. Kiencke and L. Nielsen, Automotive Control Systems for Engine, Driveline, and Vehicle, second ed., Springer-Verlag Berlin Heidelberg, Germany, 2005.

[32] G. E. Totten, Handbook of Lubrication and Tribology Volume I Application and Maintenance, second ed., CRC Press Taylor & Francis Group, Florida, 2006.

[33] Q. Ahmed and A. I. Bhatti, "Estimating SI Engine Efficiencies and Parameters in Second Order Sliding Modes," IEEE Transaction on Industrial Electronics, Vol. 57, No. 12, 2010, pp. 1-9.

[34] J. Deur, D. Pavkovic, N. Peric, M. Jansz and D. Hrovat, "An Electronic Throttle Control Strategy Including Compensation of Friction and Limp-Home Effects," IEEE Transactions on Industry Applications, Vol. 40, No. 3, May/Jun 2004, pp. 821-834.

# Appendix A

## Discrete Fuzzy PI operation

## A.1 1st area

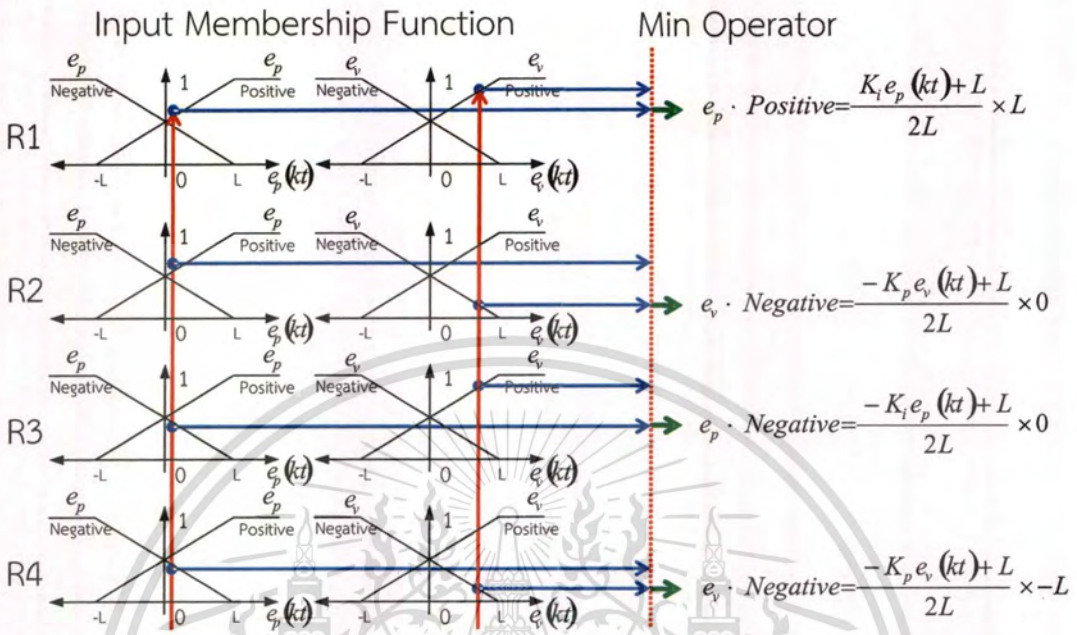


**Fig. A.1** Fuzzification, fuzzy inference and defuzzification operations of 1st area

$$COA_1 = \frac{\left(\frac{K_i e_p(kt) + L}{2L} \times L\right) + 0 + 0 + \left(\frac{-K_p e_v(kt) + L}{2L} \times -L\right)}{\frac{K_i e_p(kt) + L}{2L} + \frac{-K_p e_v(kt) + L}{2L} + \frac{-K_i e_p(kt) + L}{2L} + \frac{-K_p e_v(kt) + L}{2L}} \quad \text{(A.1a)}$$

$$COA_1 = \frac{L \times \left(\frac{K_i e_p(kt) + K_p e_v(kt) + L - L}{2L}\right)}{\frac{4L - 2K_p e_v(kt)}{2L}} \quad \text{(A.1b)}$$

$$COA_1 = \frac{L \times \left(K_i e_p(kt) + K_p e_v(kt)\right)}{2\left(2L - K_p e_v(kt)\right)} \quad \text{(A.1c)}$$

## A.2 2nd area

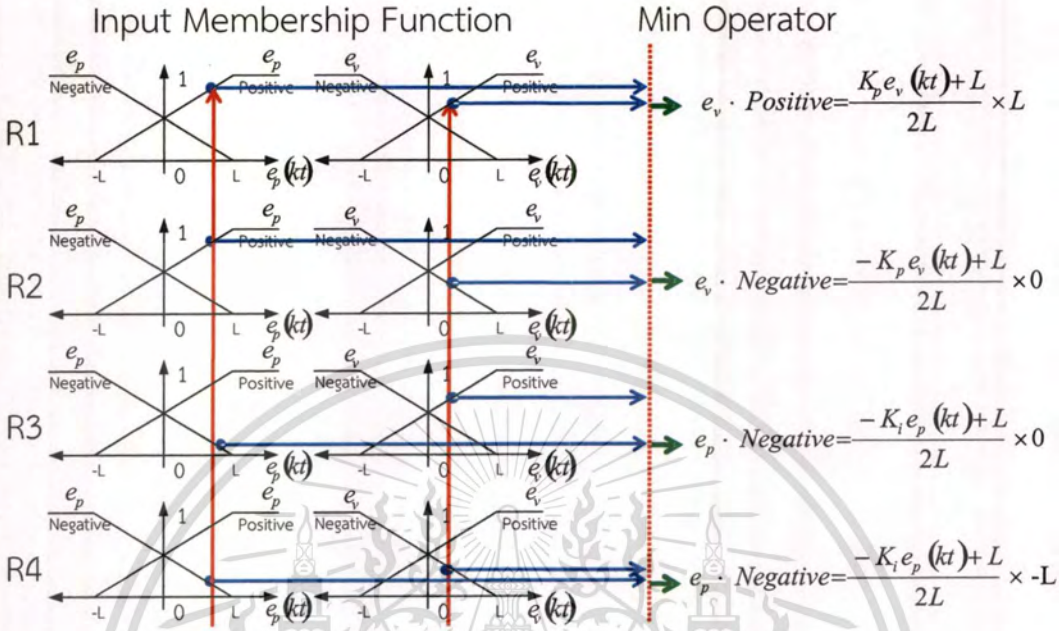


**Fig. A.2** Fuzzification, fuzzy inference and defuzzification operations of 2nd area

$$COA_2 = \frac{\left(\frac{K_p e_v(kt)+L}{2L} \times L\right) + 0 + 0 + \left(\frac{-K_i e_p(kt)+L}{2L} \times -L\right)}{\frac{K_p e_v(kt)+L}{2L} + \frac{-K_p e_v(kt)+L}{2L} + \frac{-K_i e_p(kt)+L}{2L} + \frac{-K_i e_p(kt)+L}{2L}} \quad \text{(A.2a)}$$

$$COA_2 = \frac{L \times \left(\frac{K_i e_p(kt) + K_p e_v(kt) + L - L}{2L}\right)}{\frac{4L - 2K_i e_p(kt)}{2L}} \quad \text{(A.2b)}$$

$$COA_2 = \frac{L \times \left(K_i e_p(kt) + K_p e_v(kt)\right)}{2\left(2L - K_i e_p(kt)\right)} \quad \text{(A.2c)}$$

## A.3 3rd area

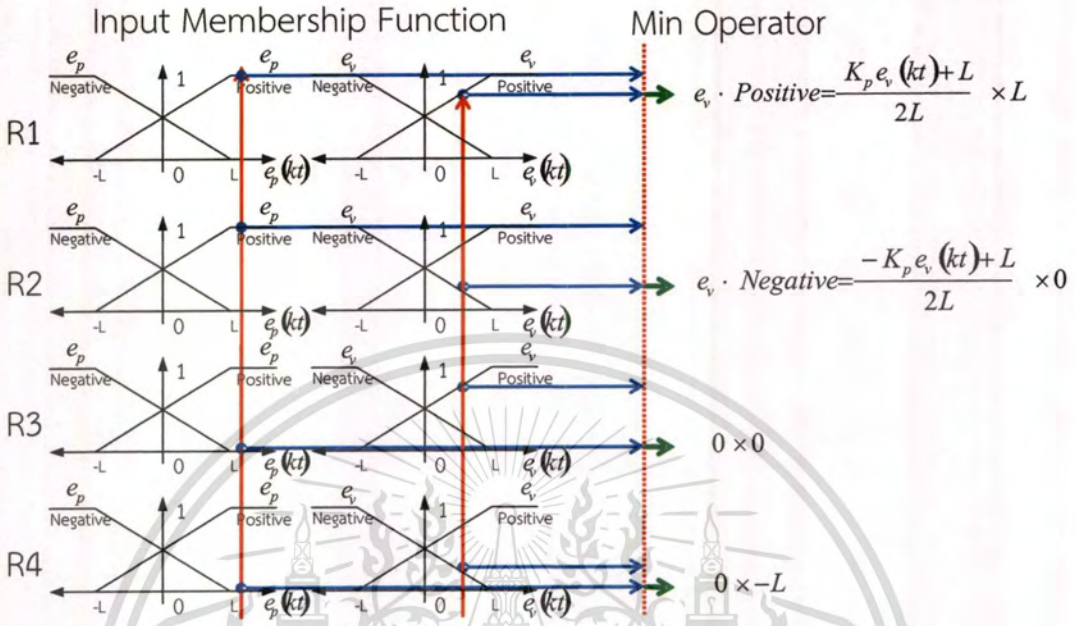


Fig. A.3 Fuzzification, fuzzy inference and defuzzification operations of 3rd area

$$COA_3 = \frac{\left(\frac{K_p e_v(kt)+L}{2L} \times L\right) + \left(\frac{-K_p e_v(kt)+L}{2L} \times 0\right) + 0 + 0}{\frac{K_p e_v(kt)+L}{2L} + \frac{-K_p e_v(kt)+L}{2L}} \quad \text{(A.3a)}$$

$$COA_3 = \frac{\left(\frac{K_p e_v(kt)+L}{2L} \times L\right) \times 2L}{2L} \quad \text{(A.3b)}$$

$$COA_3 = \frac{K_p e_v(kt)+L}{2L} \times L \quad \text{(A.3c)}$$

$$COA_3 = 0.5\left(K_p e_v(kt)+L\right) \quad \text{(A.3d)}$$

## A.4 4th area

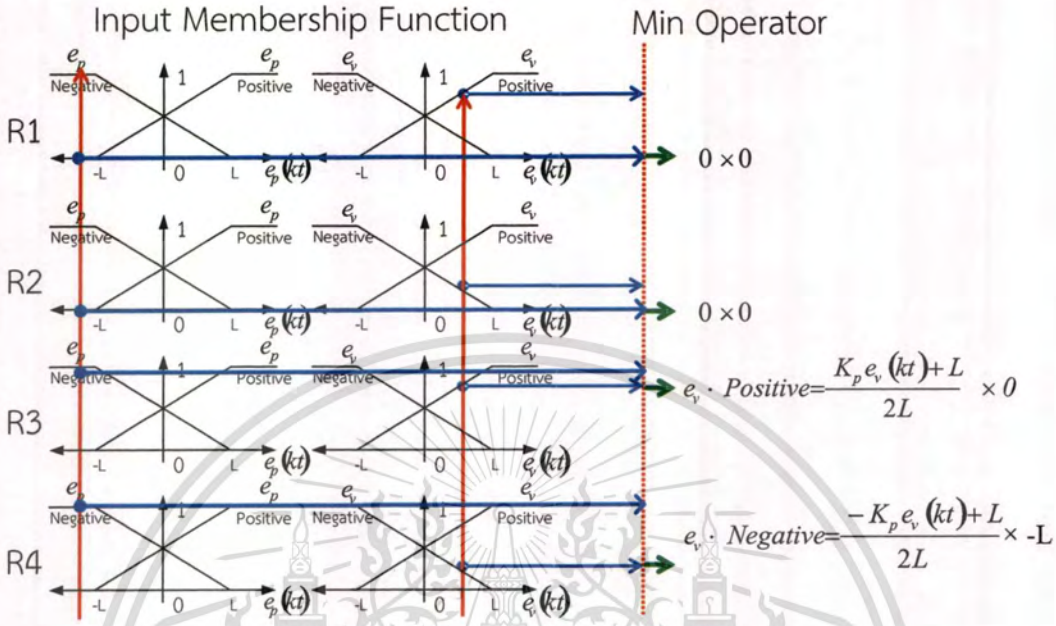


**Fig. A.4** Fuzzification, fuzzy inference and defuzzification operations of 4th area

$$COA_4 = \frac{0 + 0 + \left(\frac{K_p e_v(kt) + L}{2L} \times 0\right) + \left(\frac{-K_p e_v(kt) + L}{2L} \times -L\right)}{\frac{K_p e_v(kt) + L}{2L} + \frac{-K_p e_v(kt) + L}{2L}} \quad \text{(A.4a)}$$

$$COA_4 = \frac{\left(\frac{-K_p e_v(kt) + L}{2L} \times -L\right) \times 2L}{2L} \quad \text{(A.4b)}$$

$$COA_4 = \frac{-K_p e_v(kt) + L}{2L} \times -L \quad \text{(A.4c)}$$

$$COA_4 = 0.5\left(K_p e_v(kt) - L\right) \quad \text{(A.4d)}$$

## A.5 5th area

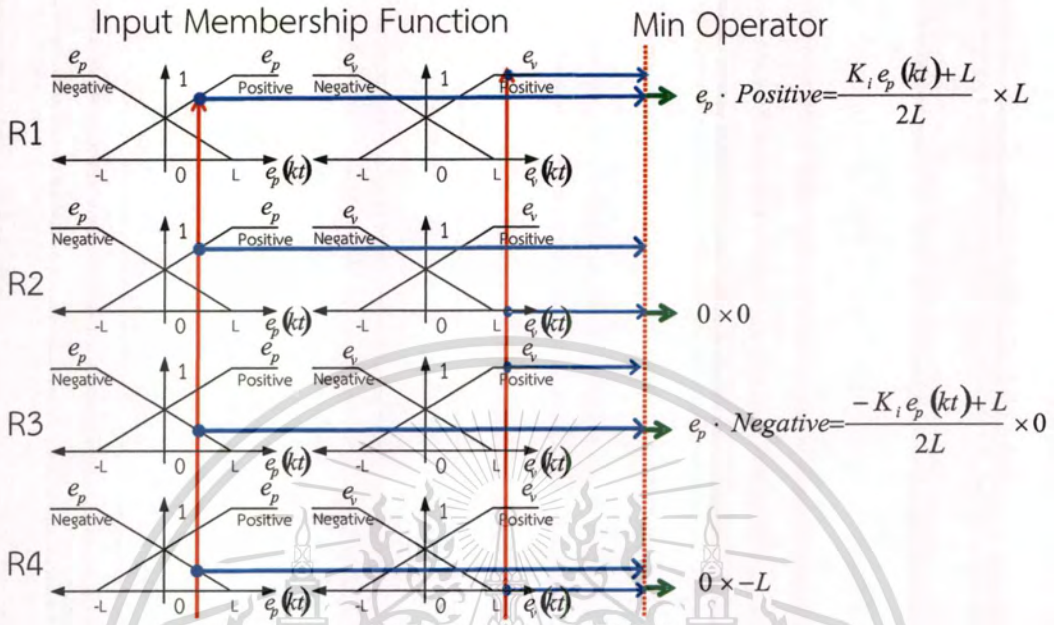


**Fig. A.5** Fuzzification, fuzzy inference and defuzzification operations of 5th area

$$COA_5 = \frac{\left(\frac{K_i e_p(kt)+L}{2L} \times L\right) + 0 + \left(\frac{-K_i e_p(kt)+L}{2L} \times 0\right) + 0}{\frac{K_i e_p(kt)+L}{2L} + \frac{-K_i e_p(kt)+L}{2L}} \quad \text{(A.5a)}$$

$$COA_5 = \frac{\left(\frac{K_i e_p(kt)+L}{2L} \times L\right) \times 2L}{2L} \quad \text{(A.5b)}$$

$$COA_5 = \frac{K_i e_p(kt)+L}{2L} \times L \quad \text{(A.5c)}$$

$$COA_5 = 0.5\left(K_i e_p(kt)+L\right) \quad \text{(A.5d)}$$

## A.6 6th area

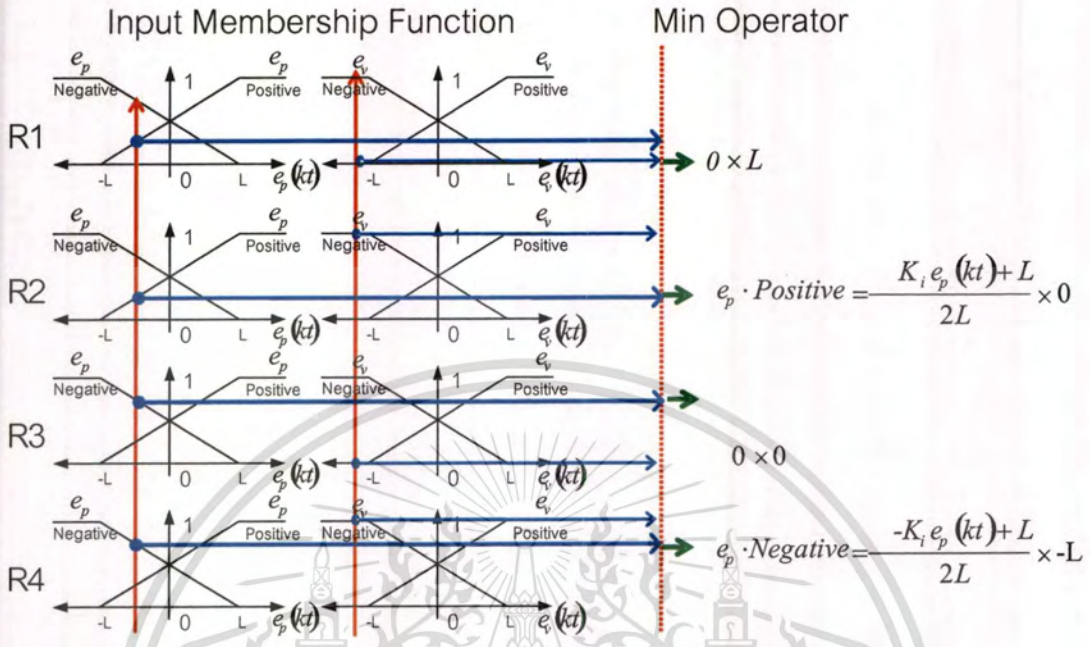


Fig. A.6 Fuzzification, fuzzy inference and defuzzification operations of 6th area

$$COA_6 = \frac{0+\left(\frac{K_i e_p(kt)+L}{2L}\times 0\right)+0+\left(\frac{-K_i e_p(kt)+L}{2L}\times -L\right)}{\frac{K_i e_p(kt)+L}{2L}+\frac{-K_i e_p(kt)+L}{2L}} \quad \text{(A.6a)}$$

$$COA_6 = \frac{\left(\frac{-K_i e_p(kt)+L}{2L}\times -L\right)\times 2L}{2L} \quad \text{(A.6b)}$$

$$COA_6 = \frac{-K_i e_p(kt)+L}{2L}\times -L \quad \text{(A.6c)}$$

$$COA_6 = 0.5\left(K_i e_p(kt)-L\right) \quad \text{(A.6d)}$$

## A.7 7th area

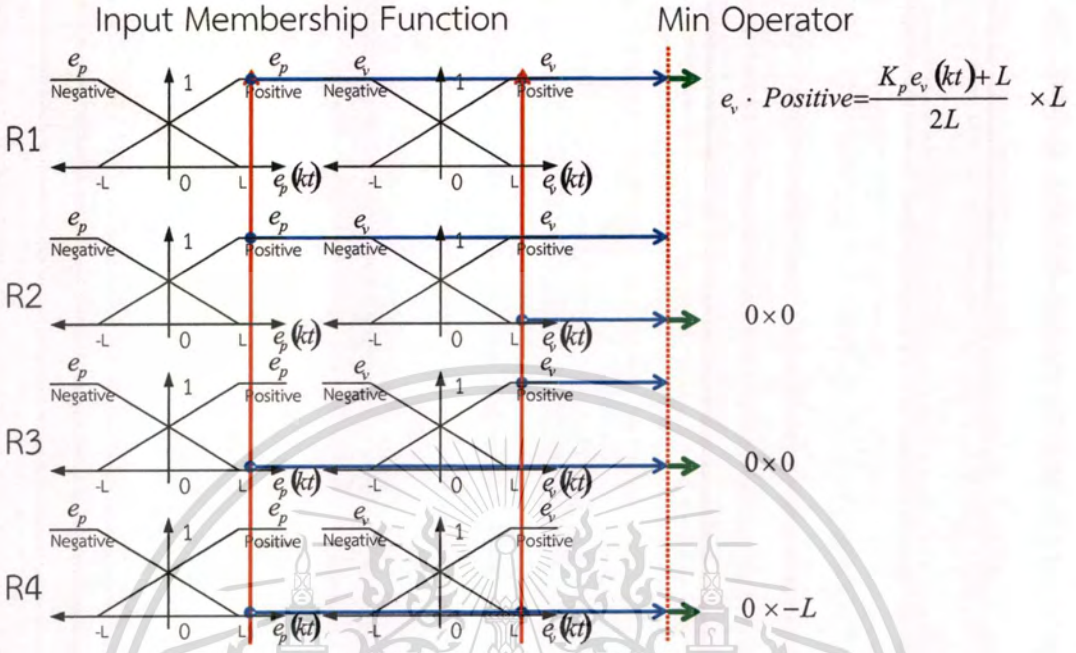


**Fig. A.7** Fuzzification, fuzzy inference and defuzzification operations of 7th area

$$COA_7 = \frac{\left(\frac{K_p e_v(kt)+L}{2L} \times L\right)+0+0+0}{\frac{K_p e_v(kt)+L}{2L}} \tag{A.7a}$$

$$COA_7 = \frac{\left(\frac{K_p e_v(kt)+L}{2L}\right) \times L}{\left(\frac{K_p e_v(kt)+L}{2L}\right)} \tag{A.7b}$$

$$COA_7 = L \tag{A.7c}$$

## A.8 8th and 9th areas

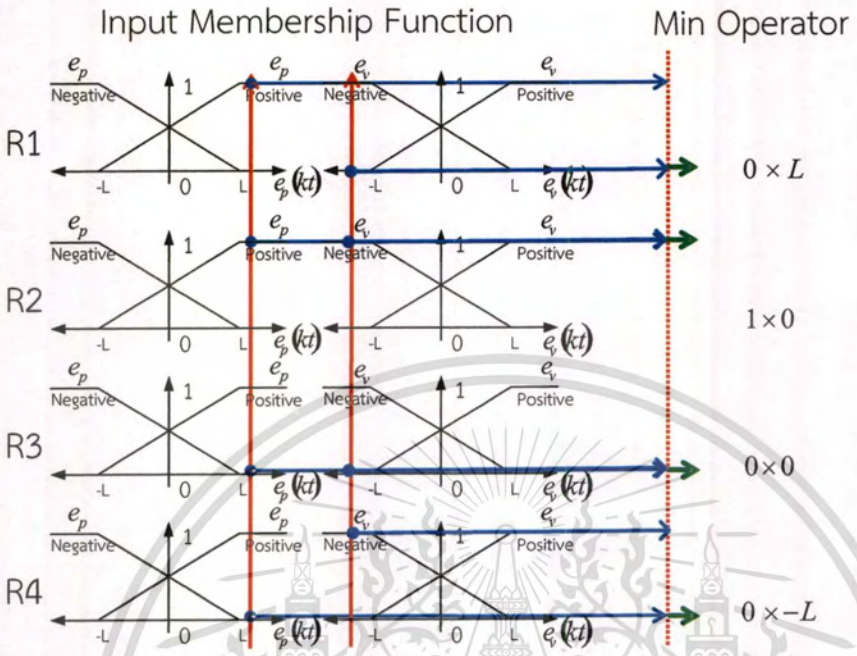


**Fig. A.8** Fuzzification, fuzzy inference and defuzzification operations of 8th and 9th areas

$$COA_{8,9} = \frac{0+(1\times 0)+0+0}{1\times 0} \quad \text{(A.8a)}$$

$$COA_{8,9} = 0 \quad \text{(A.8b)}$$

## A.9 10th area

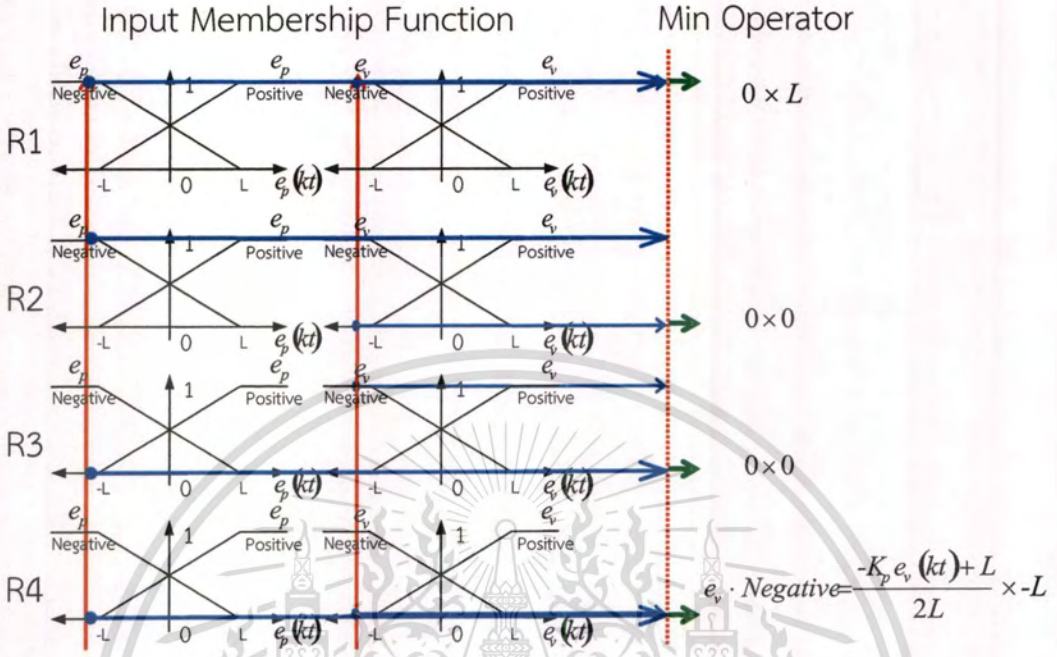


**Fig. A.9** Fuzzification, fuzzy inference and defuzzification operations of 10th area

$$COA_{10} = \frac{0+0+0+\left(\frac{-K_p e_v(kt)+L}{2L} \times -L\right)}{\frac{-K_p e_v(kt)+L}{2L}} \tag{A.10a}$$

$$COA_{10} = \frac{\left(\frac{-K_p e_v(kt)+L}{2L}\right) \times -L}{\left(\frac{-K_p e_v(kt)+L}{2L}\right)} \tag{A.10b}$$

$$COA_{10} = -L \tag{A.10c}$$

# Appendix B

# MATLAB/SIMULINK

## B.1 Area of throttle

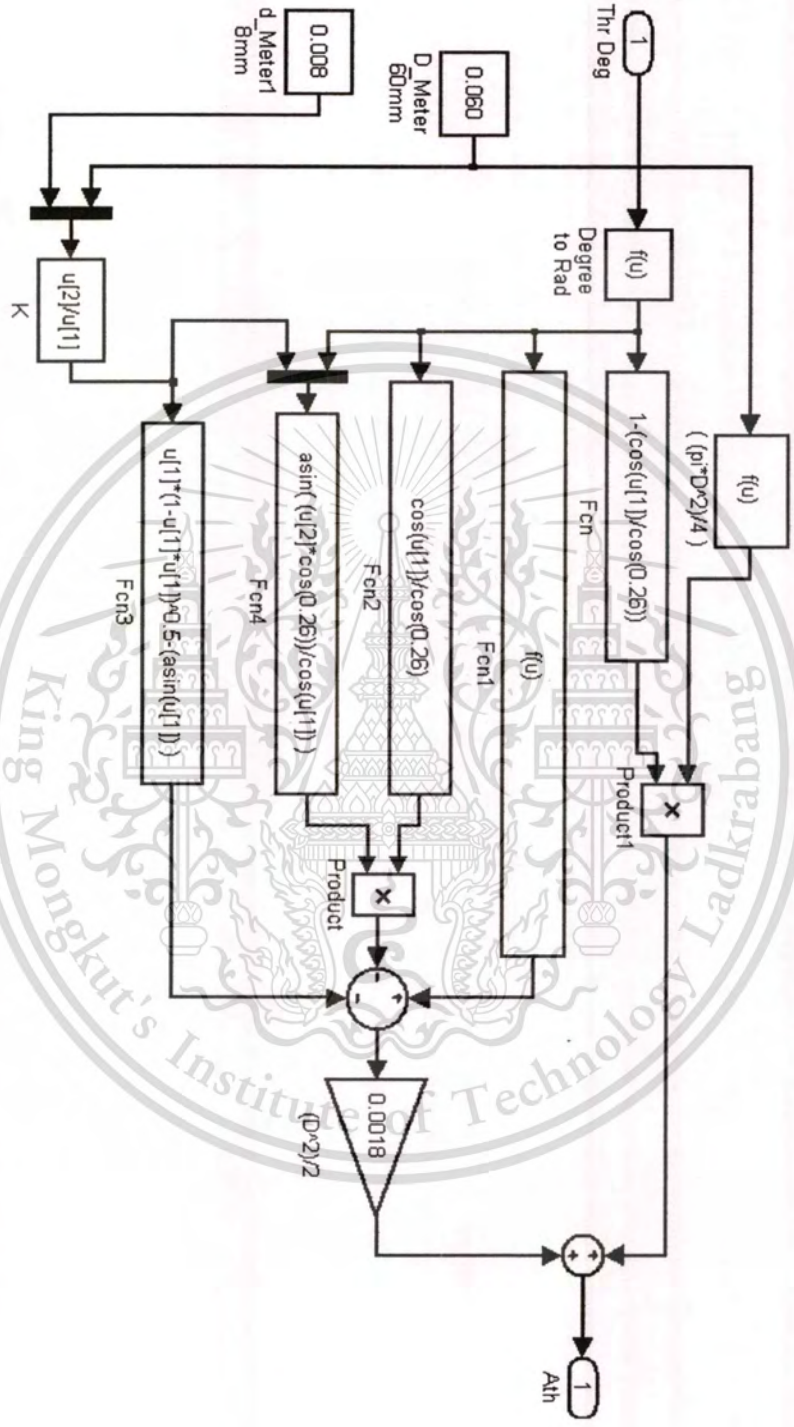


Fig. B.1 Area of throttle diagram

## B.2 Mass of air after the throttle

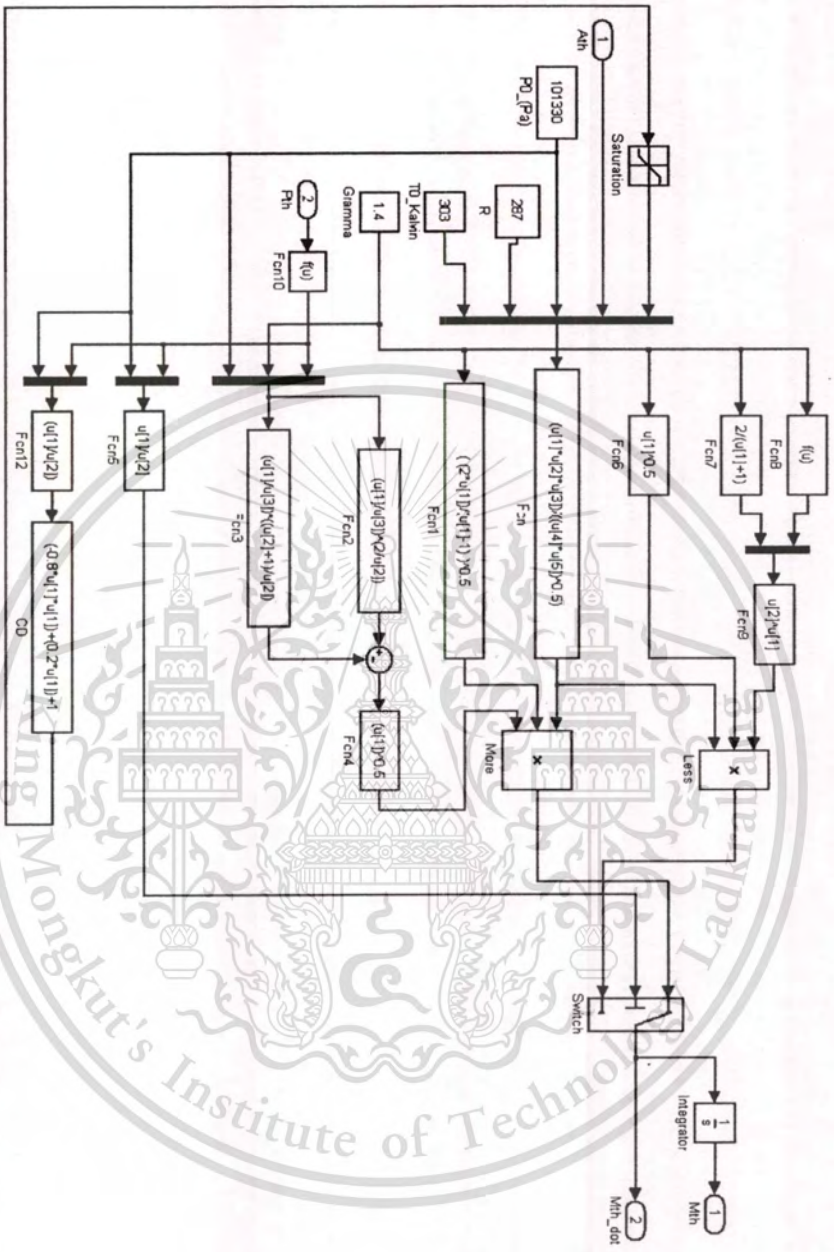


**Fig. B.2** Air mass diagram

## B.3 Volumetric efficiency

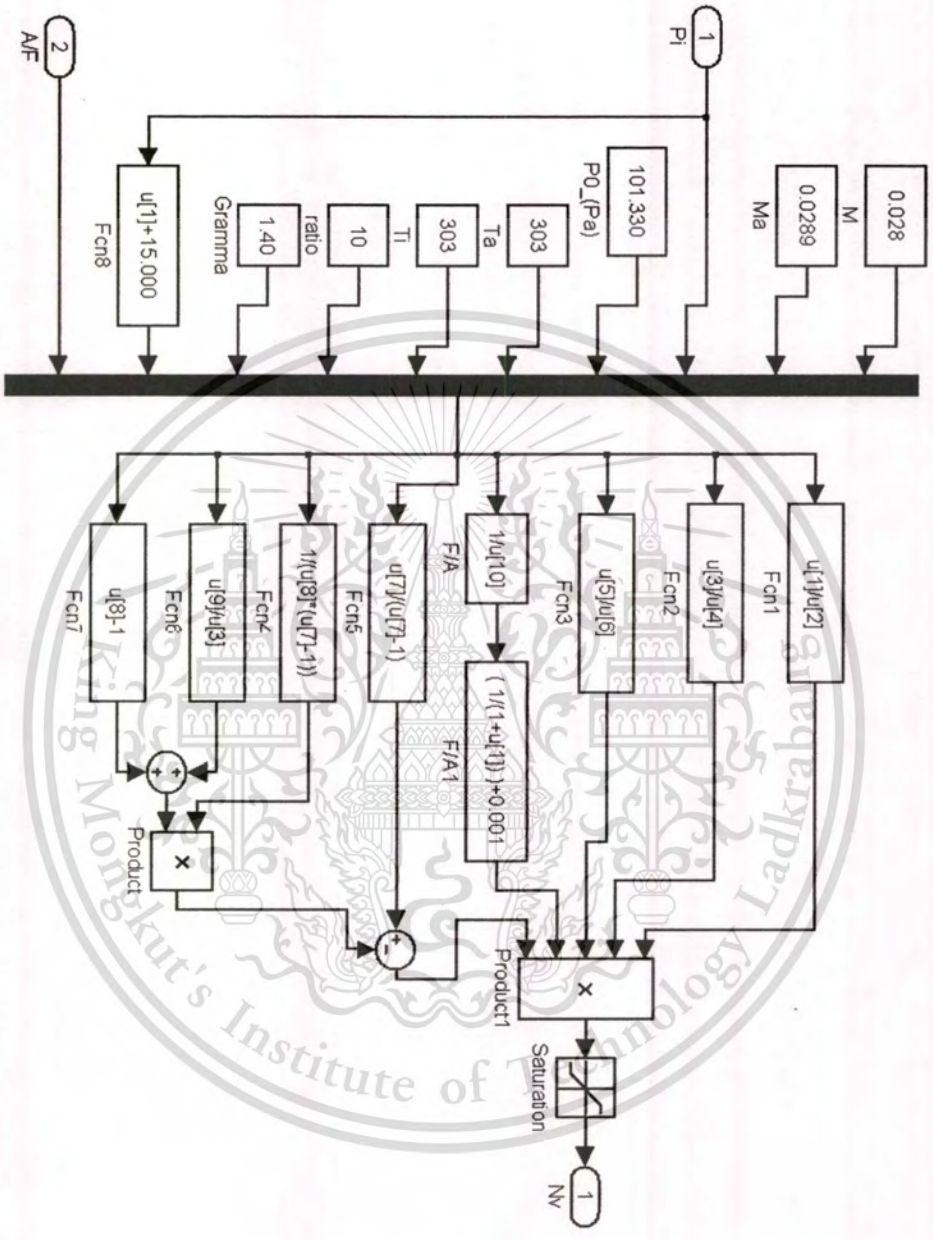


**Fig. B.3** Volumetric efficiency diagram

## B.4 Intake manifold density

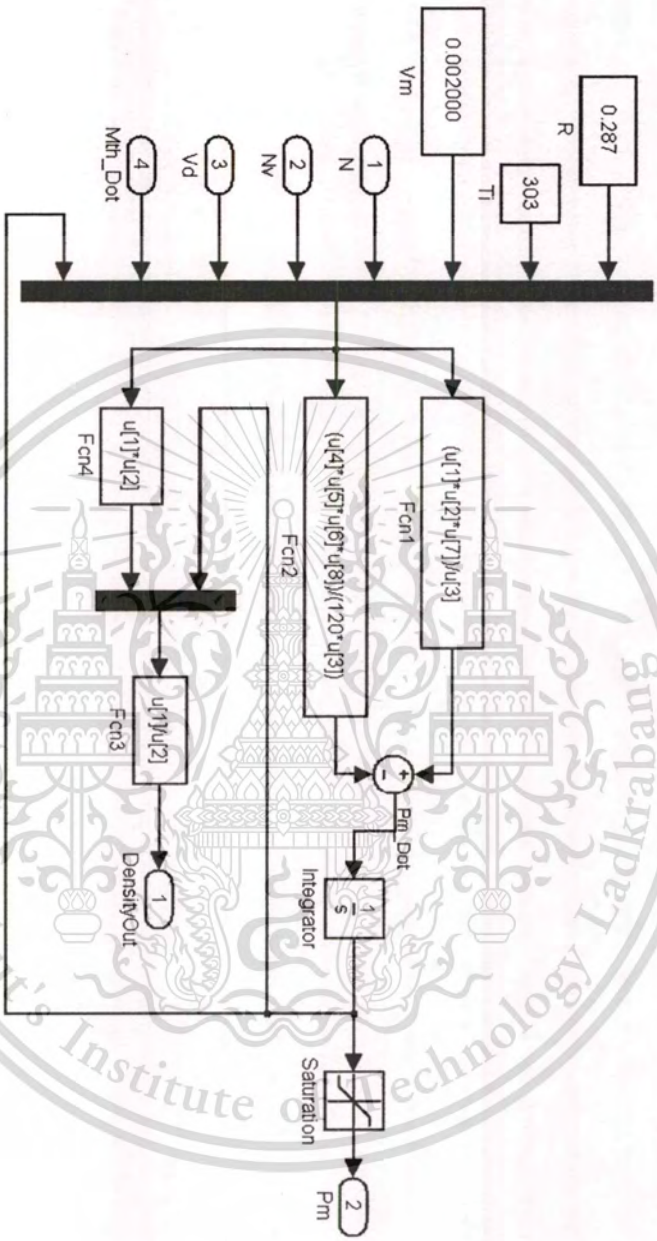


**Fig. B.4** Intake manifold density diagram

## B.5 Crankshaft

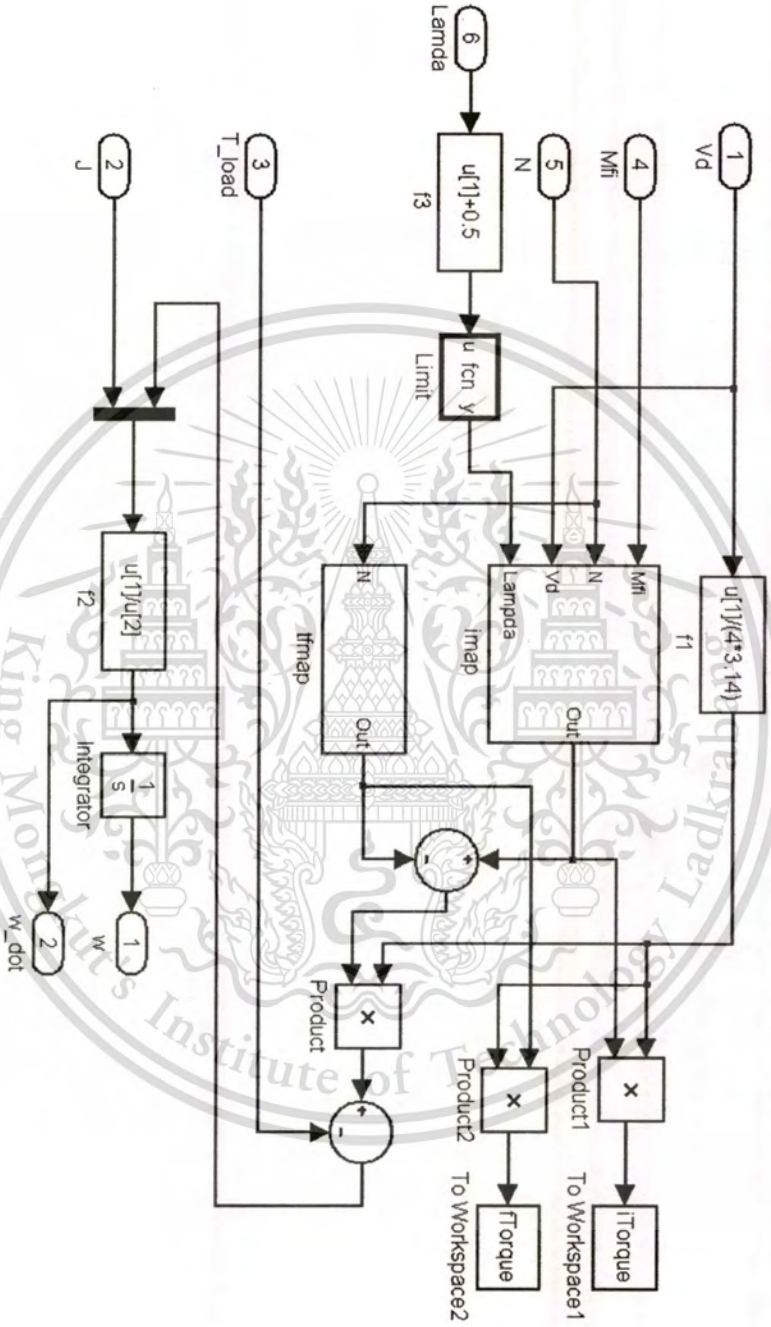


Fig. B.5 Crankshaft diagram

## B.6 Electronic throttle control

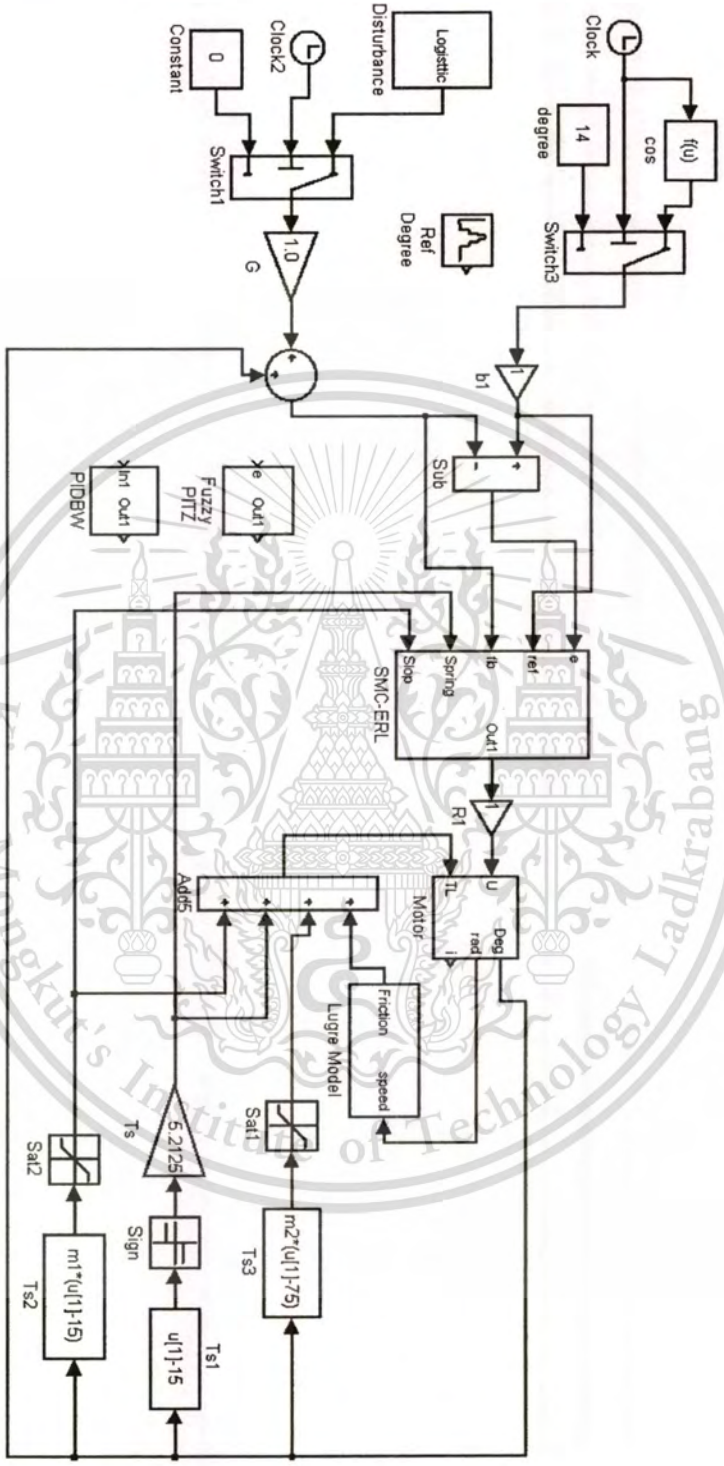


**Fig. B.6** Electronic throttle control diagram

# Appendix C

## Electronic throttle valve

For experimental ETV, the feedforward approach is utilized to prove a total number of load torque. The input signals are Pulse-Width-Modulation signals that increase the duty-cycle of the signal by ten percent every second. Concurrently, the current sources and the throttle angles are measured. The measured data are presented in Table C.1 and depicted on a load-torque characteristic in Fig C.1. As such, the Coulomb friction is approximately 5 Nm/s at 40 percent of duty cycle.

**Table C.1** The characterization of used electronic throttle valve

| Duty cycle of PWM | Current (Ampere) | Throttle angle (Degree) | Load Torque (Nm/s) |
|---|---|---|---|
| 10% | 0.105 | Close position | 0.126 |
| 20% | 0.3923 | Close position | 0.9415 |
| 30% | 0.7106 | Close position | 2.5581 |
| 40% | 1.086 | 22 | 5.2128 |
| 50% | 1.36 | 80 | 8.16 |
| 60% | 1.79 | 85 | 12.888 |

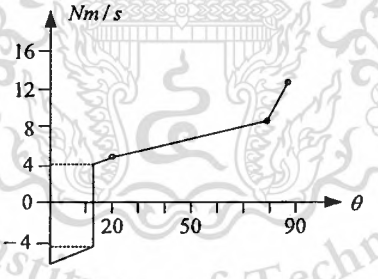


**Fig. C.1** A load-torque characteristic of the used ETV

# Appendix D

# PID controller family and experiment results

## D.1 PI Trapezoid Rule (Bilinear Approximation)

The $\frac{2}{T}\frac{(1-z^{-1})}{(1+z^{-1})}$ is employed for $s$ as follow:

$$U_{PI}(s) = K\left(1+\frac{1}{st_i}\right)e(s)$$

$$U_{PI}(z) = K\left(1+\frac{1}{t_i}\left(\frac{T}{2}\frac{(1+z^{-1})}{(1-z^{-1})}\right)\right)e(z)$$

$$U_{PI}(z) = \left(K_p + K_i\left(\frac{(1+z^{-1})}{(1-z^{-1})}\right)\right)e(z)$$

$$U_{PI}(z) = \left(\frac{K_p(1-z^{-1})+K_i(1+z^{-1})}{(1-z^{-1})}\right)e(z)$$

$$U_{PI}(z)(1-z^{-1}) = \{K_p(1-z^{-1})+K_i(1+z^{-1})\}e(z)$$

$$U_{PI}(KT)-U_{PI}(KT-1) = K_p\{e(KT)-e(KT-1)\}+K_i\{e(KT)+e(KT-1)\}$$

$$\Delta U_{PI}(KT) = K_p\{e(KT)-e(KT-1)\}+K_i\{e(KT)+e(KT-1)\}$$

where

$K_p = K$, $K_i = KT/2t_i$ and the controller diagram is shown as below

..

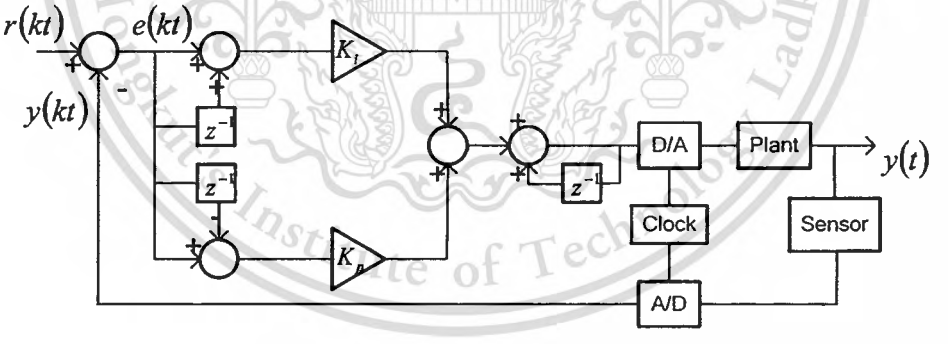


**Fig. D.1** Block diagram of PI (Bilinear Approximation) scheme

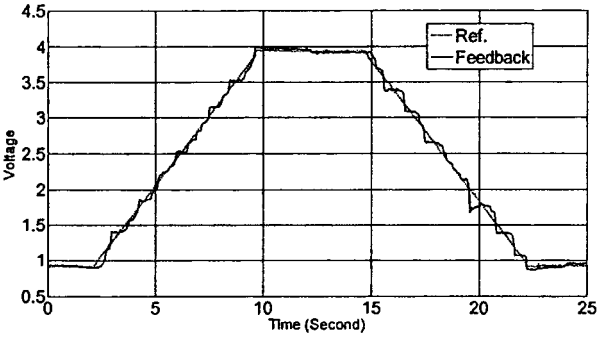


Fig. D.2 Ramp-step response of PI controller

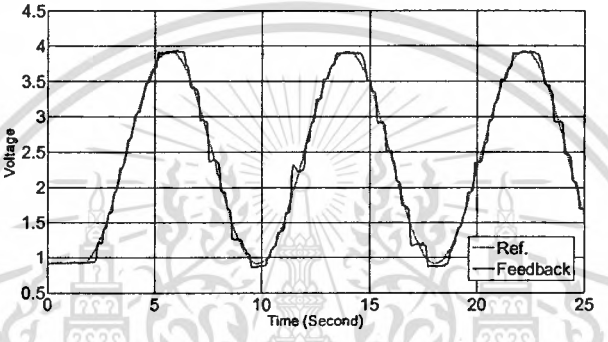


Fig. D.3 Sine-step response of PI controller

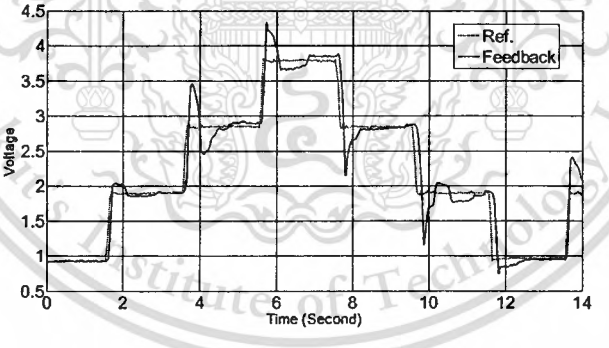


Fig. D.4 Multi-step response of PI controller

**Table D.1** Performance indices of PI control in experiment

| Acceleration | IAE (Degree) | ISE (Degree) | OV Max (Degree) | Settle Time Max (Second) |
|---|---|---|---|---|
| Ramp step | 1.1933 | 0.0979 | 0 | - |
| Sine Step | 1.5874 | 0.1814 | 0 | - |
| Multi Step | 1.8298 | 0.705 | 0.7363 | 1.15 |

## D.2 PD backward rule

The $\frac{1-z^{-1}}{T}$ is employed for $s$ as follow:

$$U_{PD}(s) = K(1+st_d)e(s)$$

$$U_{PD}(z) = K\left(1+\left(\frac{1-z^{-1}}{T}\right)t_d\right)e(z)$$

$$U_{PD}(z) = \left(K_p + K_d\left(1-z^{-1}\right)\right)e(z)$$

$$U_{PD}(KT) = K_p\{e(KT)\} + K_d\{e(KT)-e(KT-1)\}$$

where

$K_p = K$, $K_d = Kt_d/T$ and the controller diagram is shown in fig. D.5

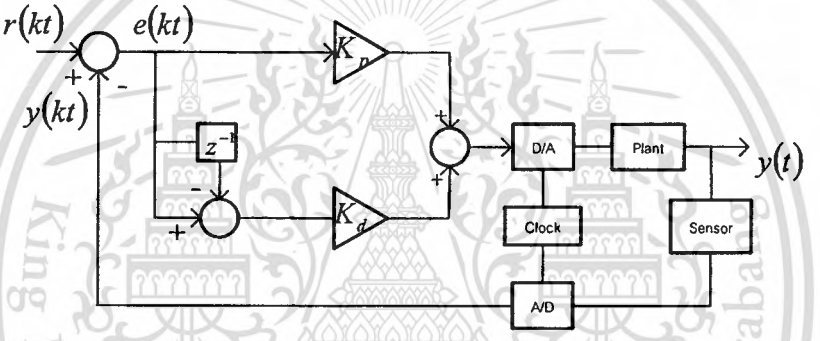


Fig. D.5 Block diagram of PD backward scheme

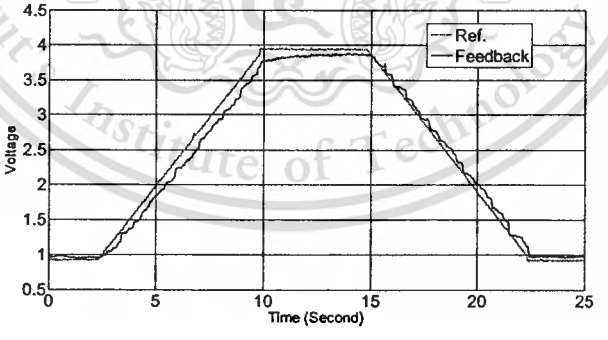


**Fig. D.6** Ramp-step response of PD controller

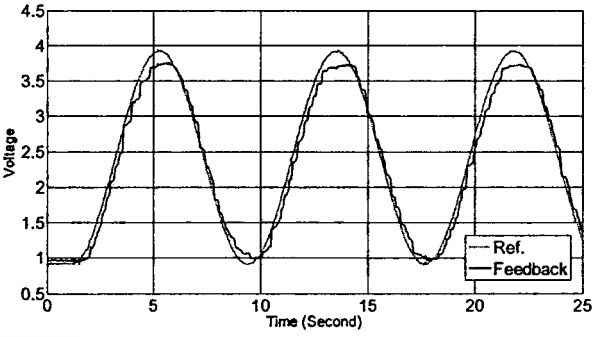


**Fig. D.7** Sine-step response of PD controller

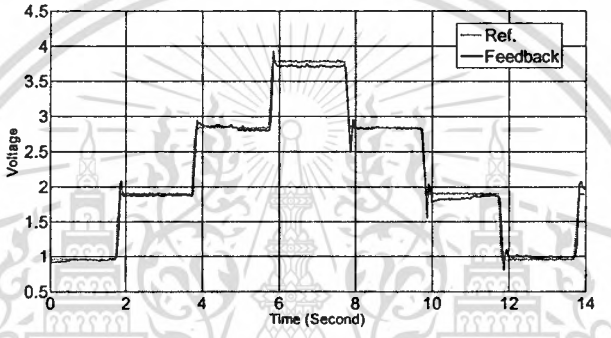


**Fig. D.8** Multi-step response of PD controller

**Table D.2** Performance indices of PD control in experiment

| Acceleration | IAE (Degree) | ISE (Degree) | OV Max (Degree) | Settle Time Max (Second) |
|---|---|---|---|---|
| Ramp step | 2.6597 | 0.3737 | 0 | Off set |
| Sine Step | 3.2316 | 0.5372 | 0 | - |
| Multi Step | 0.7663 | 0.1101 | 0.3936 | Off set |

**D.3 PD+I backward rule**

The $\frac{1-z^{-1}}{T}$ is employed for $s$ as follow:

$$U_I(s) = K\left(\frac{1}{st_i}\right)e(s)$$

$$U_I(z) = K\left(\frac{1}{t_i}\frac{T}{(1-z^{-1})}\right)e(z)$$

$$U_I(z) = \left(K_i\left(\frac{1}{(1-z^{-1})}\right)\right)e(z)$$

$$U_I(z)(1-z^{-1}) = K_i e(z)$$

$$U_I(KT) - U_I(KT-1) = K_i e(KT)$$

and

$$U_{PD}(s) = K(1+st_d)e(s)$$

$$U_{PD}(z) = K\left(1+\left(\frac{1-z^{-1}}{T}\right)t_d\right)e(z)$$

$$U_{PD}(z) = \left(K_p + K_d(1-z^{-1})\right)e(z)$$

$$U_{PD}(KT) = K_p\{e(KT)\} + K_d\{e(KT) - e(KT-1)\}$$

where

$K_p = K$, $K_d = Kt_d/T$, $K_i = KT/t_i$ and the controller diagram is shown in fig. D.9

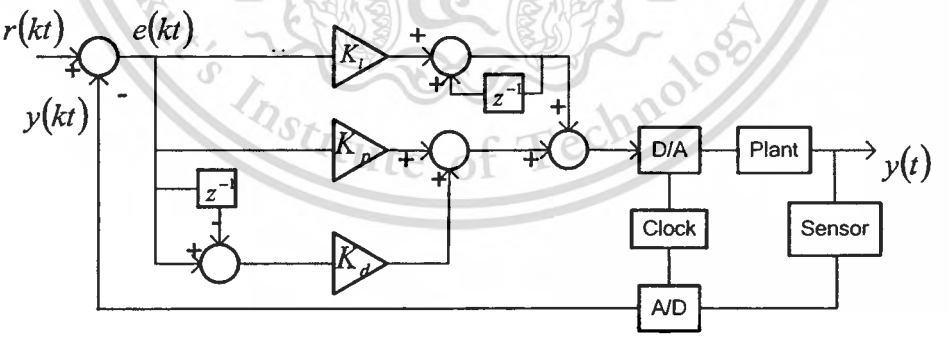


**Fig. D.9** Block diagram of PD+I backward scheme

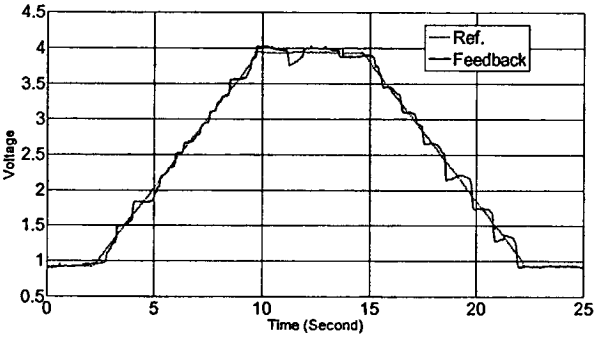


Fig. D.10 Ramp-step response of PD+I controller

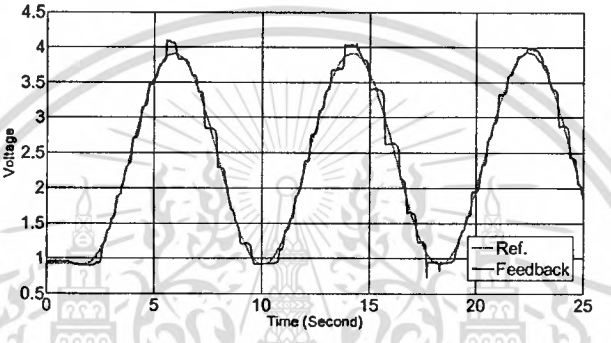


Fig. D.11 Sine-step response of PD+I controller

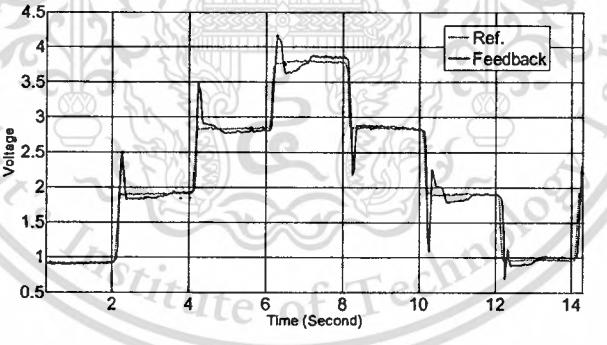


Fig. D.12 Multi-step response of PD+I controller

**Table D.3** Performance indices of PD+I control in experiment

| Acceleration | IAE (Degree) | ISE (Degree) | OV Max (Degree) | Settle Time Max (Second) |
|---|---|---|---|---|
| Ramp step | 1.431 | 0.1392 | 0 | - |
| Sine Step | 1.6857 | 0.1987 | 0.91 | - |
| Multi Step | 1.222 | 0.3524 | 1.75 | 1.62 |

# Appendix E

# Fuel Properties

**Table E.1** Data on fuel properties

| Fuel | Formula | Higher heating value, MJ/kg | Lower heating value, MJ/kg | $(A/F)_s$ |
|---|---|---|---|---|
| Gasoline | $C_nH_{1.87n}$ | 47.3 | 44.0 | 14.6/1 |
| Natural gas | $C_nH_{3.8}N_{0.1n}$ | 50.0 | 45.0 | 14.5/1 |
| Methane | $CH_4$ | 55.0 | 50.0 | 17.23/1 |
| Propane | $C_3H_8$ | 50.4 | 46.4 | 15.67/1 |
| Ethanol | $C_2H_6O$ | 29.7 | 26.9 | 9.0/1 |
| Gasohol E10 | $0.9C_nH_{1.87n}+0.1C_2H_6O$ | 45.54 | 42.36 | 14.13/1 |
| Gasohol E20 | $0.8C_nH_{1.87n}+0.2C_2H_6O$ | 43.78 | 40.45 | 13.29/1 |
| Gasohol E85 | $0.15C_nH_{1.87n}+0.85C_2H_6O$ | 32.34 | 29.06 | 9.86/1 |

# Appendix F

# Crankshaft Moment of Inertia

**Engine Mass in Motion**

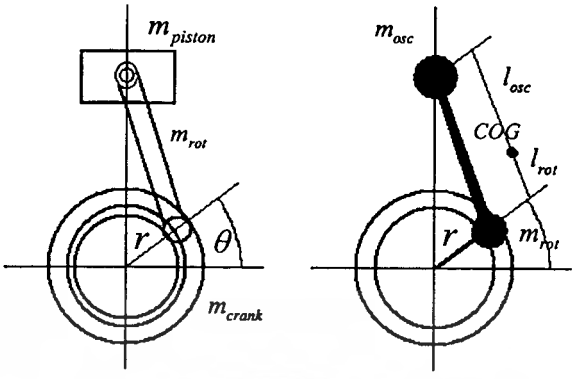


Fig. F.1 Two-mass model for oscillating and rotating masses

An oscillating portion is

$$m_{rod,osc} = m_{rod}\frac{l_{osc}}{l}, \tag{F.1}$$

and a rotation portion is

$$m_{rod,rot} = m_{rod}\frac{l_{rot}}{l}. \tag{F.2}$$

The two lengths $l_{osc}$ and $l_{rot}$ with

$$l_{osc} + l_{rot} = l \tag{F.3}$$

are defined by the location of the center of gravity of the connecting rod. Thus the oscillating mass at each cylinder is

$$m_{osc} = m_{piston} + m_{rod}\frac{l_{osc}}{l}, \tag{F.4}$$

and the rotational mass of the crankshaft portion at one cylinder

$$m_{rot} = m_{crank} + m_{rod}\frac{l_{rod}}{l}. \tag{F.5}$$

The crankshaft mass in deducted from the moment of inertia

$$m_{crank} = \frac{J_{crank}}{r^2}. \tag{F.6}$$

Thus, the moment of inertia is

$$J(\theta) = m_{rot}r^2 + m_{osc}\sum_{j=1}^{cyl}\left(\frac{ds_j}{d\theta}\right)^2, \tag{F.7}$$

as the speed of oscillating mass $v_{osc,j}$ is the time derivative of respective piston stroke $s_j$

$$v_{osc,j} = \dot{s}_j(\theta) = \dot{s}\left(\theta - (j-1)\frac{4\pi}{cyl}\right), j = 1,\ldots,cyl. \tag{F.8}$$

Appendix G

# Average performance indices of controls in experiment

**Table G.1** Average performance indices of controls in experiment

| Controller | IAE (Degree) | ISE (Degree) | OV Max (Degree) | Settling Time Max (Second) |
|---|---|---|---|---|
| PID | 1.0063 | 0.1261 | 0.6318 | 0.93 |
| PID-AW | 1.1517 | 0.1668 | 0 | 0.81 |
| **FPI-AW** | **0.933** | **0.0861** | **0** | **0.72** |
| SMC-ERL | 2.5872 | 0.7711 | 0.6671 | Off set |

# RELATED PUBLICATIONS

1. **Anurak Jansri** and Pitikhate Sooraksa, "Enhanced model and fuzzy strategy of air to fuel ratio control for spark ignition engines," An International journal Computers & Mathematics with Applications, Vol. 64, 2012, P 922-933.

2. **Anurak Jansri** and Pitikhate Sooraksa, "Simple Nonlinear Air to Fuel Ratio for Spark Ignition Engines," International Symposium on Computer, Consumer and Control 2012, 4-6 June, Taiwan.

3. **Anurak Jansri,** Thadchapong Pongsuttiyakorn and Pitikhate Sooraksa, "On Practical Control of Electronic Throttle Body," 9th International Conference on Fuzzy Systems and Knowledge Discovery, 2012, 29-31 May, Chongqing, China.

# AUTHOR BIOGRAPHY

Anurak Jansri was born in Chiang Mai, Thailand. He received B.IT. and M.Eng. degrees from King Mongkut's Institute of Technology Ladkrabang, Ladkrabang, Bangkok, Thailand, in 2002 and 2007, respectively. During 2004 to 2007, he employed in Total Access Communication Public Company Limited. His research interests include Automotive control, IT-mechatronics, development of rapid prototypes in embedded systems and computer-aided control. He received a scholarship from TRF-RGJ.PhD for achieving his Doctoral degree in electrical engineering, Faculty of Engineering, King Mongkut's Institute of Technology Ladkrabang, Ladkrabang, Bangkok, Thailand.